

https://dspace.org/

Phosphogypsum beneficiation

Msila, Xolani

2016
http://hdl.handle.net/10539/21002

Downloaded from a DSpace repository. https://dspace.org/

P H O S P H O G Y P S U M B E N E F I C I A T I O N

Xolani Msila

A Thesis submitted to the Faculty of Science, University of the Witwatersrand, in fulfilment of the requirements for the degree of Doctor of Philosophy**.**

Johannesburg, 2016

DECLARATION

I declare that this thesis is my own unaided work. It is being submitted for the Degree of Doctor of Philosophy at the University of the Witwatersrand, Johannesburg. It has not been submitted before for any degree or examination at any other University.

_____

(Signature of candidate)

_____ day of _____2016 in _____

ABSTRACT

Three alternatives for the utilisation of the phosphogypsum from the Lowveld region of South Africa were investigated in this thesis, namely (a) its suitability for use as building material; (b) its conversion to saleable ammonium sulphate and precipitated calcium carbonate; and (c) the reaction mechanism, pathway and kinetics of its thermal reduction with graphitic carbon to calcium sulphide.

The phosphogypsum contains activity concentrations of naturally occurring radioactive nuclides of uranium, thorium and their progenies that are lower than the 500 Bq/kg limit set for regulation in South Africa. The K-40 activity concentration is below the minimum detectable amount of 100 Bq/kg by gamma spectrometry. The calculated values for H_{ex}, H_{in} and I_{γ} are: 2.12 $\pm$ 0.59, 3.44 $\pm$ 0.64 and 2.65 $\pm$ 0.76 respectively. The calculated Ra_{eq} is 513 $\pm$ 76 Bq/kg. The phosphogypsum is suitable for restricted use in building materials but a final decision for its use should be taken with the consideration of scenarios of use.

The phosphogypsum was converted to ammonium sulphate and precipitated calcium carbonate in a Merseburg process that has been modified by omitting the CO_2 scrubbing towers. This modification reduced the heating requirement in the gypsum conversion reactor by 35 °C. The calcium carbonate precipitated as calcitic, scalenohedral polymorphs with a mean size of 3.4$\pm$ 0.1 µm in diameter.

A kinetic study of the reaction between phosphogypsum and graphitic carbon was carried out in the range 25 °C to 1200 °C using a TG-DSC analyser. The results showed that after the dehydration of the phosphogypsum to anhydrite the anhydrite converts to calcium sulphide via an intermediate compound, characterised by a mass loss of 11%. The average activation energy for the reduction of phosphogypsum with

graphite was determined using the Ozawa-Flynn-Wall- (OFW) and Kissinger-Akahira-Sunose (KAS) methods to be between 330-370 kJ/mol.

The reaction pathway for the thermal reduction of the phosphogypsum with graphite was studied using *in situ* Raman spectroscopy. The dehydration of the phosphogypsum to anhydrite was completed at about 142 °C. The dehydration was followed by the formation of the intermediate compound at about 900 °C. The intermediate compound, proposed to be a dehydrated Orschallite-type compound ($Ca_3[SO_4][SO_3]_2$), converted to CaS at about 1000 °C.

DEDICATION

To my mother

Lizzy Cetyiwe Msila

1927-2010

ACKNOWLEDGEMENTS

Deon Kotze (NECSA): Performed the radioactive nuclides analysis of phosphogypsum.

Benni Vilakazi (NECSA): Performed the TG-DSC analysis of the thermal reduction of phosphogypsum with graphite.

Pirow Engelbrecht (Sasol Technology): Performed the Anderson-Darling statistical analysis on the radioactive nuclides data.

Dr. Rudolf Erasmus (Wits University): Granted access to the laboratory that housed the Raman spectrometer.

Wiebke Grote (University of Pretoria): Performed some of the high temperature X-Ray powder diffraction analysis.

Sasol Management for sponsoring this work and allowing my frequent absence from work while carrying out these studies.

TABLE OF CONTENTS

ABSTRACT iii

DEDICATION v

ACKNOWLEDGEMENTS vi

LIST OF FIGURES x

LIST OF TABLES xii

DEFINITIONS xiii

LIST OF SYMBOLS xiv

CHAPTER 1 1

INTRODUCTION 1

1.1 Phosphoric acid production and phosphogypsum 1

1.2 Environmental concerns related to phosphate operations 3

1.3 Aims of the study 5

1.3.1 Evaluation of Phalaborwa phosphogypsum for use as building materials 5

1.3.2 Conversion of phosphogypsum to ammonium sulphate and precipitated calcium carbonate 5

1.3.3 Recovery of elemental sulphur from phosphogypsum 6

CHAPTER 2 9

GENERAL LITERATURE REVIEW 9

2.1 Radioactive nuclides in phosphogypsum – suitability for use as building material 9

2.1.1 Radioactive nuclides and their decay mechanism 9

2.1.2 Measurement of radioactivity 15

2.1.3 Radioactive nuclides in apatite ore 16

2.1.4 Radioactive nuclides in phosphogypsum 21

2.1.5 Impact of radioactive nuclides on human health 22

2.1.6 Decay rates equilibria 23
2.2 Conversion of phosphogypsum to ammonium sulphate and precipitated calcium carbonate 25
2.2.1 Ammonium sulphate and calcium carbonate applications 25
2.3 Sulphur recovery 26
2.3.1 Sulphur recovery from gypsum 26
2.4 Hypothesis formulation 26
2.4.1 Hypothesis 1 26
2.4.2 Hypothesis 2 26
2.4.3 Hypothesis 3 26
2.5 Analytical Techniques used 27
2.5.1 Raman spectroscopy 27
2.5.2 Inductively Coupled Plasma_Optical Emission Spectrometry 28
2.5.3 Gamma and neutron activation spectroscopy 28
2.5.4 Single particle optical sensor 29
CHAPTER 3 31
RADIOACTIVE NUCLIDES IN THE PHOSPHOGYPSUM FROM THE LOWVELD REGION OF SOUTH AFRICA – SUITABILITY FOR USE AS BUILDING MATERIAL 31
3.1 Introduction 31
3.2 Published Research Article: Radioactive nuclides 32
CHAPTER 4 52
CONVERSION OF PHOSPHOGYPSUM INTO AMMONIUM SULPHATE AND PRECIPITATED CALCIUM CARBONATE IN A MODIFIED MERSEBURG PROCESS 52
4.1 Introduction 52
4.2 Published Research Article: Modified Merseburg process 54
CHAPTER 5 75
THERMAL REDUCTION OF PHOSPHOGYPSUM TO CALCIUM SULPHIDE USING GRAPHITE 75
5.1 High temperature X-Ray powder diffraction 75
5.1.1 Gypsum dehydration 25-650 °C 77

5.2 Thermogravimetric analysis 82
5.3 In situ Raman spectroscopy 82
5.4 Research Article: TG kinetics 83
5.5 Published Research Article: Raman spectroscopy 100
CHAPTER 6 121
CONCLUSIONS AND RECOMMENDATION 121
6.1 Suitability of the Lowveld phosphogypsum for use in building materials 121
6.2 Conversion of the Lowveld phosphogypsum to ammonium sulphate and precipitated calcium carbonate 122
6.3 Thermal sulphate reduction of the Lowveld phosphogypsum using carbonaceous material to calcium sulphide 123
6.3.1 Reaction mechanism pathway 123
6.4 Recommended future research 125
6.4.1 Radioactive nuclides in phosphogypsum 125
6.4.2 Modified Merseburg process 125
6.4.3 Thermal reduction of phosphogypsum 125
Publications and papers under review 126
REFERENCES 127
Appendix A: Flynn – Wall – Ozawa method: Data for E_a calculation 136
Appendix B: Kissinger – Akahira – Sonuse method: Data for E_a calculation .. 137
Appendix C: High temperature X-Ray diffractometer set-up 138
Appendix D: Diffractogram of the Phalaborwa phosphogypsum 140
Appendix E: Diffractogram of the LAB_6 standard used for peak position verification of the X-Ray diffractometer 141
Appendix F: Diffractogram of phosphogypsum and graphite reaction mixture at temperature 25-1080 ºC under continuous nitrogen flow. ... 142
Appendix G: Gamma-ray spectrum of the grab sample from the pile 143

LIST OF FIGURES

Figure 1.1: The number of phosphate and phosphoric acid operations that are active the world (Abouzeid, 2008) 2

Figure 1.2: Aerial view of phosphate/phosphoric facilities showing alongside the stockpiles of phosphogypsum/Phosphate indicated with red arrows: (2a) Florida, USA; (2b) Louisiana, USA; (2c) Dorowa, Zimbabwe; (2d) Phalaborwa, South Africa 4

Figure 1.3: Gypsum - Ammonium Carbonate (Merseburg) process (reproduced from Alienov, 1998) 6

Figure 1.4: Averaged and the standard deviation of FOB prices of sulphur to Alberta, US West Coast, Houston, Nola Flora and Spot TAMPA for the period January 2003 – July 2013 (Source: InterChem) 7

Figure 2.1: Chart of radionuclides in a plot of Z versus N (www.nndc.bnl.gov/chart/) 11

Figure 2.2: Transition diagram for decay modes of a radioactive nuclide, with mass number A and atomic number Z (shown are α, β±, emissions, EC denotes electron capture). http://www2.lbl.gov/abc/ 13

Figure 2.3: The mechanism of γ radiation, the matter penetration ability by α, β and γ radiation. 15

Figure 2.4: Natural decay series of Uranium-238 showing the modes of decay (α = alpha; β =beta) and the half-lives of the daughter nuclides (Coles *et al.*, 1978) 18

Figure 2.5: Natural decay series of Uranium-235 showing the modes of decay (α = alpha; β =beta) and the half-lives of the daughter nuclides (Coles *et al.*, 1978) 19

Figure 2.6: Natural decay series of Thorium-232 showing the modes of decay (α = alpha; β =beta) and the half-lives of the daughter nuclides (Coles *et al.*, 1978). 20

Figure 2.7: Depiction of decay rates (A) of arbitrary parent nuclides N_1 and daughter nuclide N_2 and the state of secular equilibrium 24

Figure 2.8: Schematic diagram of a gamma spectrometer (https://tu-dresden.de) 29

Figure 2.9: Schematic diagram of the Auto dilution system of the Nicomp 780 Accusizer system 30

Figure 3.1: The calculated H_{ex}, H_{in}, I_{γ} and Ra_{eq} in the LSA phosphogypsum-error lines indicate the standard deviation 42

Figure 3.2: The ratio of activity concentrations for ^{238}U, ^{235}U, ^{232}Th and their progenies in the LSA phosphogypsum 44

Figure 3.3: Probability plots of activity concentrations of: (14a) U-238; (14b) U-235; (14c) Ra-228, (14d) Th-228, (14e) Ra-226 and (14f) Th-232 46
Figure 4.1: PFD of the Merseburg process with modification/omission highlighted in red 53
Figure 4.2: Temperature profile of ammonium carbonate formation in the original Merseburg; modified Merseburg and modified Merseburg and gypsum replaced with anhydrite 63
Figure 4.4: PSD of the Merseburg PCC 65
Figure 5.1: Reaction between gypsum and carbonaceous material 25-650 °C under nitrogen flow 78
Figure 5.3: Ball and stick model of Gypsum showing the water layer in the 010 plane 81
Figure 5.4: Thermographs of phosphogypsum reaction with graphite in molar ratios (PG:C) of 1:2, 1:3 and 1:4 89
Figure 5.7: Normalised mass loss for the reaction between phosphogypsum and graphite 92
Figure 5.8: First derivative of the thermographs of phosphogypsum reduction with graphite at heating rates 15, 20, 25 and 30 ºC/min; A indicates the dehydration of gypsum to hemihydrate and B indicates the formation of an intermediate compound 93
Figure 5.10: Plot according to Kissinger-Akahira-Sunose Method (KAS) 95
Figure 5.11: Activation energies calculated according to the OFW and KAS methods 96
Figure 5.12: Room temperature Raman spectrum of the carbonaceous materials before heating 108
Figure 5.13: Room temperature Raman spectrum of graphite heated under continuous N_2 flow to 1080 °C 108
Figure 5.14: First derivatives of the thermographs of phosphogypsum + carbonaceous material (1:3 molar ratio) 111
Figure 5.15: Raman spectrum of CaO 112
Figure 5.16: Raman spectra of graphite: gypsum reaction at 900 °C- black; 1000 °C - turquoise, 1080 °C (30min)-green & 1080 °C (60min)-red 113
Figure 5.17: Wire or sticks model of Orschallite ($Ca_3[SO_4][SO_3]_2 \cdot 12H_2O$) from Diamond crystal visualisation software [black - O^{2-}; green - Ca^{2+}; red - S^{4+}; blue - S^{6+}] 114

LIST OF TABLES

Table 1.1: Typical composition of phosphate ores (Gulbrandsen, 1966; Mar and Okazaki, 2012) 2

Table 2.1: Summary of the radioactive decay mechanism 14

Table 2.2: Activity concentrations in the process material of the phosphate plant in the Lowveld of South Africa (van der Westhuizen, 2004) 16

Table 2.3: K-40, Th-232 and Ra-226 concentrations in phosphogypsum from countries other than South Africa 21

Table 2.4: Concentration of Radium-226 [C_{Ra}], Thorium-232 [C_{Th}] and Potassium-40 [C_K] and calculated Radium Equivalent [Ra_{eq}] in building bricks from countries other than South Africa 22

Table 3.1: Activity concentrations of ^{40}K, ^{232}Th and ^{226}Ra in phosphogypsum from countries other than RSA 34

Table 3.2: Activity concentrations of the radioactive nuclide the LSA phosphogypsum 39

Table 3.3: Activity concentrations of ^{40}K, ^{232}Th and ^{226}Ra in building bricks from other countries 40

Table 3.4: The scenarios of use for building materials 42

Table 4.1: Experimental conditions and materials for Merseburg process ... 59

Table 4.2: The main ICP_OES conditions for measurement of metals in phosphogypsum 60

Table 4.3: The NICOMP Accusizer 780 settings 60

Table 4.4: Bruker Raman spectrometer settings 61

Table 4.5: ICP analysis of the phosphogypsum and the modified Merseburg process products 69

Table 5.1: The review of studies on thermal dehydration of $CaSO_4.xH_2O$ over the period 1964 to 2009 75

Table 5.2: Experimental setting for kinetic studies 88

Table 5.3: Band positions (cm^{-1}) for phosphogypsum before and after heating to 1080 °C and assignments 106

DEFINITIONS

Absorbed dose: total energy absorbed from ionizing radiation per mass of the absorber. Gray (Gy) =1 J/kg = 100 rad.

Dose equivalent: measure of the biological health risk, absorbed dose x Quality factor: Sieverts (Sv) = 100 rem, where the quality factor is used to modify the absorbed dose by multiplying to obtain a quantity called the equivalent dose. It is used because some types of radiation, such as α particles, are more biologically damaging internally than other types such as the β particles. The factor is determined by the US Nuclear Regulatory Commission (NRC) and is the same basic quantity as the radiation weighting factor as defined by the International Commission on Radiological Protection.

Electron capture is one process that unstable atoms can use to become more stable. During **electron capture**, an **electron** in an atom's inner shell is drawn into the nucleus where it combines with a proton, forming a neutron and a neutrino. The neutrino is ejected from the atom's nucleus.

Grab sampling is a sampling technique which is a single sample or measurement taken at a specific time or over as short a period, as feasible. Grab samples provide an immediate sample, and are thus preferred for some tests.

Radiation exposure: amount of ionizing radiation that produces 2.58 Coulombs per cm^3 of STP air Roentgen (R)

Radioactivity: a measure of the number of nuclear disintegrations per second: 1 Becquerel (Bq) = 1 disintegration / second; One Curie = 3.7×10^{10} Bq.

LIST OF SYMBOLS

σ- Alpha

β- Beta

γ - Gamma

λ- Activity

Γ - Irreducible representation

CHAPTER 1

INTRODUCTION

1.1 Phosphoric acid production and phosphogypsum

Phosphate ore is available in abundance on earth and there are over fifty phosphate processing operations in the world. Ten of these operations are in Africa and one of these is in the Lowveld region of South Africa as shown in Figure 1.1.

The wet process of phosphoric acid production involves the digestion of fluoro-apatite ore ($Ca_{10}(PO_4)_6F_2$) with sulphuric acid (H_2SO_4) as described by Equation 1.1 (Al-Jundi *et al.*, 2008; Pereira and Bilal, 2012). The phosphoric acid production also produces hydrogen fluoride (HF) as a by-product. Aluminium silicate (Al_2SiO_5) and caustic soda (NaOH) are added, followed by a flocculent for the removal of the fluorides in the phosphoric acid. The settled coagulated solids are removed from phosphoric acid by filtration.

Equation 1.1 also shows that along with each ton of phosphoric acid (H_3PO_4) produced, 1.7 tons of calcium sulphate dihydrate ($CaSO_4.2H_2O$), commonly known as gypsum or specifically phosphogypsum, is produced as a by-product.

$$Ca_{10}(PO_4)_6F_2 + 10H_2SO_4 + 20H_2O \rightarrow 10CaSO_4 \cdot {}^{1}\!/\!_{2}\, H_2O + 6H_3PO_4 + 2HF \quad \ldots(1.1)$$

Each year approximately 550 kilotons of phosphogypsum are generated as a by-product. The phosphogypsum is stored in waste stacks alongside the phosphoric acid manufacturing facility.

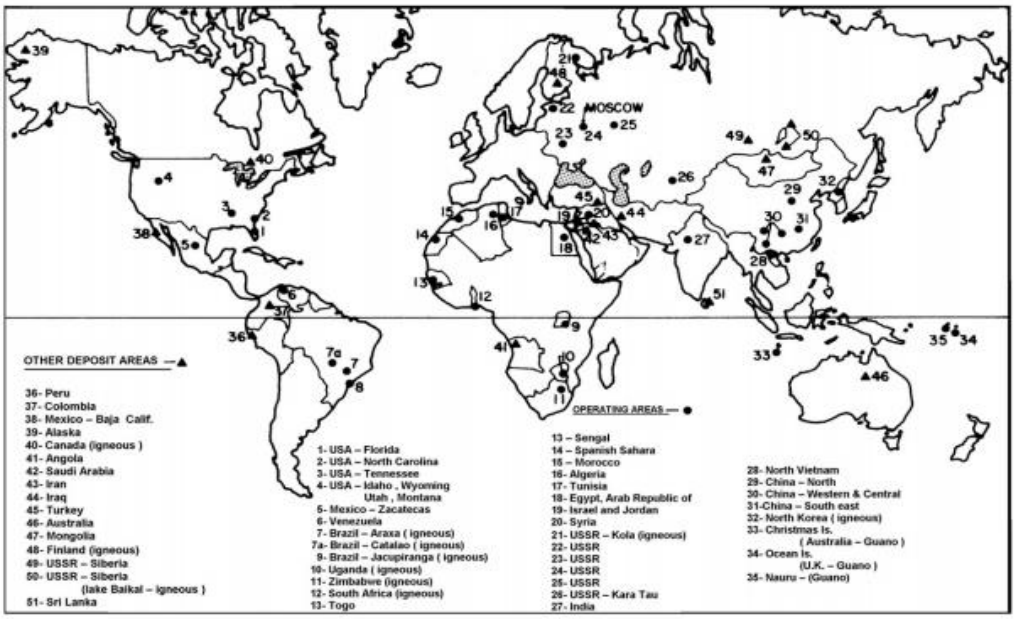


Figure 1.1: The number of phosphate and phosphoric acid operations that are active the world (Abouzeid, 2008)

A typical composition of phosphate ores is shown in Table 1.1. Appreciable amounts of the metal impurities (Si, Al, Fe, Mg, Na, K, Ti, S, F and Cl are expected to be present in both the phosphoric acid and the phosphogypsum.

Table 1.1: Typical composition of phosphate ores (Gulbrandsen, 1966; Mar and Okazaki, 2012)

Element oxides	Typical XRF results
SiO_2	0.8 - 36.5
Al_2O_3	1.7 - 8.2
Fe_2O_3	0.3 - 6.4
MgO	0.3 - 2.2
CaO	44.0 - 71.0
Na_2O	0.2 - 2.2
K_2O	0.0 - 1.2
TiO_2	0.0 - 0.5
P_2O_5	6.1 -33.6
SO_3	0.2 - 1.1
F	3·1
Cl	0.0 - 0.2
organic matter	2·1
Uranium averages	0·009

1.2 Environmental concerns related to phosphate operations

The mining and processing of phosphate rock, all over the world, is usually associated with stockpiles of phosphogypsum and other phosphate waste. Figure 1.2 shows some examples from (2a) Louisiana – USA, (2b) Florida – USA, (2c) Dorowa – Zimbabwe and (2d) Phalaborwa – SA. The excess water from the phosphogypsum stacks in Phalaborwa is pumped back into the phosphoric acid plant for reuse but there exists a possibility for some acidic water and sulphate (SO_4^{2-}) to leach into the ground water and surrounding aquatic systems. The aerial view of Phalaborwa in Figure 1.2d shows the natural water stream Ga-Selati River that runs along the phosphoric acid production complex into the Oliphants River. The Oliphants River runs through a major nature reserve, the Kruger National Park, and is a source of drinking water to wildlife in this reserve. Although sulphates are not toxic in low concentrations, at very high aqueous concentrations sulphates have been reported to have adverse health impacts on animals. At a concentration of about 1200 mg/l in water SO_4^{2-} causes a significant but clinically mild increase in stool mass in adult humans (Heizer, 1997).



Figure 1.2: Aerial view of phosphate/phosphoric facilities showing alongside the stockpiles of phosphogypsum/Phosphate indicated with red arrows: (2a) Florida, USA; (2b) Louisiana, USA; (2c) Dorowa, Zimbabwe; (2d) Phalaborwa, South Africa

The concentration of sulphates is restricted to 500 mg/l SO_4^{-2} in ground water and 2000 mg/l SO_4^{-2} in industrial effluents (Wagner and van Niekerk, 1987). There is agreement in the reports by Loneragan *et al*., (2001) and Cammack *et al*., (2010) that high levels of sulphate in water result in reduced water intake by animal feedlots and affect the quality of their carcasses. However, the concentrations reported by these authors where the adverse effects were experienced are different. Loneragan *et al.*, (2001) observed the adverse effect on animals that drank water with concentrations of SO_4^{2-} > 500 mg/l, where Cammack *et al*., carried out a controlled study and reported the concentration of 1200 mg/l.

1.3 Aims of the study

The aim of this study is to investigate ways of utilising the Phalaborwa phosphogypsum by means of value addition, either by converting it to materials of industrial, economic or social benefit such as building materials, ammonium sulphate, and calcium carbonate or by converting it to elemental sulphur.

1.3.1 Evaluation of Phalaborwa phosphogypsum for use as building materials

This study evaluates the suitability of the phosphogypsum from Phalaborwa, South Africa for the manufacturing of building materials such as bricks, boards etc. with reference to (i) the South African Nuclear Regulation Act 47 of 1999 of South Africa and its regulations and (ii) the associated risks of radioactivity as quantified in terms of: radium equivalent (Ra_{eq}), internal and external hazard indices (H_{in} and H_{ex}), and concentration index (I_{γ}), and these will be evaluated against the international guidelines. The outcome of this study is published in the article: Msila X, Labuschagne F, Barnard W, Billing, DG (2016) Radioactive nuclides in phosphogypsum from the Lowveld region of South Africa. *South Africa Journal of Science*, vol. 112, no. 1, pp 98-102. http://dx.doi.org/10.17159/sajs.2016/20150102. The article forms the basis of Chapter 3 of this Thesis.

1.3.2 Conversion of phosphogypsum to ammonium sulphate and precipitated calcium carbonate

This study evaluates the technical feasibility of converting the Phalaborwa phosphogypsum ($CaSO_4.2H_2O$) into ammonium sulphate ($(NH_4)_2SO_4$) and precipitated calcium carbonate ($CaCO_3$) in a Merseburg process that has been modified by omitting the carbon dioxide (CO_2) absorption towers

(C16 and C17 in Figure 1.3) and instead forming the ammonium carbonate ($(NH_4)_2CO_3$) in the gypsum ($CaSO_4.2H_2O$) convertor.. The outcome of this study is published in the article: Msila X, Billing D, Barnard W (2016) Capture and storage of CO_2 in phosphogypsum – the modified Merseburg process. *Clean Technology and Environment Policy.* Published online 26/03/2016, DOI: 10.1007/s10098-016-1157-4. The article forms the basis of Chapter 4 of this Thesis.

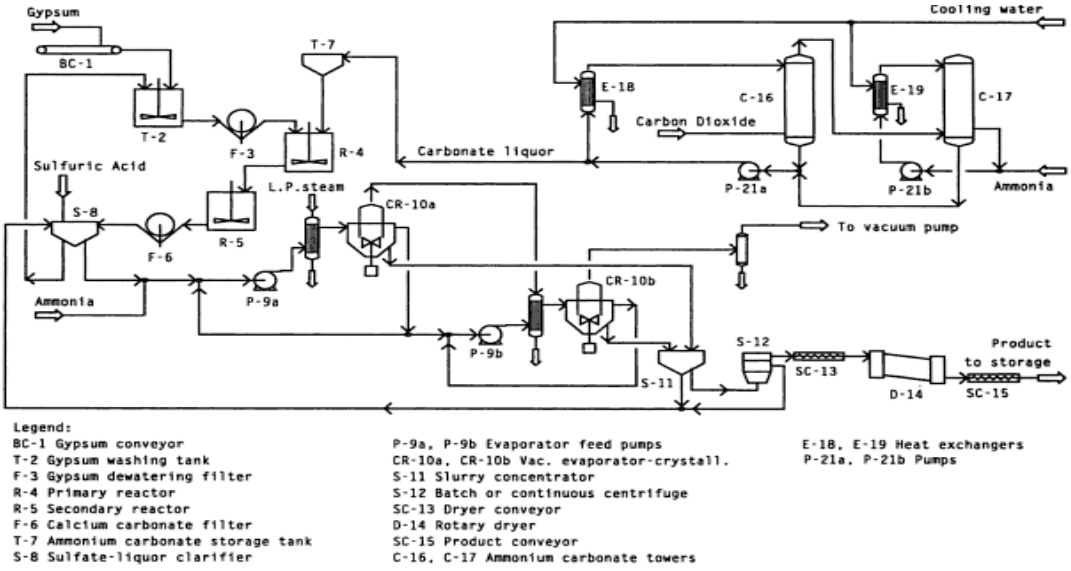


Figure 1.3: Gypsum - Ammonium Carbonate (Merseburg) process (reproduced from Alienov, 1998)

1.3.3 Recovery of elemental sulphur from phosphogypsum

The African continent is a major importer of sulphur (Ratlabala, 2003). Countries like Zambia and the Democratic Republic of Congo (DRC) import large tonnages of sulphur at a high cost to manufacture sulphuric acid for the reduction of oxidised ores such as in the production of phosphoric acid. Over 95% of phosphate production is consumed in fertilizers (Abouzeid, 2008)

South Africa alone by 2009 had imported 1.5 million tons of sulphur per year from the Middle East and Canada (Mokaila, 2003). The demand for sulphur is also expected to increase in line with increased fertiliser usage.

Sulphur is cheap but the costs are inflated by the cost of transportation. Figure 1.4 shows the average free on board (FOB) prices of sulphur as delivered to Alberta (Canada), US West Coast, Houston, Nola Flora (New Orleans) and a spot price in Tampa (Florida). The error bars indicate the standard deviation between the average prices. The unpredictability of the increase in the sulphur price such as that experienced in 2008 poses a serious risk to the production of phosphoric acid and as a result to the fertilizer industry, the major consumer of phosphoric acid. For this reason the fertilizer industry has a vested interest in alternative sources of sulphur. One possible source of sulphur is the sulphate thermal reduction followed by sulphide stripping and elemental sulphur production through the PIPco or Iron process.

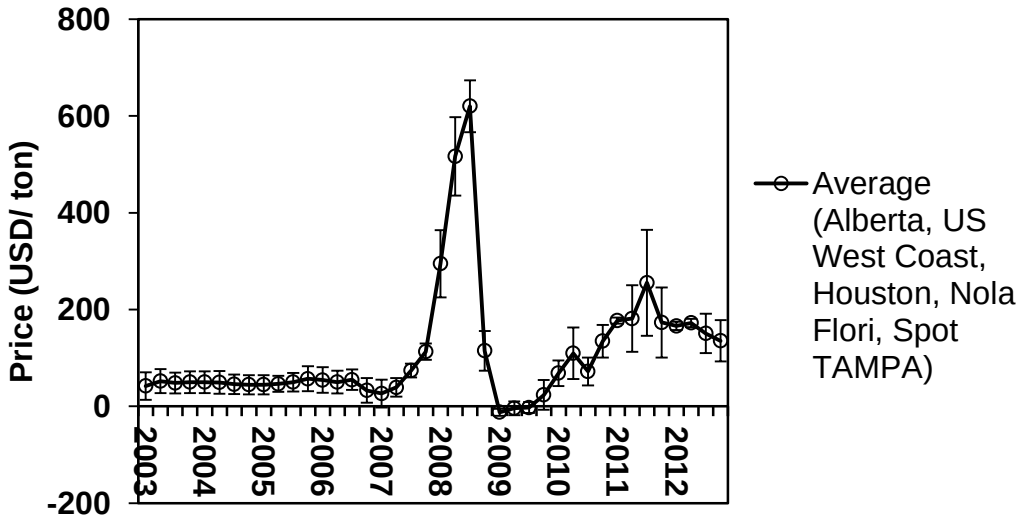


Figure 1.4: Averaged and the standard deviation of FOB prices of sulphur to Alberta, US West Coast, Houston, Nola Flora and Spot TAMPA for the period January 2003 – July 2013 (Source: InterChem)

This study will focus on probing the reaction mechanism pathway and the kinetics of the reduction of phosphogypsum to calcium sulphide (CaS)

using graphite. The CaS can be converted to precipitated calcium carbonate and hydrogen sulphide (H_2S) as shown in Equation 1.3. The H_2S can be converted to elemental sulphur in variety of processes such as: The traditional Claus process in Equation 1.4; The two step PIPco process (Ray *et al*., 1990) as described by Equations 1.5 – 1.6.

$$CaS(s) + H_2O(l) + CO_2(g) \rightarrow CaCO_3(s) + H_2S(g) \quad \text{(1.3)}$$

$$2H_2S(g) + SO_2(g) \rightarrow 3S(s) + 2H_2O(l) \quad \text{(1.4)}$$

$$H_2S(g) + \tfrac{1}{2}O_2(g) \rightarrow SO_2(g) + H_2O(g) \quad \text{(1.5)}$$

$$2H_2S(g) + SO_2(g) \rightarrow 2H_2O(l) + 3S(s) \quad \text{(1.6)}$$

The outcome of the study is published in the articles: (a) Msila X, Barnard W, Billing DG (2015) Raman spectroscopic study of the thermal reduction of phosphogypsum with a carbonaceous material. *Spectrochimica Acta Part A: Molecular and Biomolecular Spectroscopy*, pp 317-322, DOI: 10.1016/j.saa.2015.04.017 (b) Msila X, Barnard W, Billing D (2016) TG-DSC kinetics study of phosphogypsum reduction with graphite. *Journal of thermal analysis and calorimetry*. (In review). These two papers form the basis of Chapter 5 of this Thesis

CHAPTER 2

GENERAL LITERATURE REVIEW

2.1 Radioactive nuclides in phosphogypsum – suitability for use as building material

2.1.1 Radioactive nuclides and their decay mechanism

An atom is characterised by the positive charge (Z_e) in its nucleus and the atomic mass. The number of protons (Z) in the nucleus is known as the atomic number and it determines the element's identity. The nucleus also contains a varying number of neutrally charged particles called neutrons (N) with a similar mass to protons. The mass number (A) of an element is the sum of the number of protons and the number of neutrons (Z+N). An arbitrary element (X) can therefore be represented as:

$$^{A}_{Z}X_{N}$$

The N is usually omitted in the nomenclature and the oxygen atom is represented as: $^{16}_{8}O$

For elements with less than 20 protons (Z < 20) the number of protons and neutrons is approximately the same. For Z > 20 the nucleus tends to be neutron-rich as is shown by the deviation from the line Z=N in Figure 2.1. The energy released by combining the neutrons and the protons to make the nucleus is called the binding energy. The binding energy therefore increases more and more at Z > 20. These elements with a

large number of protons will tend to be unstable due to the higher Coulombic repulsion force between protons caused by high packing density.

The nuclei with a higher number of protons tend to release energy and particles (decay) in order to form new nuclides in the energy stable zone indicated by the black colour in Figure 2.1. The modes of decay are alpha (α), beta (β) and spontaneous fission. The nuclei with N > 150 tend to decay by spontaneous fission i.e. splitting of heavy nuclide to two nuclei of approximately the same mass number (A). The different colours in the radionuclide charts indicate the different modes of decays.

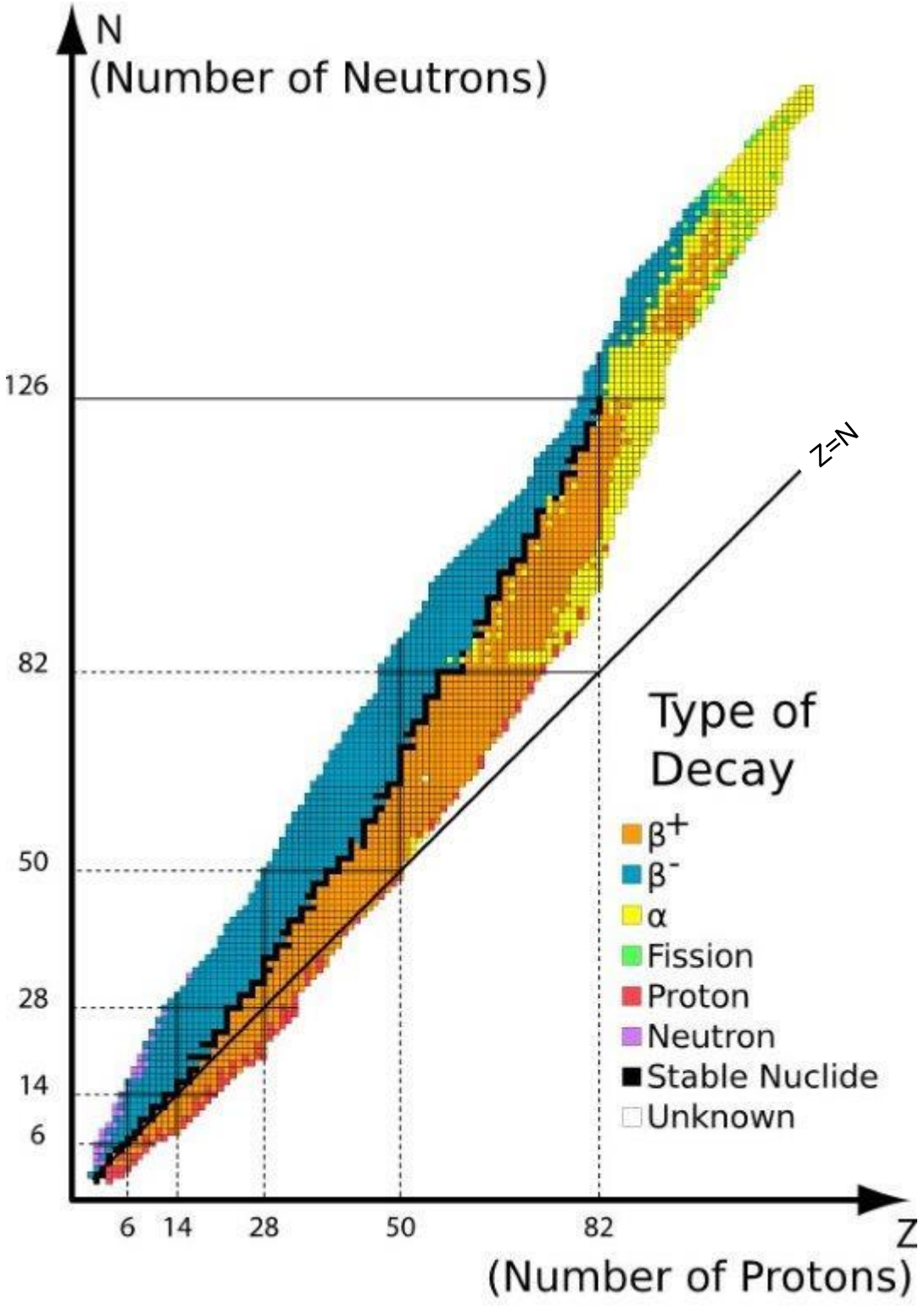


Figure 2.1: Chart of radionuclides in a plot of Z versus N (www.nndc.bnl.gov/chart/)

The nuclei of N > 83 tend to decay by alpha (α) emission. The alpha decay mechanism can be expressed as shown in Equation 2.1:

$$ {}^{A}_{Z}X \rightarrow {}^{A-4}_{Z-2}Y + \alpha + Q \quad \text{.....(2.1)} $$

where Q is the energy released by the decay process, and alpha is a particle equivalent to a ${}^{4}_{2}He$ nucleus.

Unstable nuclei can also undergo negative beta decay as shown in Equation 2.2:

$$ {}^{A}_{Z}X \rightarrow {}^{A}_{Z+1}Y + \beta^{-} + \bar{\nu} + Q_{\beta^-} \quad \text{.....(2.2)} $$

OR

positive beta decay as in Equation 2.3.

$$ {}^{A}_{Z}X \rightarrow {}^{A}_{Z-1}Y + \beta^{+} + \nu + Q_{\beta^+} \quad \text{.....(2.3)} $$

where $Q_{\beta+}$ and $Q_{\beta-}$ represent the energy release during the beta (β) decay, ν represents neutrino and $\bar{\nu}$ represents antineutrino

OR

electron capture where an electron in an orbital close to the nucleus reacts with a proton to form a neutron. The alpha, beta and spontaneous fission mechanism can leave the nucleus excited and the excited nucleus can release the energy by emitting gamma-ray (γ). Figure 2.2 depicts the mechanism of decay from the parent nucleus ${}^{A}_{Z}X$ into different daughter nuclei.

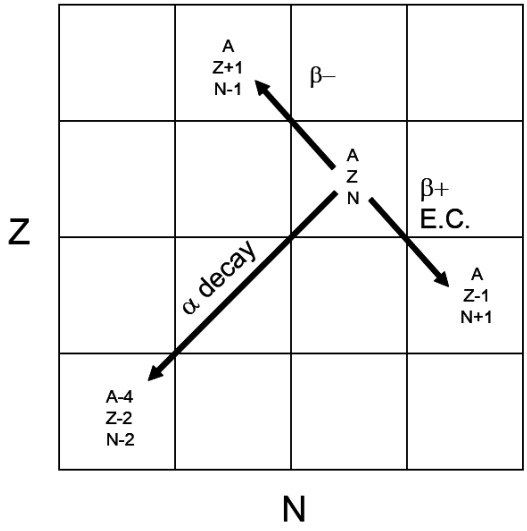


Figure 2.2: Transition diagram for decay modes of a radioactive nuclide, with mass number A and atomic number Z (shown are α, β±, emissions, EC denotes electron capture). http://www2.lbl.gov/abc/

Table 2.1 summarises the various decay mechanisms, the forms of energy, particle or photon released by each mechanism type. The gamma (γ) decay is a massless photon that has the ability to penetrate human tissue and is classified as indirect ionising radiation. An example is given in Figure 2.3 where the barium nucleus emits the gamma ray to result in an energetically stable nucleus. (http://www.epa.gov/radiation .accessed on 4.12.2015)

Table 2.1: Summary of the radioactive decay mechanism

Decay Type	Emitted Particle	ΔZ	ΔA	Occurrence
Alpha (α)	$^{4}_{2}He^{2+}$	-2	-4	N>83
Beta (β)	Energetic e^{+}, γ	+1	0	$m[^{A}Z] > m[^{A}(Z+1)] + m[^{0}_{-1}e^{-}]$ (Parent nucleus) > (Daughter nucleus) + (electron)
Proton Emission	Energetic e^{-}, γ	-1	0	$m[^{A}Z] > m[^{A}(Z-1)] + m[^{0}_{+1}e^{+}]$ (Parent nucleus) > (Daughter nucleus) + (positron)
Electron capture	ν	-1	0	$m[^{A}Z] + m[^{0}_{-1}e^{-}] > m[^{A}(Z-1)]$ (Parent nucleus) + (electron) > (Daughter nucleus)
Gamma (γ)	Photon	0	0	Any excited nucleus

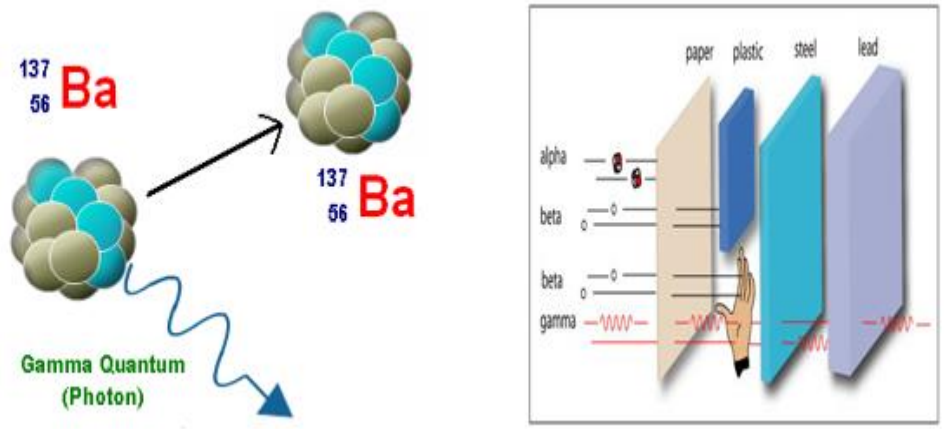


Figure 2.3: The mechanism of γ radiation, the matter penetration ability by α, β and γ radiation.

2.1.2 Measurement of radioactivity

The specific activity (Bq/kg) of the radionuclides is measured with a gamma-ray spectrometer fitted with a photon counter. The activity per mass unit for each radionuclide detected is calculated using Equation 2.4.

$$A_{Ei} = {}^{N_{Ei}}\!\!\diagup\!\!_{(\varepsilon_E \times t \times \gamma_d \times M_s)} \quad \text{.....(2.4)}$$

where N_{Ei} is the Net Peak Area of a peak at energy E,

ε_E is the detection efficiency at energy E,

t is the counting time,

γ_d is the number of gammas per disintegration of this nuclide for a transition at energy E, and M_s is the mass in kg of the measured sample.

The standard international units of measure for number of decays per second or activity is the Becquerel (Bq) named after the discoverer of radioactivity, Henri Becquerel (Genet, 1995). The alternative units are Curie after Pierre and Marie Curie (Curie, 1904 and Curie, 1911).

2.1.3 Radioactive nuclides in apatite ore

Worldwide average radionuclide activity concentrations in the earth's crust are about: 40 Bq/kg of radium; 40 Bq/kg of thorium; and 400 Bq/kg of potassium (ECRP, 1999). Uranium, thorium and their daughter products exist in apatite ores of sedimentary origin (El-Taher and Makhluf, 2010; Pereira and Bilal, 2012) in concentrations above earth crust averages. The radioactive nuclides in the phosphate process material in the Lowveld and the results are given in Table 2.2.

Table 2.2: Activity concentrations in the process material of the phosphate plant in the Lowveld of South Africa (van der Westhuizen, 2004)

Radioactive nuclide	Activity concentration (Bq/kg)	
	Phosphate rock	Tailings
^{238}U	140	260
^{226}Ra	140	270
^{210}Pb	120	Not reported
^{232}Th	470	310
^{228}Ra	550	330
^{228}Th	550	350

Uranium, radium and thorium occur in three natural decay series headed by uranium-238; uranium-235 and thorium-232 (Garcia-Talavera *et al*., 2001; van der Westhuizen, 2004). The radionuclides formed from the

uranium-238; uranium-235 and thorium-232 decay series. The mode of decay and their half-lives are shown in Figures 2.4 to 2.6.

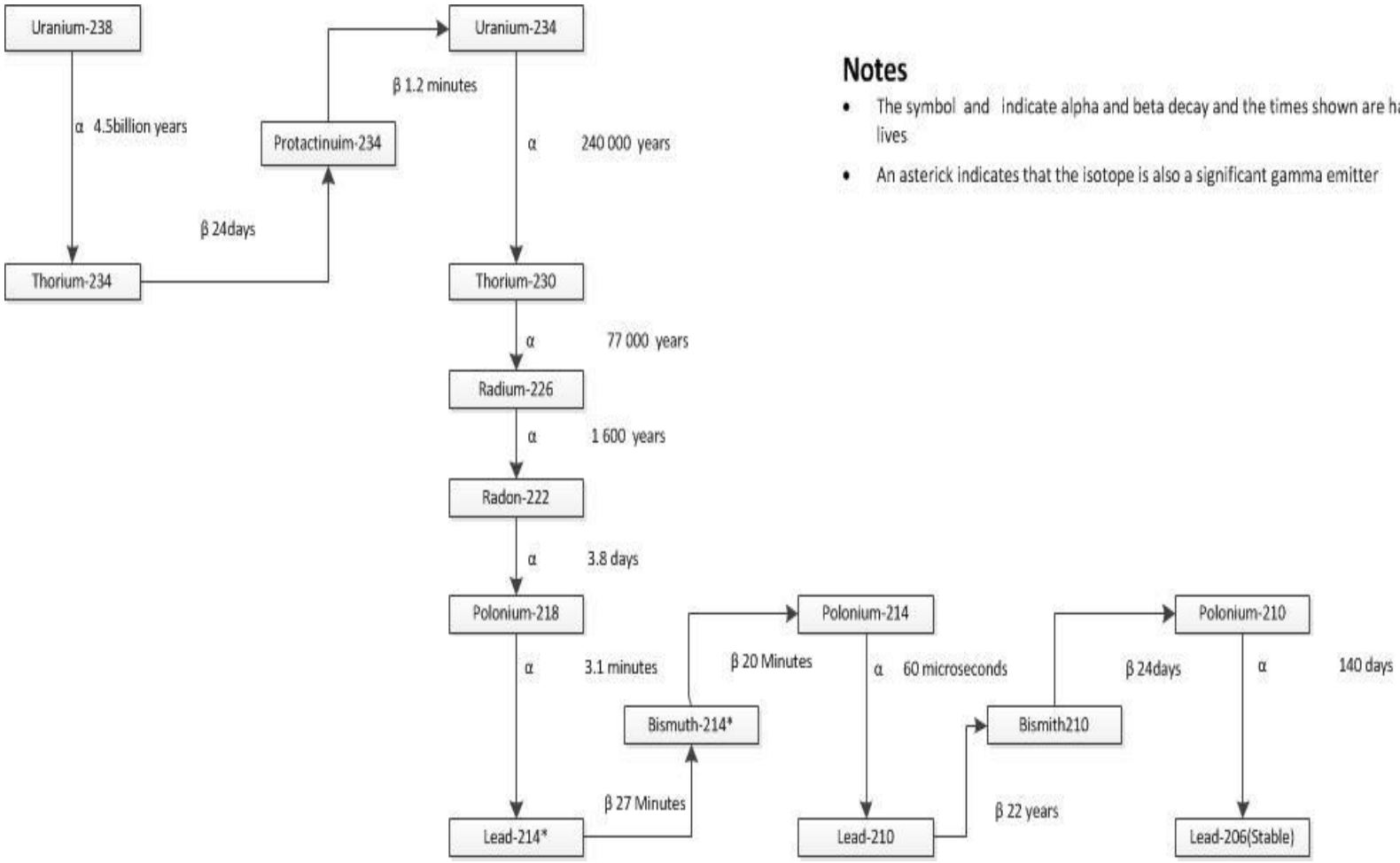


Figure 2.4: Natural decay series of Uranium-238 showing the modes of decay (α = alpha; β =beta) and the half-lives of the daughter nuclides (Coles *et al.*, 1978)

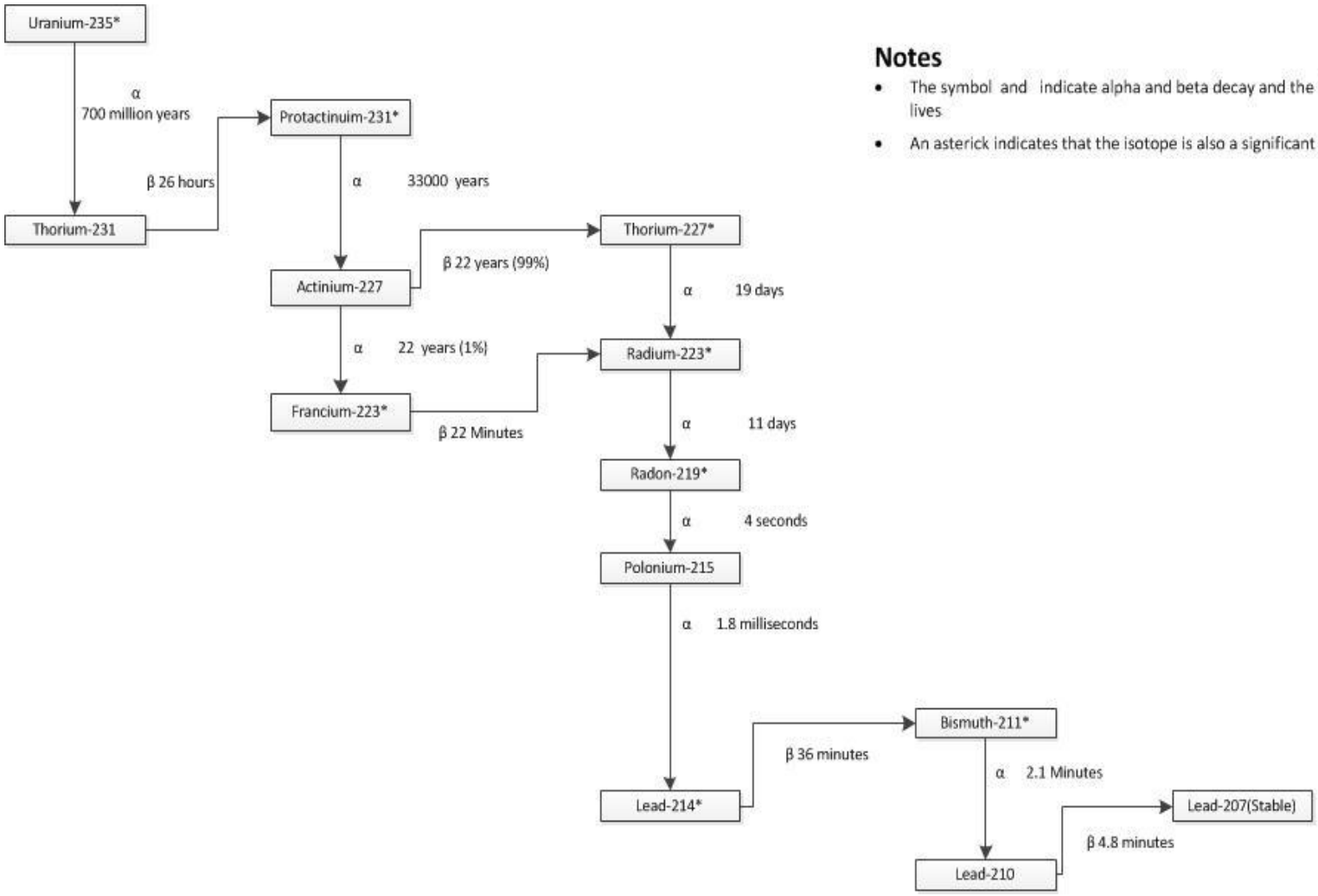


Figure 2.5: Natural decay series of Uranium-235 showing the modes of decay (α = alpha; β =beta) and the half-lives of the daughter nuclides (Coles *et al.*, 1978)

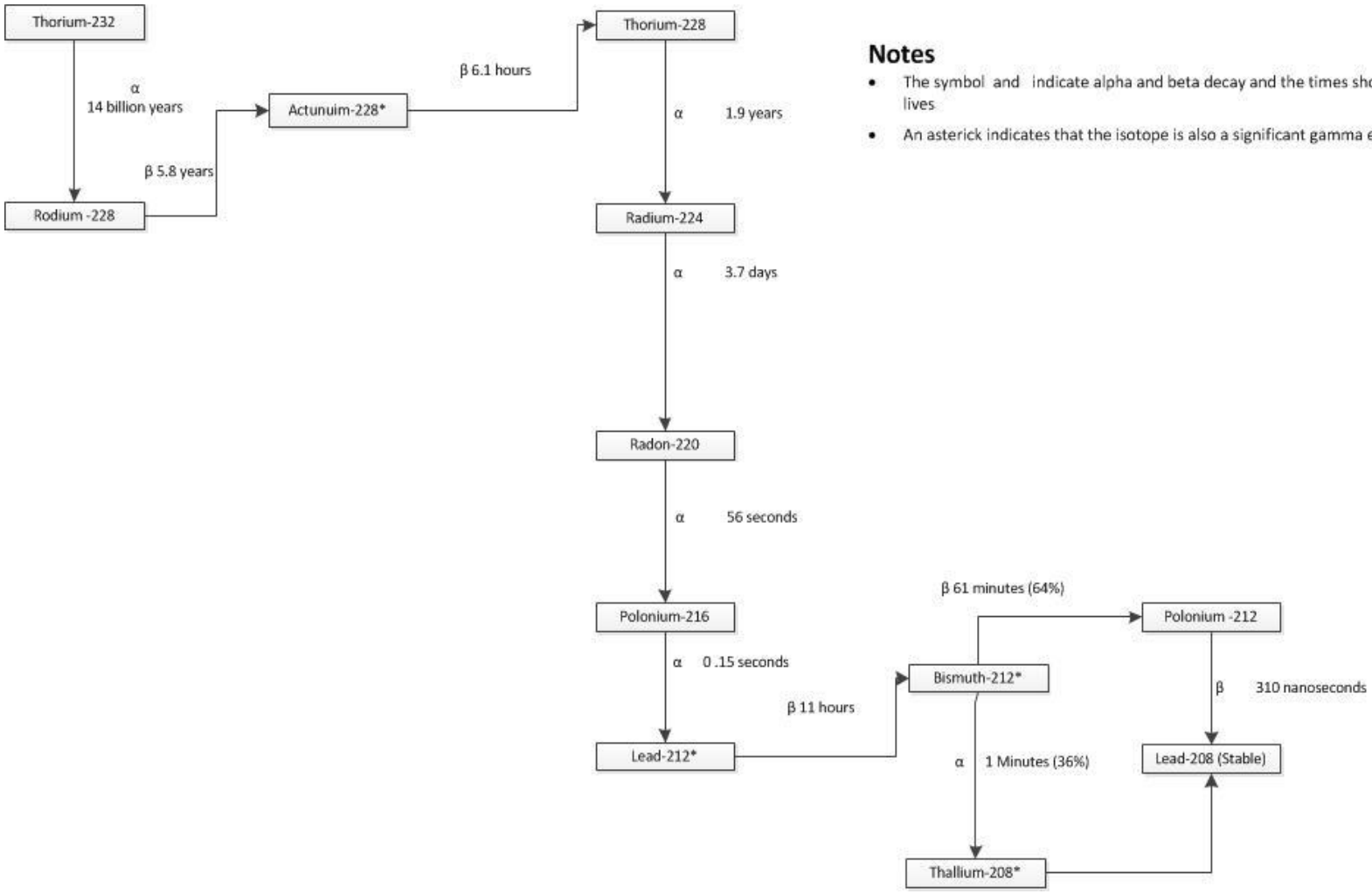


Figure 2.6: Natural decay series of Thorium-232 showing the modes of decay (α = alpha; β =beta) and the half-lives of the daughter nuclides (Coles *et al.*, 1978).

The progenies of radionuclides in Figures 2.4-2.6 are therefore also present in the apatite ore in appreciable concentrations depending on the age of the ore and their respective half-lives.

2.1.4 Radioactive nuclides in phosphogypsum

Although part of the radionuclides from the ore ends up in the phosphate fertilisers (Pfister *et al.,* 1976), phosphogypsum generated from the processing of apatite ore contains appreciable activity concentrations of these radionuclides: uranium-235, uranium-238 and thorium-232 and their natural decay products (Balakrishnan *et al.*, 2012; Dias *et al.*, 2010). Radioactive nuclide concentrations and the calculated radium equivalent values in phosphogypsum from countries other than South Africa are listed in Table 2.2. The term radium equivalent reported in the right-most column of Table 2.2 is described and discussed in detail in Chapter 3.

Table 2.3: ^{40}K, ^{232}Th and ^{226}Ra concentrations in phosphogypsum from countries other than South Africa

Country	Number of samples	^{40}K	^{232}Th	^{226}Ra	Ra_{eq}	Reference
		(Bq/kg)				
Jordan	15	40	-	376	-	Al-Jundi *et al.*, 2008
Serbia	-	8.7	8.7	439	452	Rajkovic and Toskovic, 2002
Egypt	-	-	-	-	439	Hussein, 1994

(- indicates not reported)

When phosphogypsum is considered for use as a building material, regional regulatory controls of radioactive materials should be taken into

consideration as a measure of radiation exposure or potential exposure to inhabitants. In the case of South Africa it must be tested against the requirements of the South African Nuclear Regulation Act 47 of 1999 of South Africa and its regulations. There are several other indices that are internationally recognised for hazard quantification of radioactive nuclides contained in building materials. Several studies, done in different countries, show that the building materials such as bricks contain appreciable concentrations of radioactive nuclides. Some of the findings are listed in Table 2.3.

Table 2.4: Concentration of Radium-226 [C_{Ra}], Thorium-232 [C_{Th}] and Potassium-40 [C_K] and calculated Radium Equivalent [Ra_{eq}] in building bricks from countries other than South Africa

Country	Number of Sample	C_{Ra}	C_{Th}	C_K	Ra_{eq}	Reference
		Bq/kg				
Norway	6	104	62	1058	276	Stranden, 1976
Greece	6	49	24	670	135	Papastefanou *et al*., 1983
Australia	25	41	89	681	220	Beretka & Mathew,1985
Netherlands	14	39	41	560	141	Ackers *et al*., 1985
Egypt	1	20	14	204	56	El-Thaway & Higgy, 1995
India	1	48	52	381	152	Kumar *et al*., 1999
Sri Lanka	24	35	72	585	183	Hewamanna *et al*., 2001
India	-	18	19	238	46	Ravisankar *et al*., 2011
India	-	47	20	349	114	Viruthagiri *et al*., 2011

(- indicates not reported)

2.1.5 Impact of radioactive nuclides on human health

Ghissassi *et al.* (2009) described the health effect of radiation to humans in the review study in the following manner:

"*Alpha (α) particles, consisting of two protons and two neutrons, are an ionising type of radiation with low capacity to penetrate living tissue (less than 0.1 mm). Beta (β) particles are electrons or positrons that are less ionising, but more penetrating (up to a few millimetres)….." "….. Epidemiological evidence shows a number of radionuclides that emit alpha (α) or beta (β) particles increase cancer risks at several anatomical sites. Radon exposure occurs mainly through contamination of indoor air by radon released from soil and building materials. Combined analyses of case-control studies now estimate that residential exposure to radon gas is the leading cause of lung cancer after tobacco smoke (8-15% attributable risk in Europe and North America).*"

The presence of Ra-226 in phosphogypsum is of particular importance since it directly decays to Rn-222. The Rn-222 is a gas with a half-life of 3.8 days. It decays via alpha which gives.

2.1.6 Decay rates equilibria

As the radioactive nuclides decay their concentration decreases at the rate determined by their decay kinetics and is described by Equation 2.5.

$$-\left(dN/dt\right) = \lambda_1 N_1 \quad \text{.....(2.5)}$$

where λ is the decay constant of a specific radio nuclide in s^{-1} and N is the number of the radionuclide atoms. The activity concentration of the radionuclide N is given by Equation 2.6.

$$Activity\,(A) = -\left(dN/dt\right) = \lambda N \quad \text{..... (2.6)}$$

The integral of Equation 2.6 is described by Equation 2.7

$$\int dN/N = \lambda \int dt \quad \text{..... (2.7)}$$

And therefore:

$$\ln N = -\lambda t + c \quad \text{..... (2.8)}$$

The concentration of the daughter radionuclides increases at the same rate of parent decay. But if the daughter radionuclide is also unstable it also decays. The state when the rate (Λ) of parent and daughter radionuclide decays is the same is referred to as secular equilibrium. The state of secular equilibrium requires that the parent radionuclides have a much longer half-life than the daughter radionuclide. The state of secular equilibrium for arbitrary radioactive nuclides N_1 and N_2 can be represented as in Figure 2.7.

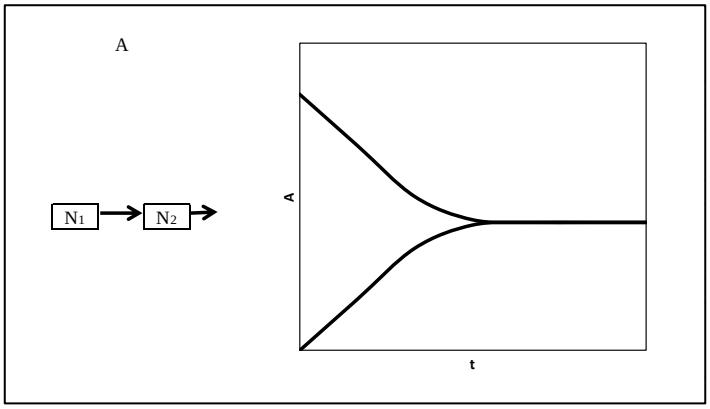


Figure 2.7: Depiction of decay rates (A) of arbitrary parent nuclides N_1 and daughter nuclide N_2 and the state of secular equilibrium

Expressed mathematically, if N_1 is the concentration of the parent radioactive nuclides and N_2 is the daughter concentration:

$$\partial N_2 / \partial t = \lambda_1 N1 - \lambda_2 N_2 \quad \text{.....(2.9)}$$

And secular equilibrium is where

$$\partial N_2 / \partial t = 0 \quad \text{.....(2.10)}$$

in natural ores are in a state of secular equilibrium the equilibrium can be disturbed when the ores are mined and processed. The disturbance of secular equilibrium can result in the partitioning of the parent and/or daughter radioactive nuclide concentrations into the product(s) or by-products of the process as reported by Al-Jundi *et al.*, 2008.

2.2 Conversion of phosphogypsum to ammonium sulphate and precipitated calcium carbonate

2.2.1 Ammonium sulphate and calcium carbonate applications

The phosphogypsum can be converted to the saleable products: ammonium sulphate and precipitated calcium carbonate using ammonium hydroxide. The details of the process of conversion are covered in section 4.1 and the application of ammonium sulphate and calcium carbonate are covered in sections 4.1.1 to 4.1.3.

2.3 Sulphur recovery

2.3.1 Sulphur recovery from gypsum

Sulphur recovery from gypsum proceeds by thermal reduction via the formation of calcium sulphide, followed by sulphide stripping with carbon dioxide and finally the production of elemental sulphur in the PIPco or Iron processes (Nengovhela, 2008).

2.4 Hypothesis formulation

2.4.1 Hypothesis 1

Phosphogypsum from Phalaborwa, South Africa contains low levels of radioactive nuclides and therefore can be exempted from regulation control in South Africa. The phosphogypsum also has sufficiently low levels of radioactive nuclide and is suitable for use in building materials.

2.4.2 Hypothesis 2

Phalaborwa phosphogypsum can be consumed in large quantities by converting it to high value ammonium sulphate and precipitated calcium carbonate in a modified Merseburg process.

2.4.3 Hypothesis 3

The reduction of gypsum is preceded by dehydration to a soluble anhydrite that converts to an intermediate compound before the final transformation to calcium sulphide. This hypothesis will be tested by following the reaction pathway from gypsum dehydration to gypsum reduction using High Temperature X-ray Powder Diffraction, Thermogravimetric analysis, and *in situ* Raman spectroscopy.

2.5 Analytical Techniques used

2.5.1 Raman spectroscopy

2.5.1.1 Classical theory of Raman spectroscopy

The polarizability, α, represents the ability of an applied electric field, *E,* to induce a dipole moment, μ_{in}, in an atom or molecule (Klinowski, 2003 and Nakamoto, 1978).

$$\mu_{in} = \alpha E \quad \text{.....(2.11)}$$

From Equation 2.11, the equation for the polarizability of an atom or molecule can be derived and this is shown in Equation 2.12.

$$\mu_{in} = \alpha_0 E_{\max} \cos(2\pi \nu_{in} t) + \frac{E_{\max} r_{\max}}{2}\left(\frac{\partial \alpha}{\partial r}\right)\left\{\cos(2\pi t(\nu_{in} + \nu) + \cos(2\pi t(\nu_{in}^{`} - \nu))\right\}$$

…2.12

According to classical theory the first term contains the variable ν_{in}, which is the frequency of the incoming light. This term relates to the outgoing, scattered photon that has the same frequency as the incoming photon. This term defines Rayleigh scattering. The second term contains two cosines. One contains the variable ν_{in}, which relates to an outgoing, scattered photon that increases in frequency by some amount ν, which is the frequency of the molecular motion. The last cosine term contains the variable ν_{in}, which relates to a scattered photon that decreases its frequency by the same amount, ν. These two terms therefore define stokes and anti-stokes Raman scattering (Ball, 2001; Nakamoto, 1978).
The two terms show that incoming photons will shift their frequencies, up and down, by amounts equal to certain motions of the molecules. This is the basis of Raman spectroscopy. This equation also gives a gross

selection rule for what are called Raman active vibration modes. The second term that is multiplying the last two cosine terms. The term $\left(\frac{\partial \alpha}{\partial r}\right)$ is the change in the polarizability with nuclear position. If that derivative equals zero, the entire second term is zero and there will be no Raman scattering. Thus, we have as a gross selection rule: A molecular motion will be Raman-active only if, $\left(\frac{\partial \alpha}{\partial r}\right) \neq 0$ that is unless the polarizability changes during the vibration.

2.5.2 Inductively Coupled Plasma_Optical Emission Spectrometry

In the Inductively Coupled Plasma_Optical emission spectrometry (ICP_OES) The analysis are carried out in samples of liquid form. A sample is nebulized into the core of the inductively coupled argon plasma, with temperature in excess of 10 000 °C. The elements are atomized exited at this temperature. As they relax they emit light of characteristic wavelength. The light is collected and passed through gratings to resolve it into spectra of its constituents. The light spectrum is amplified into measurable intensities that are converted to elemental concentration by comparison with calibration standards.

2.5.3 Gamma and neutron activation spectroscopy

Gamma ray spectrometry is an analytical method that allows the identification and quantification of gamma emitting isotopes in a variety of matrices. In one single measurement and with little sample preparation, gamma ray spectrometry allows for the detections of several gamma emitting radioactive nuclides in the sample. The measurement gives a spectrum of lines, the amplitude of which is proportional to the activity of the radionuclide and its position on the horizontal axis gives an idea on its

energy. A schematic diagram of a gamma spectrometer is shown in Figure 2.8

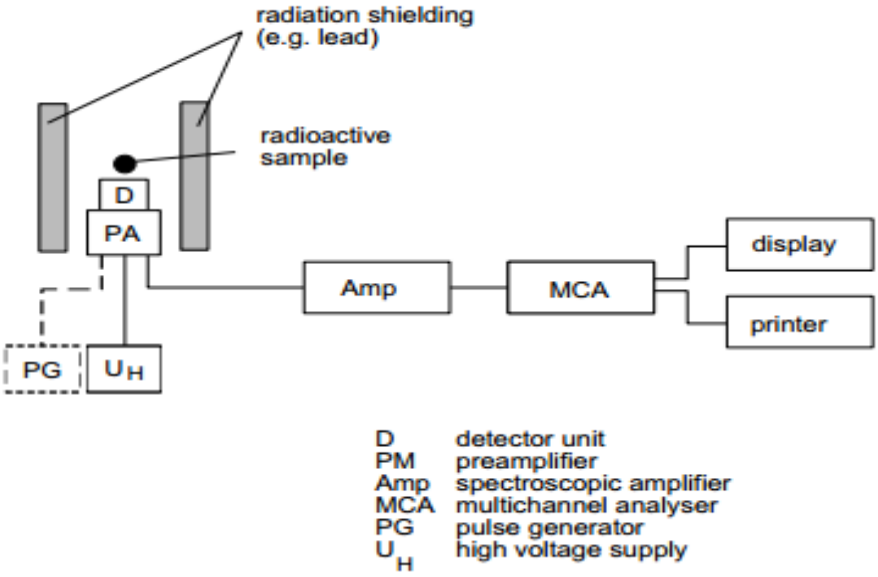


Figure 2.8: Schematic diagram of a gamma spectrometer (https://tu-dresden.de)

2.5.4 Single particle optical sensor

Particles in gas or liquid suspension flow through a small photozone of uniform illumination produce by a laser diode. The particle in suspension is sufficiently dilute when the particles pass one at a time through the illuminated region. The passage through the sensing zone causes a detectable pulse, which the magnitude depends on the diameter of the particle and the principle of detection which could be light scattering or obscuration. A PSD is constructed one particle at time by comparing the detected pulse to a standard calibration curve obtained from a set of uniform particles of known size. Figure 2.9 is the schematic dilution system.

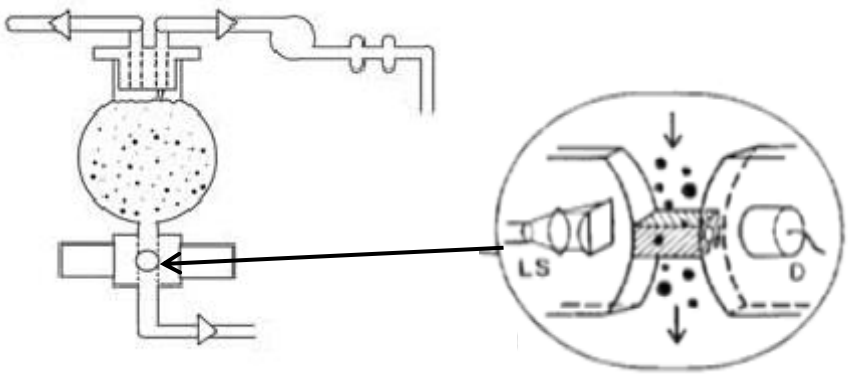


Figure 2.9: Schematic diagram of the Auto dilution system of the Nicomp 780 Accusizer system

A few drops of a concentrated liquid suspension or wet powder is manually introduced into the mixing chamber containing a filtered diluent such as water. The particles are mixed using a magnetic stirrer. Under a computer command a filtered diluent flows into the mixing chamber by means of a variable-speed precision gear pump creating a positive pressure causing some of the diluted solution to flow through the sensor region.

The particle concentration, c, in the fluid entering the sensor decreases exponentially with time, t according to:

$$c = c_0 \exp^{(-t/\tau)} \quad \text{.....(2.9)}$$

Where

$$\tau = V/F \quad \text{.....(2.10)}$$

Where V is the volume of the mixing chamber and F is the diluent flow rate.

CHAPTER 3

RADIOACTIVE NUCLIDES IN THE PHOSPHOGYPSUM FROM THE LOWVELD REGION OF SOUTH AFRICA – SUITABILITY FOR USE AS BUILDING MATERIAL

3.1 Introduction

The *National Nuclear Regulator Act* 47 of 1999 of South Africa seeks:

> *"To provide for the establishment of a National Nuclear Regulator in order to regulate nuclear activities, for its objects and functions, for the manner in which it is to be managed and for its staff matters; to provide for safety standards and regulatory practices for protection of persons, property and the environment against nuclear damage; and to provide for matters connected therewith*."

The Act exempts radioactive material on the basis of exposure or potential exposure from all or some aspects of regulatory control. The gamma-ray spectrometry analysis of the phosphogypsum was carried out at the laboratory at NECSA's RadioAnalysis Laboratories.

This chapter will evaluate the radioactivity of the Lowveld phosphogypsum, its suitability for use as a building material in South Africa, against the requirements of this Act and also against international hazard indices for international suitability. The results of the evaluation were accepted for publication by the South African Journal of Science (Impact Factor 0.957). The article is in paragraph 3.2. The lead author did the interpretation of the results and wrote the manuscript for publication. The second author did the process sampling and arranged for the analysis to be carried out. The third and fourth authors supervised the work.

3.2 Published Research Article: Radioactive nuclides

Radioactive nuclides in the phosphogypsum from the Lowveld region of South Africa – suitability for use as building material

Xolani Msila - Sasol Dyno Nobel, 486 Brandbach Road, Ekandustria, Bronkhorstspruit, 1021, South Africa; xolani.msila@sasol.com, +2713 933 6072, +2782 456 2468 (To whom correspondence should be addressed)

Frans Labuschagne - Sasol Dyno Nobel, 486 Brandbach Road, Ekandustria, Bronkhorstspruit, 1021, South Africa; frans.labuschagne@sasol.com , +2713 933 6017

Werner Barnard - Sasol Technology R&D, 1 Klasie Havenga Road, Sasolburg, 1947, South Africa; werner.barnard@sasol.com, +2716 960 6219

David Gordon Billing - School of Chemistry, University of the Witwatersrand, Johannesburg, WITS 2050, South Africa; dave.billing@wits.ac.za, +2711 717 6759

Abstract

In this study, we evaluated the suitability of phosphogypsum from the Lowveld region of South Africa (LSA), for the manufacturing of building materials, with reference to (a) the *National Nuclear Regulator Act 47 of 1999* of South Africa and (b) the radioactivity associated risks as quantified in terms of the external and internal hazard indices, the activity concentration index and the radium equivalent. The distribution of radioactive nuclides in the LSA phosphogypsum was also examined.

Analyses of 19 samples of the LSA phosphogypsum show that phosphogypsum contains lower activity concentrations of naturally occurring radioactive nuclides of uranium and thorium and their progeny than the 500 Bq/kg limit set for regulation in South Africa. The potassium-40 (^{40}K) activity concentration was below the minimum detectable amount of 100 Bq/kg. The values obtained for external and internal hazard indices and the activity concentration index (I_γ) were: 2.12±0.59, 3.44±0.64 and 2.65±0.76 respectively. The calculated radium equivalent Ra_{eq} was 513±76 Bq/kg. The final decision regarding phosphogypsum's suitability for use as a building material should consider scenarios of use

Key Words: apatite; radioactive nuclides; radiation hazard indices; Anderson–Darling; secular equilibrium

Introduction

A phosphoric acid production facility has been in operation in the Lowveld region of South Africa (LSA) since the 1960s. The process of producing phosphoric acid involves the digestion of fluoro-apatite ore ($Ca_{10}(PO_4)_6F_2$) with sulphuric acid as shown in Equation 3.1. Each year, tons of calcium sulfate dihydrate ($CaSO_4.2H_2O$) or gypsum, or specifically phosphogypsum, is produced as a by-product. The LSA phosphogypsum is stored in waste stacks alongside the phosphoric acid factory.

$$Ca_{10}(PO_4)_6F_2 + 10H_2SO_4 + 20H_2O \rightarrow 10CaSO_4.2H_2O + 6H_3PO_4 + 2HF \quad \text{.....(3.1)}$$

In a country like South Africa, that has a challenge to provide low cost or affordable housing (Ajayi, 2012), the use of phosphogypsum to manufacture building material is an attractive option. The manufacturing of low cost prefabricated building material from gypsum has in the recent past been demonstrated by Rajkovic and Toskovic (2002). But the

solubility of uranium, thorium and their daughter products that exist in apatite ores (Pereira and Bilal, 2012; Garcia *et al*., 2001), result in these radioactive nuclides partitioning between the phosphoric acid and the phosphogypsum (Dias *et al*., 2010; Al-Jundi *et al*., 2008), during the processing of the ore. Rajkovic and Toskovic (2002), Al-Jundi *et al*. (2008) and Hussein (1994) studied phosphogypsum from Serbia, Jordan and Egypt respectively. Hussein did not report on the activity concentrations of potassium-40 (^{40}K), thorium-232 (^{232}Th) and radium-226 (^{226}Ra) but the results of radioactive nuclide activities from Serbia and Jordan are given in Table 3.1.

Table 3.1: Activity concentrations of ^{40}K, ^{232}Th and ^{226}Ra in phosphogypsum from countries other than RSA

Country	Samples	^{40}K	^{232}Th	^{226}Ra
		(Bq/kg)		
Serbia	-	8.7	8.7	439
Jordan	15	40	-	376
Egypt		Not reported		

The worldwide average activities of ^{226}Ra, ^{232}Th and ^{40}K in the earth's crust are about: 40; 40 and 400 Bq/kg, respectively (ECRP, 1999). Humans are therefore exposed to this naturally occurring radioactive material (NORM). If the material used for the construction of human dwellings contributes additional radioactivity to the naturally occurring radioactive material, radiation exposure increases. The presence of these

radioactive nuclides impurities in the LSA phosphogypsum can limit its use as building material.

In this study we evaluated the suitability of the LSA phosphogypsum for the manufacturing of building materials, with reference to (a) the *National Nuclear Regulator Act 47 of 1999* of South Africa and (b) the radioactivity associated risks as quantified in terms of the external (H_{ex}) and internal (H_i) hazard indices, the activity concentration index (I_γ) and the radium equivalent (Ra_{eq}). The effect of ore processing on the distribution of the radioactive nuclides was also examined.

Materials and method

Nineteen representative samples of LSA phosphogypsum were taken during the production of phosphoric acid for analysis.

Sample preparation

The phosphogypsum was dried overnight in an oven at 80 °C. About 100 g of the dried phosphogypsum was transferred to a stainless grinding vessel (containing a stainless steel grinding balls and block) with a swing mill. Milling was performed at 960 rpm for one minute to obtain a fine powder. The process was repeated until 0.5 kg of homogeneous fine powder was generated.

Gamma analysis

A standard glass container was filled with phosphogypsum and the mass recorded. The container was closed with a lid and sealed airtight with the aid of epoxy resin. The prepared sample was allowed to stand for 3 weeks

so that radon-222 (and some of its progeny) reached radioactive equilibrium with radium-226. The γ-spectrum was acquired on a high purity germanium detector calibrated for the standard glass container geometry. The detector was housed in a lead shield to reduce background radiation. Gamma spectrum analysis was performed with Genie^{TM} 2000 Model S501 Gamma Analysis software. The weighted average activity of bismuth-214 and lead-214 was calculated and reported for radium. Thorium-228 was calculated from lead-212 and thalium-208. Radium-228 was determined from actinium-228. Potassium-40 was measured directly.

Uranium and thorium analysis by neutron activation analysis

Aliquots of the powder were transferred into irradiation capsules. Uranium and thorium standards were prepared by transferring known amounts of these elements from certified reference solutions into capsules and evaporated to dryness. Samples and standards were sequentially transferred with a pneumatic system into an in-core position of the SAFARI-1 reactor and irradiated with neutrons for a fixed time. After irradiation, the sample was transferred to a detector to measure neutrons emitted by products formed from fission of uranium-235.

The emission of neutrons between samples and standards was compared to calculate the uranium concentration in the sample. After a prolonged period, the irradiated samples and standard were measured on a gamma detector to determine neptunium-239 and protactinium-231. These nuclides formed from the neutron activation of uranium-238 and thorium-232 respectively. By comparing the activities of the nuclides in the standards and samples, the uranium-238 and thorium-232 sample activities were calculated.

For the determination of the presence of discrete radionuclides and calculations of their activities, the following gamma ray transitions (in keV) were chosen: ^{40}K (1460.8), ^{208}Tl (510.8, 583.1 and 860.5), ^{212}Pb (238.6 and 300.1), ^{214}Pb (241.9, 295.2 and 351.9), ^{214}Bi (609.3, 1120.3, 1238.1 and 1764.5) and ^{228}Ac (338.3, 911.1 and 968.9), ^{239}Np (228.2 and 277.6), ^{231}Pa (300.1 and 302.7), ^{235}U (185).

The activity of the sample (Bq/kg) is calculated using Equation 3.2:

$$A = 1000 \times \frac{\left(N/T\right)}{m\varepsilon P_\gamma} \quad \text{.....(3.2)}$$

where N is net counts of the photopeak, T is the live time of measurements (sec), m is the mass of the sample used (g), ε is the counting efficiency of the specific radioactive nuclide's energy and P_γ is the gamma transition probability through the specific energy.

The error was calculated using the formula in Equation 3.3:

$$uncertainity = \sqrt{\sum \sigma_{ni}^2 + \frac{1}{3}\sum \sigma_{si}^2} \quad \text{.....(3.3)}$$

where , σ_{ri} is the individual random error and σ_{si} is the individual systematic error

Radiation indices

From the activity concentrations of the radioactive nuclides, H_{ex}, H_i, I_γ and Ra_{eq} were calculated using the formulae in Equations 3.4–3.7

respectively. The formulae and their applications are comprehensively defined by the European Commission for Radiation Protection (ECRP, 1999).

$$H_{ex} = C_{Ra}/370 + C_{Th}/258 + C_K/4180 \quad \text{.....(3.4)}$$

$$H_{in} = C_{Ra}/185 + C_{Th}/259 + C_K/4810 \quad \text{.....(3.5)}$$

$$I_\gamma = C_{Ra}/300 + C_{Th}/200 + C_K/3000 \quad \text{.....(3.6)}$$

$$Ra_{eq} = C_{Ra} + 1.43C_{Th} + 0.077C_K \quad \text{.....(3.7)}$$

where C_{Ra}, C_{Th} and C_K are activities of ^{226}Ra, ^{232}Th and ^{40}K in Bq/kg, respectively (Mehdizadeh *et al*., 2011; Radenkovic *et al*., 2011).

Results and discussion

Radionuclides concentrations in phosphogypsum

The average activity concentrations of the radioactive nuclides: uranium-238 (^{238}U), uranium-235 (^{235}U), radium-228 (^{228}Ra), thorium-238 (^{238}Th), ^{226}Ra, ^{232}Th and ^{40}K in the LSA phosphogypsum are presented in Table 3.2. According to the *National Nuclear Regulatory Act, 47 of 1999 of South Africa,* an operation or material is excluded from regulation if activity concentration of the naturally occurring radioactive nuclides of

uranium, thorium and their progeny are each below 500 Bq/kg. The limit for ^{40}K is 10 000 Bq/kg.

Table 3.2: Activity concentrations of the radioactive nuclide the LSA phosphogypsum

Radioactive nuclide	^{238}U	^{235}U	^{228}Ra	^{228}Th	^{226}Ra	^{232}Th	^{40}K
	Bq/kg						
Average	31	1	404	253	109	189	<100
σ	20	1	70	160	18	155	-
No. of samples	19						

The results confirm that the activity concentrations measured in the 19 LSA phosphogypsum samples are all below the regulation limits set by the *National Nuclear Regulator Act 47 of 1999* of South Africa for ^{238}U, ^{235}U, ^{228}Ra, ^{226}Ra, ^{228}Th, and ^{232}Th. The activity concentration of ^{40}K in the LSA phosphogypsum was determined to be below the minimum detectable limit of 100 Bq/kg. Numerous studies (Papastafanou *et al*., 1983; Beretka and Mathew, 1985; Ackers *et al*., 1985; El-Thaway and Higgy, 1985; Kumar *et al*., 1999; Hewamana, 2001; Ravinsakar *et al*., 2011; Viruthagisi and Ponnarisi, 2011; Dhanya *et al*., 2012) have revealed that building materials contain appreciable activity concentrations of radioactive nuclides ^{226}Ra, ^{232}Th and ^{40}K. There are limited data available on the radiological safety of phosphogypsum use as building material beyond the study by Rajkovic and Toskovic (2002) and therefore to put the results obtained for LSA phosphogypsum into perspective, some of the results obtained for bricks from several countries are presented in Table 3.3.

Table 3.3: Activity concentrations of ^{40}K, ^{232}Th and ^{226}Ra in building bricks from other countries

Country	Reference	Samples	^{226}Ra	^{232}Th	^{40}K
			Bq/kg		
Greece	Papastefanou *et al*., 1983	6	49	24	670
Australia	Beretka and Mathew, 1985	25	41	89	681
Netherlands	Ackers *et al*., 1985	14	39	41	560
Egypt	El-Thaway and Higgy	1	20	14	204
India	Kumar *et al*., 1999	1	48	52	381
Sri Lanka	Hewamana, 2001	24	35	72	585
India	Ravinsakar *et al*., 2011	Not reported	18	19	238
India	Dhanya *et al*., 2012	Not reported	47	20	349

Average activity concentration of ^{226}Ra in the bricks listed in Table 3.3 ranges from 18–104 Bq/kg. This is lower than the average activity concentration in the LSA phosphogypsum (109 $\pm$ 18 Bq/kg). Similarly, the average activity concentration of ^{232}Th in the bricks ranges from 14 to 89 Bq/kg which is lower than the average in the LSA phosphogypsum ^{232}Th

(189 ± 155 Bq/kg). The activity concentration of ^{40}K (<100 Bq/kg) is lower in the LSA phosphogypsum compared to the range of activity concentrations reported for the bricks (204–1058 Bq/kg).

Radiation hazard indices (External, Internal, Activity concentration and Radium equivalent)

The LSA phosphogypsum is rich in ^{228}Ra compared to the ^{232}Th and as a result the activity concentration of the former is used in the place of the activity of the latter to calculate the hazard indices in Equations 3.4–3.7. The calculated hazard indices H_{ex}, H_{in}, I_{γ} and the Ra_{eq} are plotted in Figure 3.1. The error bars in Figure 3.1 represents the standard deviation of the results of the 19 LSA phosphogypsum samples. The values obtained for H_{ex}, H_{in} and I_{γ} were 2.12±0.59, 3.44±0.64 and 2.65±0.76 respectively. The calculated Ra_{eq} is 513±76 Bq/kg.

The Hex and Hi are both above the value of 1 and therefore the phosphogypsum is flagged against unrestricted use as the building material.

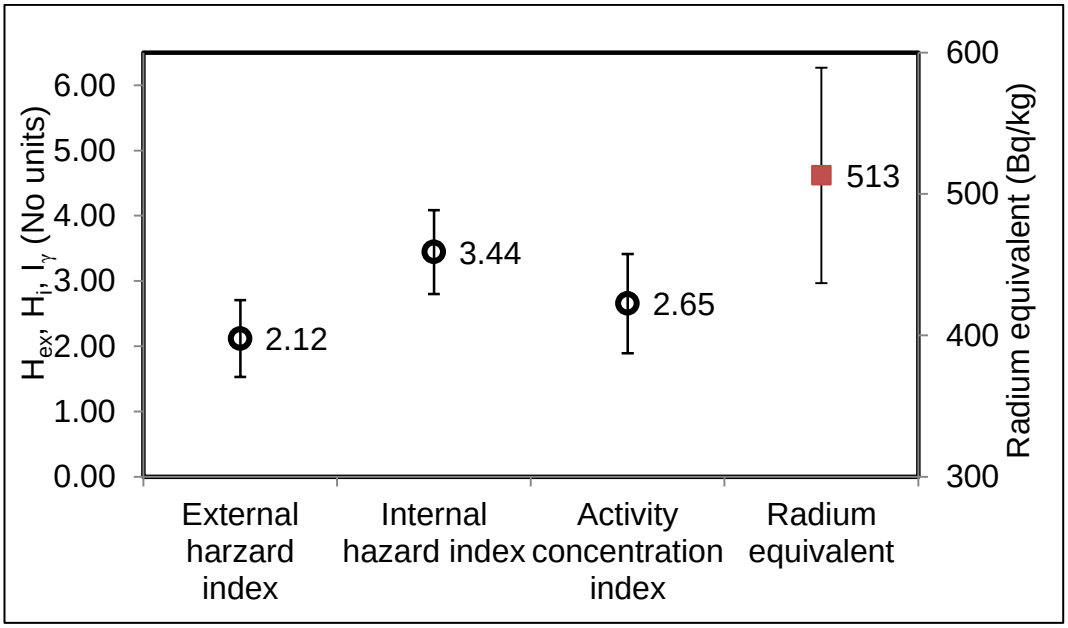


Figure 3.1: The calculated H_{ex}, H_{in}, I_γ and Ra_{eq} in the LSA phosphogypsum- error lines indicate the standard deviation

The assessment of a material's suitability for use as a building material should be based on scenarios where the material is used. The scenarios for use at different dose criteria are given in Table 3.4 (ECRP, 1999). The activity concentration index, $I_{\gamma,}$ should be evaluated against these criteria. If the I_γ is 1 or less, the material can be used as building material, without restriction, as far as radioactivity is concerned, whereas if the I_γ is above 1 and less than or equal to 6, the material should be used superficially. These activity concentrations are equivalent to radioactivity dose of 1 mSv year for bulk usage and artificial usage respectively.

Table 3.4: The scenarios of use for building materials

Dose criteria	0.3 mS/year	1 mSv/year
Material used in bulk amount, e.g. Bricks	$I_\gamma \leq 0.5$	$I_\gamma \leq 1$
Superficial and other material with restricted use: tiles, and boards	$I_\gamma \leq 2$	$I_\gamma \leq 6$

The Ra_{eq} as defined in Equation 3.5 is calculated from the activity concentrations of ^{226}Ra, ^{232}Th and ^{40}K. Equation 3.2 is based on the estimation that 1 Bq/kg of ^{226}Ra; 0.7 Bq/kg of ^{232}Th and 13 Bq/kg of ^{40}K generate the same γ-rays dose rate (Mehdizadeh *et al*., 2011; Uosif, 2011; Le Nhu *et al*., 2011). According to Mondal *et al*. (2006) and supported by El-Taher and Makhluf (2010), the I_γ=1 is equivalent to the Ra_{eq} of 370 Bq/kg. The calculated Ra_{eq} of 513$\pm$76 Bq/kg for LSA phosphogypsum is consistent with the activity concentration ($1<I\gamma<6$).

Radioactive nuclides distribution in LSA phosphogypsum

A simplified definition of secular equilibrium is found in Zhang *et al*., (2010) Activity of daughter radionuclides build up to that of the parent in about seven half-lives and thereafter, parent activity (λ_1) is the same as the activity of its progeny (λ_2). It follows therefore that at the state of secular equilibrium, the ratio of the activity of the parent to that of the daughter is 1 ($\lambda_1 / \lambda_2 = 1$). This phenomenon is known as secular equilibrium. The secular equilibrium observed in natural ores can be disturbed by mineral processing. Al-Jundi *et al*. (2008) showed that concentration of ^{238}U and its decay products ^{210}Pb and ^{226}Ra originating from apatite ore are partitioned during processing in such a way that ^{238}U accumulates in the phosphate fertilizer while ^{228}Ra, ^{226}Ra and ^{210}Pb accumulate in the phosphogypsum. This partitioning behavior can be attributed to the very low aqueous solubility of radium sulfate and lead sulfate relative to that of uranium sulfate as almost all the ^{228}Ra and ^{226}Ra reported by Van der Westhuizen (2004) as present in the phosphate rock is observed in the LSA phosphogypsum.

The ratios of activity concentrations in the LSA phosphogypsum for ^{238}U, ^{235}U, ^{232}Th and their progeny in the natural decay series are plotted Figure 3.2. Although the linear trend of the ratio of these two radionuclides is close to unity, there is a poor correlation between their activities as shown

by the regression coefficient (R^2) of 0.133. The uranium radioactive nuclide ^{238}U is also in disequilibrium with its progeny ^{226}Ra. Similarly, disequilibrium is also observed between ^{232}Th versus ^{228}Ra and ^{228}Ra versus ^{228}Th.

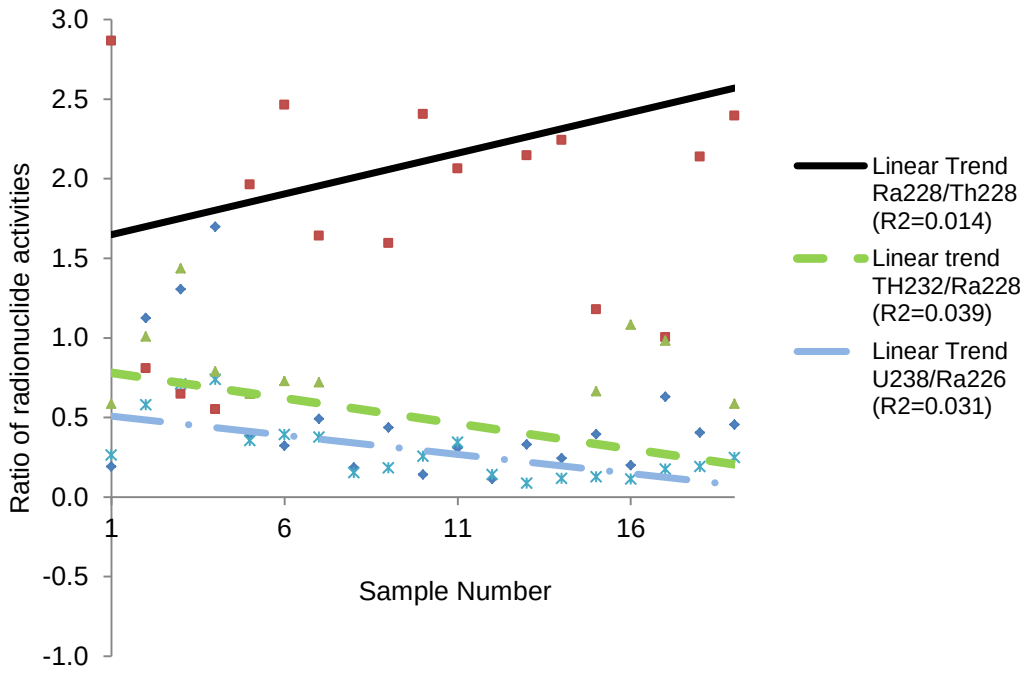


Figure 3.2: The ratio of activity concentrations for ^{238}U, ^{235}U, ^{232}Th and their progenies in the LSA phosphogypsum

In order to assess the randomness versus systematic distribution of the radioactive nuclides concentration in the phosphogypsum, a test for normal distribution was performed. The Anderson–Darling statistics have been shown to give appropriate empirical distribution function statistics for detecting departure from normality, even with small samples of less than twenty five (Stephens,1974). For the Gaussian distribution test, the statistics are based on the squared difference between the normal and the empirical data. If the calculated *p*-value is less than a chosen alpha (one minus the confidence interval), the null hypothesis, that the data come from that distribution, is rejected. The Anderson–Darling (AD) test was performed on the radioactive nuclide activity concentration data using the

statistical software Minitab® 16 statistical software to evaluate the distribution pattern of the activity concentration in the LSA phosphogypsum. The results obtained are presented in the probability plot in Figure 3.3:a–f.

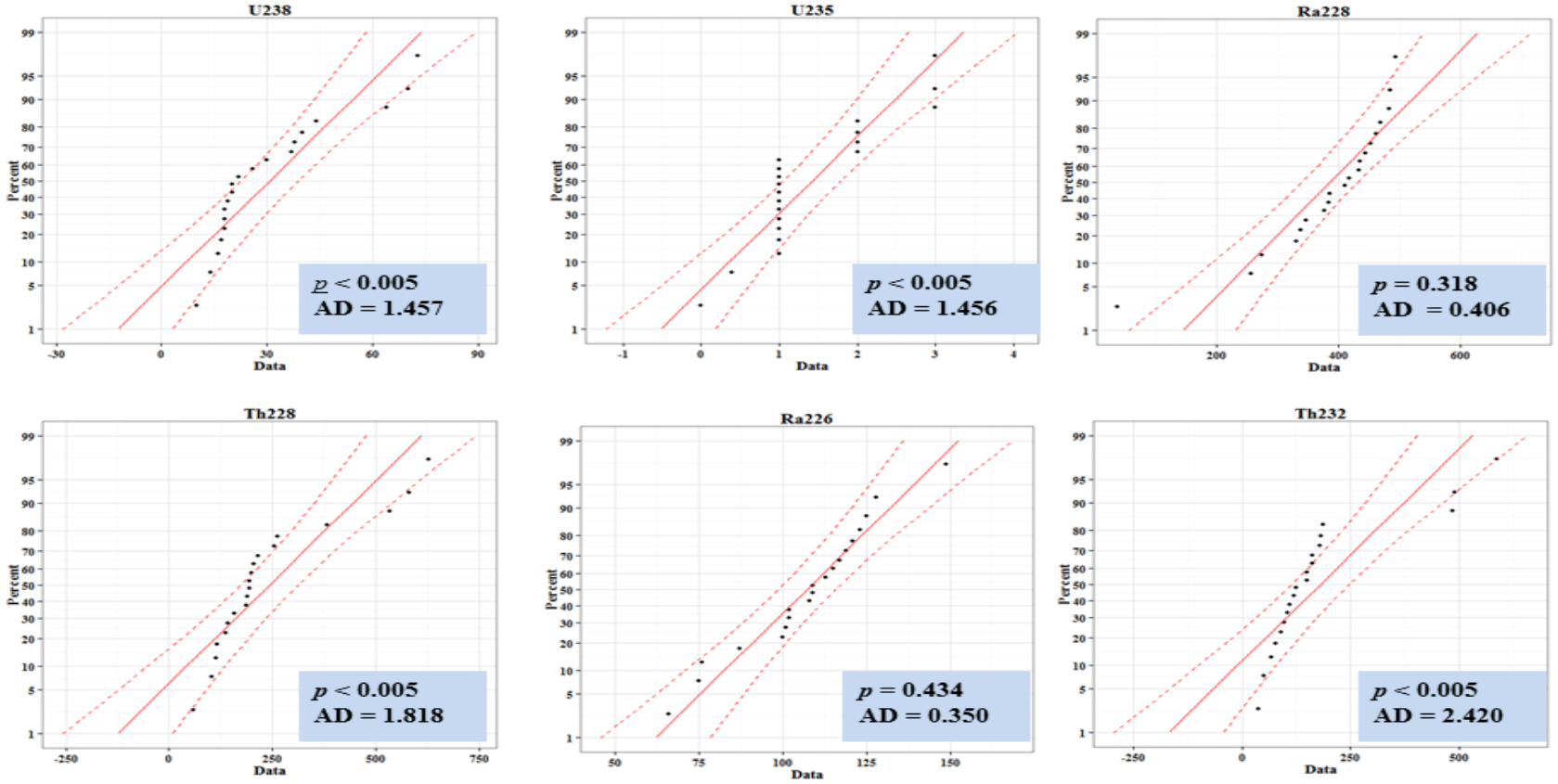


Figure 3.3: Probability plots of activity concentrations of: (14a) U-238; (14b) U-235; (14c) Ra-228, (14d) Th-228, (14e) Ra-226 and (14f) Th-232

At 95% confidence level, a *p* value of less than 0.05 indicates no deviation from a Gaussian distribution. Contrary to the *p* value, the smaller the AD value the closer is the distribution is to Gaussian. This behaviour (normal distribution) is observed for the activity concentration of the radioactive nuclides: ^{238}U ^{235}U, ^{228}Th and ^{232}Th in the LSA phosphogypsum. The contrary is observed for the ^{228}Ra and ^{226}Ra activity concentrations. The calculated *p* values are 0.318 and 0.434 respectively and the Anderson–Darling values are 0.406 and 0.350 respectively. This can be attributed to the low solubility of radium sulfate which results in accumulation in the phosphogypsum rather than the phosphoric acid.

Conclusion and recommendation

The LSA phosphogypsum contains appreciable amounts of the radioactive nuclides: ^{238}U; ^{235}U; ^{228}Ra; ^{228}Th; ^{226}Ra; ^{232}Th and below-detectable levels of ^{40}K. The average activities are below the limits set by the *National Nuclear Regulator Act 47 of 1999* of South Africa. The phosphogypsum is therefore excluded from regulatory control. The calculated results of hazard indices: H_{ex}, H_{in}, I_{γ} and Ra_{eq} indicate that the LSA phosphogypsum can be utilised as building material if used superficially or with restriction. A final decision on the usability of the material can be made when the scenario of use is known and a more representative sample of the aged bulk material is analysed. The radioactive nuclides and their progenies are not in secular equilibrium in the LSA phosphogypsum and the distribution ^{238}U, ^{235}U, ^{232}Th and ^{228}Th deviates from Gaussian.

References

Ackers, J.G., Den Boer, J.F., De Jong, P. and Wolschrijin, R.A. (1985) Radioactivity and radon exhalation rates of building materials in the Netherlands*. Science of the Total Environment*, vol. **45**, pp 151-156.

Ajayi, J.R. *Strategies for sustainable housing co-operatives in South Africa,* PhD Theses, Nelson Mandela Metropolitan University Port Elizabeth, 2012.

Al-Jundi, J., Al-Ahmad, N., Shehadeh, H., Afaneh, F., Maghrabi, M. and Gerstmann, U. (2008) Investigation on the activity concentrations of U-238, Ra-226, Pb-210 and K-40 in Jordan phosphogypsum and fertilizer. *Radiation Protection Dosimetry*, vol*.* **131,** no. 4, pp 449-454.

Beretka, J. and Mathew, P.J. (1985) Natural radioactivity of Australian building materials, industrial waste by-products. *Health Physics,* vol. **48**, no. 1, pp 87-95.

Department of Energy, National Nuclear Regulator Act 47 of 1999 available at: http://www.energy.gov.za/files/esources/nuclear/act47.pdf (accessed: 4 December 2015)

Dhanya, B., Umadevi, A.G., Jose, P.A., Rajagopalan, M. and Jojo, P.J. (2012) A study on activity concentration of natural radionuclide of building materials in Kochi. *International Journal of Fundamental Physical Sciences*, vol. **2**, no. 3, pp 41-43.

Dias, N.M.P., Caires, E.F., Pires, L.F., Bacchi, M.A. and Fernandes, E.A.N. (2010) Radiological impact of phosphogypsum surface application in a no-till system in Southern Brazil. *Pesquisa Agropecuaria Brasileira, vol.* **45**, pp 1456-1464.

El-Taher, A. and Makhluf, S. (2010) Natural radioactivity levels in phosphate fertilizer and its environmental implications in Assuit governorate, Upper Egypt. *Indian Journal of Pure and Applied Physics*, vol. **48**, pp 697-702.

El-Thaway, M.S. and Higgy, R.H. (1985) Natural radioactivity in different types of bricks fabricated and used in the Cairo region. *Applied Radiation Isotopes,* vol. **46,** no. 12, pp 1401-1406.

European Commission. Radiation Protection 112: Radiological protection principles concerning the natural radioactivity of building materials. Brussels: Directorate-General: Environment, nuclear safety and civil production; 1999.

Garcia-Talavera, M., Leadermann, J.P., Decombaz, M., Daza, M.J. and Quintana, B. (2001) Coincidence summing corrections for the natural decay series in γ-ray spectrometry. *Journal of Radiation Isotopes*, vol. **54**, pp 769-776.

Hewamanna, R., Sumithrarachchi, C.S., Mahawatte, P., Nanayakkara, H.L.C. and Ratnayakhe, H.C. (2001) Natural radioactivity and gamma dose from Sri Lankan clay bricks used in building construction. *Applied Radiation Isotopes*, vol. **54**, pp 365-369.

Hussein, E.M. (1994) Radioactivity of phosphate ore, superphosphate and phosphogypsum in Abu Zaabal phosphate plant, Egypt. *Health Physics*, vol. **48**, pp 87-95.

Kumar, V., Ramachandra, T.V. and Prasad, R. (1999) Natural radioactivity of Indian building materials and by products. *Applied Radiation Isotopes*, vol. **51**, no. 1, pp 93-96.

Le Nhu, S., Nguyen, T.B., Truong, Y., Nguyen, T.N., Nguyen, T.L. and Nguyen, V.P. Natural radioactivity in common building materials used in Vietnam 11255. WM2011 Conference; 2011 February 27-March 03; Phoenix, AZ; 2011

Mehdizadeh, S., Faghihi, R. and Sina, S. (2011) Natural radioactivity in building materials in Iran. *Nukleonika*, vol. **56,** no. 4, pp 363-368.

Mondal, T., Sengupta, D. and Mandal, A. (2006) Natural radioactivity of ash and coal in major thermal power plants of West Bengal**,** India**.** *Current Science*, vol. **91,** no. 10**,** pp 1387–1393.

Papastefanou, C., Manolopolou, M. and Charalambous, S. (1983) Exposure from the radioactivity in the building materials. *Health Physics*, vol. **45**, pp 349-361.

Pereira, F. and Bilal, E. (2012) Phosphoric acid extraction and rare earth recovery from apatites of the Brazilian phosphate ores. *Romanian Journal of Mineral Deposits, vol.* **85**, no. 2, pp 49-52.

Radenkovic, M.B., Alshikh, S.M., Andric, V.B. and Miljanic, S.S. (2009) Radioactivity of sand from several renowned public beaches and assessment of the corresponding environmental risks. *Journal of Serbian Chemical Society,* vol. **74**, no. 4, pp 461-470.

Rajkovic, M.B. and Toskovic, D.V. (2002) Investigation of the possibilities of phosphogypsum application for building partitioning walls - elements of a prefabricated house. *Acta Periodica Technolgica*, vol. **33**, pp 71-92.

Ravisankar, R., Vanasundari, K., Chandrasekaran, A., Suganya, M., Eswaran, P. and Vijayagopal, P. (2011) Measurement of Natural radioactivity in brick samples of Namakkal, Tamilnadu, India using gamma-ray spectrometry. *Archives of Physics Research*, vol. **2**, no. 2, pp 95-99.

Stephens, M.A. (1974) EDF Statistics for Goodness of Fit and Some Comparisons. *Journal of American Statistical Association*, vol. 69, pp 730–737.

Uosif, M.A.M. (2011) Specific activity of ^{226}Ra, ^{232}Th, and ^{40}K for Assessment of radiation hazards from building materials commonly used in Upper Egypt. SDU. *Journal of Science*, vol. **6**, no. 2, pp 120-126.

Van der Westhuizen, A.J. Rail transport of igneous phosphate rock. *International Atomic Energy Agency conference*, Szczyrk, Poland. 2004.

Viruthagiri, G. and Ponnarasi, K. (2011) Measurement of natural radio activity in bricks samples. *Advances in Applied Science Research,* vol. **2**, no. 2, pp 103-108.

Zhang, Q., Burman, C. and Amols, H. (2014) Transient and secular radioactive equilibrium revisited. [Article on the Internet]. Available online at http://arxiv.org/ftp/arxiv/papers (accessed: 4 December 2015)

CHAPTER 4

CONVERSION OF PHOSPHOGYPSUM INTO AMMONIUM SULPHATE AND PRECIPITATED CALCIUM CARBONATE IN A MODIFIED MERSEBURG PROCESS

4.1 Introduction

Waste phosphogypsum and effluent carbon dioxide are available in abundance but are of low commercial value. With the addition of ammonia these two low-value materials can be converted using the Merseburg process to relatively high value products, namely ammonium sulphate and precipitated calcium carbonate. In the Merseburg process the ammonium carbonate is formed from the reaction of carbon dioxide and aqueous ammonium solution in carbon dioxide scrubbing towers. In this study, a modification of the process by omitting the carbon dioxide scrubbing towers (C-16 and C-17 in Figure 1.3) and instead forming ammonium carbonate in the primary gypsum converting reactor (R- 4 in Figure 4.1) is evaluated.

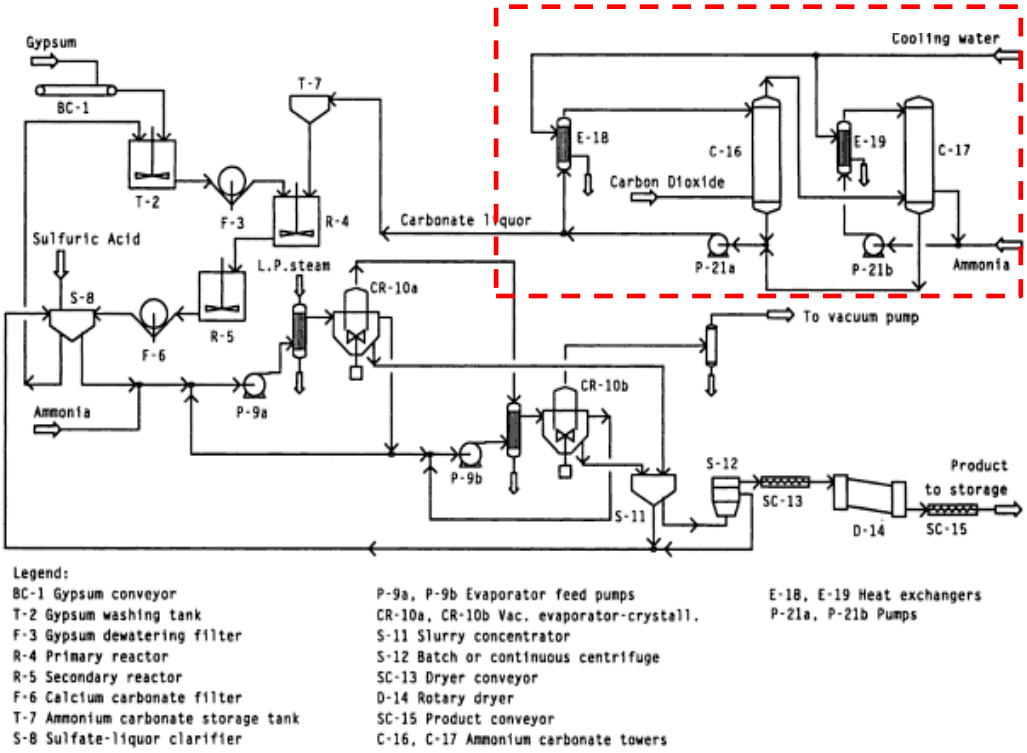


Figure 4.1: PFD of the Merseburg process with modification/omission highlighted in red

The omitted process units are highlighted in red in the process flow diagram in Figure 4.1 and the blue lines indicate the re-routing of the ammonium hydroxide and carbon dioxide lines. The focus of the study is on the process parameters such as temperature, pH and reaction kinetics that may be affected by the modification, as well as the characterisation of the product ammonium sulphate and precipitated calcium carbonate.

The outcome of this study has been published by the Clean Technology and Environmental Policy Journal (Impact Factor 1.934). The lead author designed the experiments, carried out the analysis, interpreted the results and prepared the manuscript for publication. The second and third authors supervised the work.

4.2 Published Research Article: Modified Merseburg process

Capture and storage of CO_2 into waste phosphogypsum – the modified Merseburg process

Mr. Xolani Msila - Sasol Dyno Nobel, 486 Brandbach Road, Ekandustria, Bronkhorstspruit, 1021, South Africa; e-mail: xolani.msila@sasol.com, Tel: +2713 933 6072, Fax: +27115224186

Prof. David Gordon Billing - School of Chemistry, University of the Witwatersrand, Johannesburg, WITS 2050, South Africa.

Dr. Werner Barnard - Sasol Technology Research and Development, 1 Klasie Havenga Road, Sasolburg, 1947, South Africa.

Abstract

We evaluated the chemical sequestration of carbon dioxide into the phosphogypsum from the Lowveld region of South Africa. The phosphogypsum was converted to saleable ammonium sulphate and precipitated calcium carbonate in a modified Merseburg process. The heat from the ammonium carbonate formation exorthemicity increased the temperature in the gypsum conversion reactor contents by 35 ºC, significantly reducing the heating requirements to achieve the reaction temperature of 70 ºC. The modified process will lower capital layout but no fundamental energy superiority or inferiority to the original Merseburg process. The gypsum conversion efficiency of 95% was achieved. The purity of the ammonium sulphate produced is comparable to the chemical grade, commercially available in South Africa. The calcium carbonate precipitated as calcitic, scalenohedral polymorphs with a mean size of 3.4 µm in diameter. The economic feasibility study must be done to determine the cost

implication of the omission of the carbon dioxide scrubbing towers in the modified Merseburg process.

Key words: Carbon capture and storage, Merseburg process, phosphogypsum, ammonium sulphate, precipitated calcium carbonate

4. Introduction

4.1. Background

The global economic development is closely associated with the rise in the total carbon emissions from fossil fuel consumption. South Africa is the 13th largest emitter of carbon dioxide (CO_2) with the total of 119 mega metric tons of carbon emission in 2012 (Boden, 2011). During the 2009 Copenhagen climate change negotiations, South Africa voluntarily announced that it would act to reduce domestic greenhouse gases emissions by 34 per cent by 2020 and 42 per cent by 2025 from business subject to the availability of adequate financial, technological and other support (KPMG, 2010). Carbon capture and storage technologies for the mitigation of CO_2 emission into atmosphere are at different levels of development and application. These technologies include but not limited to: pre-combustion, post-combustion and oxy-fuel combustion (Kanniche *et al*., 2010), chemical looping and oxygen transport membrane, utilisation of carbon dioxide into Enhanced Oil Recovery in oil extraction processes, microalgae production (Li *et al*., 2006), chemicals and fuels production (Abidin *et al*., 2011; Mendes *et al*., 2014).

The global economic development is also driving the increase in the demand for chemical fertilizers, including the phosphate based fertilizers. The fertilizer production increased from the annual 3 mega metric tons in 1751 to 9449 mega metric tons in 2011 (Boden *et al*., 2015). China alone accounts for 39% consumption in 2015 (HIS, 2016). The phosphoric acid [H_3PO_4] used in the phosphate based fertilizers is produced via the

digestion of apatite [$Ca_{10}(PO_4)_6F_2$] ore with sulphuric acid [H_2SO_4]. The reaction is described by Equation 4.1 (Al-Jundi *et al*., 2008; Pereira and Bilal, 2012; Chou *et al*., 1995; Chou *et al*., 1996).

$$Ca_{10}(PO_4)_6F_2 + 10H_2SO_4 + 20H_2O \rightarrow 10CaSO_4.2H_2O + 6H_3PO_4 + 2HF \ldots. (4.1)$$

Every ton of phosphoric acid produced, generates 1.7 tons of gypsum or specifically phosphogypsum as a by-product. Approximately 500 kilotons of phosphogypsum is produced annually from the phosphoric acid production plant in the Lowveld of South Africa.

4.1.1. Ammonium sulphate and precipitated calcium carbonate production

There are two known processes of producing ammonium sulphate: (a) the direct reaction of ammonia, ammonia solution or ammonia containing gas with sulphuric acid (b) the gypsum process where calcium sulphate is reacted with ammonium carbonate (Robinson, 1953) solution to form ammonium sulphate and the precipitated calcium carbonate (PCC). The later process also known as the Merseburg process was originally developed in Germany and was used in Austria, India, Pakistan and the United Kingdom (Alienov, 1998; Kontrec *et al*., 2011). The Merseburg process is described by Equation 4.2.

$$CaSO_4.2H_2O + CO_2 + 2NH_4(OH) \rightarrow CaCO_3 + (NH_4)_2SO_4 + 3H_2O \ldots\ldots\ldots (4.2)$$

Stoichiometrically, for every 1.0 ton of ammonium sulphate produced, 0.9 tons of PCC is also produced and 1.6 tons of gypsum and 0.4 tons CO_2 are consumed. South Africa has an opportunity to sequestrate up to 0.2% of its CO_2 emission and 100% of its phosphogypsum generation through the Merseburg. Chou *et al.,* (1995) are the latest to evaluate the Merseburg process on pilot scale and the concluded that the process is technically feasible for flue gas desulfurization gypsum. In a follow up study, Chou *et al*., (1996) concluded that the Merseburg process was also economically viable although the crystal size of ammonium sulphate produced was in the range 1.2 – 3.3 millimetres. They also estimated that a compaction unit to produce granules of ammonium sulphate as usually required by the fertilizer industry would make the process uneconomical. In this study we carried out a bench scale technical feasibility of the Merseburg process modified by omitting the CO_2 scrubbing towers in an attempt to reduce the capital layout. In this modified process the ammonium carbonate is formed directly in the gypsum conversion reactor. The modified process products ammonium sulphate and PCC were also characterized with regards to metal impurities and the crystal morphology, respectively.

4.1.2. Impurities in ammonium sulphate

The apatite ore is a host to heavy metals impurities such as cadmium (Cd), lead (Pb), arsenic (As), mercury (Hg) and nickel (Ni) (Dawson *et al*., 1996; Mar and Okazaki, 2012; Meck *et al*., 2011). Phosphogypsum as the by-product of apatite ore digestion contains some of these impurities (Rajkovic and Toskovic, 2002). Since ammonium sulphate is used in fertilizers (Liske *et al*., 2001; Robinson, 1953) and chemical fertilizers are known to contribute heavy metals into soils they are applied to (Atafar *et al*., 2010; Savci, 2012). High concentration of heavy metals in agricultural soil results in high concentrations in food grown in such soil (Orisakwe *et al*., 2012). For these reasons the fate of the heavy metal impurities during

the conversion of phosphogypsum to ammonium sulphate must be understood.

4.1.3. PCC

PCC is a multi-functional mineral filler extensively used in paper, paint, plastics, cosmetics, food, rubber, pharmaceutical and textile industries (Liske *et al*., 2001; Unkrainczyk *et al*., 2007). Paper made from PCC as a filler has better optical qualities as measured by brightness, whiteness, yellowness and opacity and better physical qualities as measured by breaking length, tear index and burst index, than that produced with ground calcium carbonate (GCC) as a filler (Tutus *et al*., 2013). The particle size and shape affects both the rheology (Michel-Sanchez 2005) and the optical properties (Tutus *et al*., 2013) of PCC-based coating. Amaya *et al*., (2011) showed that the particle size and crystal morphology of pigments used as either filler or in coating can have significant effect on optical performance of paper. In turn the size and shape of solution grown crystals is influenced by amongst other parameters: the degree of supersaturation; concentration and the type of impurities in solution; and the pH of the solution (Kubota *et al*. 2000; Loffelmann and Mersmann 2002; Vedantham 2004). The worldwide consumption of PCC has been reported by de Beers (2014) to be 74 mega tons in 2011.

The crystal morphology of PCC produced from a Merseburg process has not been reported before. The polymorphs of calcium carbonate are vaterite, aragonite and calcite (Vedantham 2004). Vaterite is the least thermodynamically stable form with hexagonal crystals and is rarely seen in natural occurring minerals (Piskin and Ozdemir 2012). Aragonite is the metastable form that belongs to orthorhombic-bipyramidal, space group - *Pmcn* (de Villiers 1971; Jarosch and Heger 1986; Kostov and Kostov 2006; Skinner *et al*. 1994). It slowly degrades to calcite. Calcite belongs

to the trigonal-rhombohedral, space group - $R\bar{3}c$ (Skinner *et al*. 1994). It is the most important of the three polymorphs in industrial applications (Reksten 1990; Scheetz and White 1977; Smyth 1997). According to Kontrec *et al*. (2011) calcite appears in various crystal forms: scalenohedral, rhombohedral, spheriohedral etc. but the scalenohedral is favoured in most industrial applications.

4.2. Experimental

Ammonium hydroxide solution (17%) was prepared by diluting a commercial 30% solution. The Reactions were carried out at atmospheric pressure in a bench scale 0.5 liter reactors fitted with a mechanical stirrer and a thermo-couple, connected to water bath circulation for temperature control. The variables in the experiments carried out are shown in Table 4.1.

Table 4.1: Experimental conditions and materials for Merseburg process

	Run #1	Run #2	Run #3	Run #4
Phosphogypsum (g)	0	0	80	80
Anhydrite (g)	0	63	0	0
NH_4OH	100 g (17%)			
CO_2 flow rate	l0 $L.min^{-1}$(Excess)			
Temperature	No heating		70 ºC	
Measurements	T & pH		T, pH, % gypsum conversion	

The measurements in Run #1-3 were taken every 5 minutes for 60 minutes. Run #4 was sampled after 0, 2, 3, 4, 5 and 7 hours. The samples were filtered through a Whatman filter paper and the solids were washed with water. The filtrate from the 7 hours reaction was acidified with 0.1N sulphuric acid to pH 3.0 before the reactor was heated to 95 ºC to

saturate the solution in order to precipitate the ammonium sulphate. The ammonium sulphate was filtered through the Whatman filter paper. The solid contents samples and the recovered ammonium sulphate were dried in an oven at 100 ºC. Samples of the solid contents, phosphogypsum were dissolved using nitric acid and the ammonium sulphate was dissolved in water. The solutions were analysed by ICP-OES in the general conditions shown in Table 4.2.

Table 4.2: The main ICP_OES conditions for measurement of metals in phosphogypsum

Nebulizer	Glass concentric
Spray Chamber	Glass cyclonic
Nebulizer Gas Flow ($dm^3.min^{-1}$)	0.7
Power (W)	1150
Plasma Gas Flow ($dm^3.min^{-1}$)	12
Auxiliary Gas Flow ($dm^3.min^{-1}$)	0.5

Table 4.3: The NICOMP Accusizer 780 settings

Detection method	Light extinction
Stirring rate (r.p.m.)	1500
Diluent flow rate ($cm^3.min^{-1}$)	60
Calculation range (μm)	1.5 – 500

Table 4.4: Bruker Raman spectrometer settings

Wavelength (nm)	532
Power (mV)	10
Scan time (s)	15

The PCC was analysed by (a) a NICOMP's Accusizer 780 (Dynamic Light Scattering combined with Zeta potential technique) for particle side distribution under the conditions given in Table 4.3) and (b) a Raman spectrometer equipped with charge coupled device detector under the experimental conditions in Table 4.4. (c) SEM (Mag = 5000x, EHT = 3.00 kV and WD 5.5 mm).

4.3. Results and Discussion

The Merseburg has been previously proven to be technically feasible. The purpose of this study was to evaluate the technical feasibility after the original process was modified by omitting the CO_2 scrubber. This section reports on the effect of the modification on the reactor temperature and the pH. The process products are characterised against their potential use.

4.3.1. Temperature in the gypsum conversion reactor

Figure 4.2 shows the average temperature increase (ΔT) in the reactor due to the ammonium carbonate formation during the reaction of NH_4OH and CO_2. The error bars in Figure 4.2 indicates the standard deviation (σ) of triplicate measurements. This temperature profile is the reflection of the ammonium carbonate scrubbing tower in the original Merseburg process. The ammonium carbonate formation is an exothermic reaction, ΔH = -674

kJ/mol. The ΔT for ammonium carbonate formation was compared with the ΔT when either gypsum or anhydrite was added during the ammonium carbonate formation. This temperature profile is the reflection of the ammonium carbonate in the gypsum convertor in the modified Merseburg process. ΔT of approximately 40 ºC was observed for the ammonium carbonate formation reaction and approximately 37 ºC for the reaction of anhydrite.

A reduction of about 38% in ΔT [$(\Delta T_{anhydrite} - \Delta T_{gypsum}) / \Delta T_{anhydrite}$] was observed when anhydrite was replaced with the phosphogypsum. The lower ΔT of $\pm$ 23 ºC, observed with gypsum addition can be attributed to the release of water of crystallisation from the co-occurring gypsum conversion (Equation 4.2), resulting in more energy dissipation. Although the modified process may show advantage in terms of capital layout, based on these results, the modified process has no fundamental energy conservation advantage or disadvantage over the original process.

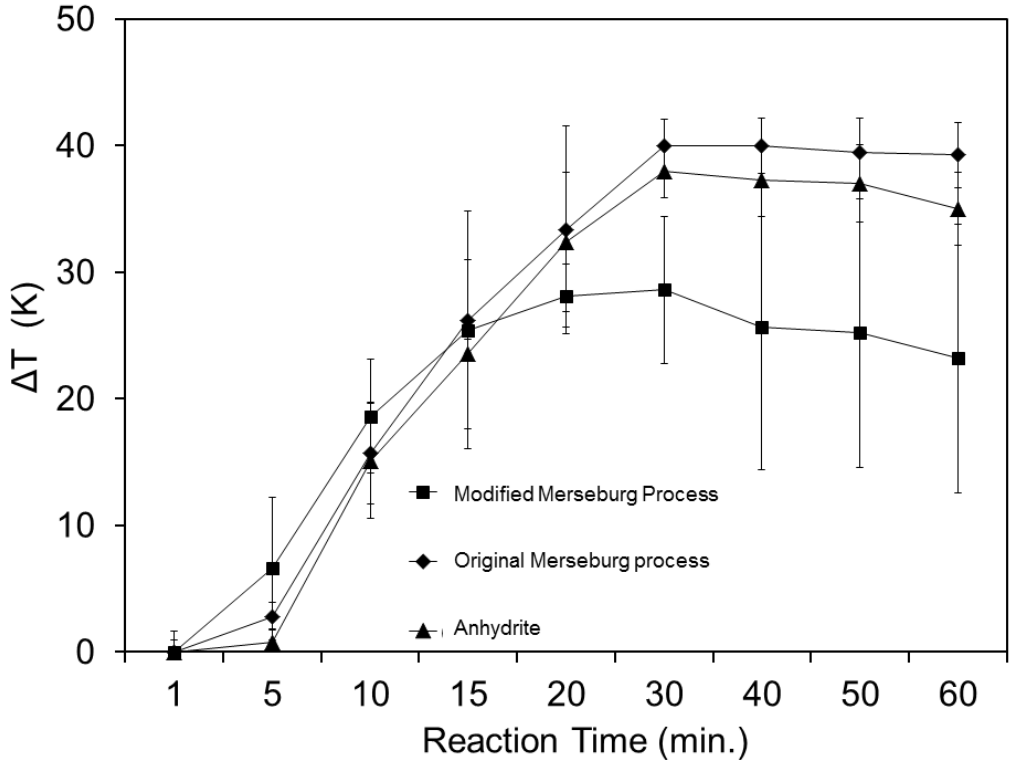


Figure 4.2: Temperature profile of ammonium carbonate formation in the original Merseburg; modified Merseburg and modified Merseburg and gypsum replaced with anhydrite

4.3.2. Ammonium sulphate precipitation

The pH in the gypsum conversion reactor was monitored over the 7 hours of reaction as the solids in the reactor changed from phosphogypsum to mainly PCC. The results of the average of triplicate pH measurements in Run #4 are shown in Figure 4.3. The error bars depict a standard deviation (σ) of triplicate measurements. The pH of the mother liquor dropped from 12 to about 8.

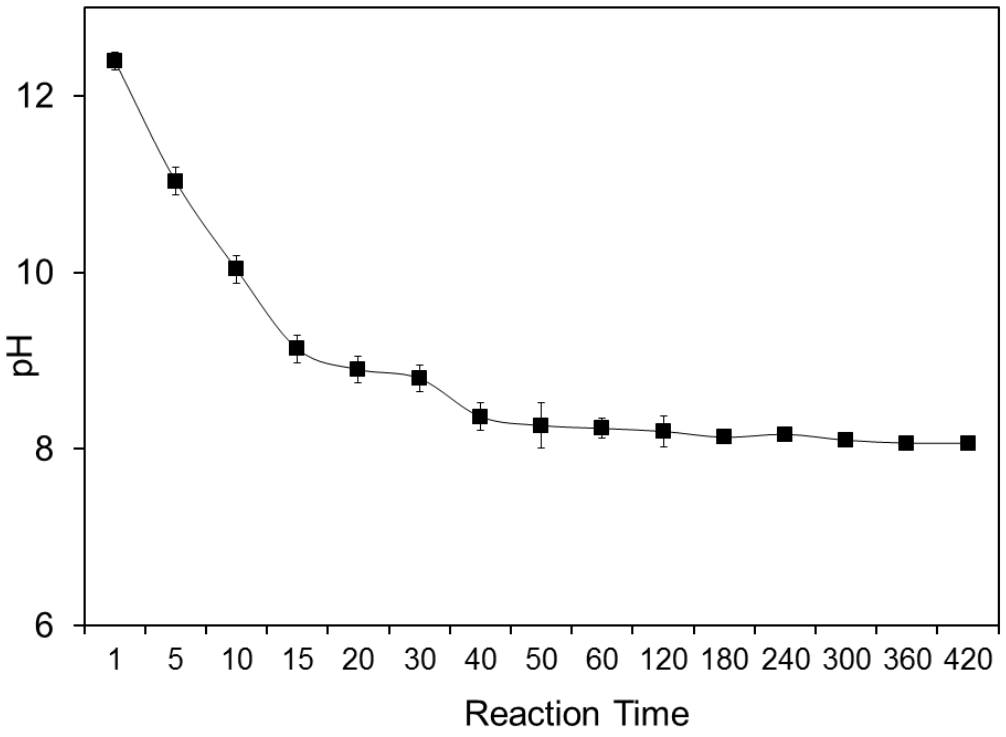


Figure 4.3: Average pH during modified Merseburg reaction

The conversion of gypsum was calculated to be 95% after 7 hours of reaction. The optimal design of the gypsum convertor may result in less ammonia gas loses and more conversion efficiencies such as the 98% reported by Chou *et al* (1995). The consumption of all phosphogypsum waste produced annually in the Lowveld, South Africa would reduce the CO_2 emission by 0.2%.

The pH of 8 is not suitable for the precipitation of ammonium sulphate and therefore after the separation of the PCC the mother liquor was acidified with a weak H_2SO_4 solution to a pH of 3.5 and the temperature of the reactor contents was increased to 80 ºC.

4.3.3. Particle size distribution of PCC

The particle size distribution (PSD) in crystal systems is a function of (1) degree of supersaturation; (2) impurities and (3) retention/crystal growth time. The crystallisation conditions were not optimised in this study but the formed crystals diameters are comparable to those reported by Piskin and Ozdemir (2012). In three experiments carried out the mean particle size of the crystal formed were found to be with an average diameter of 3.4 μm, a median of 2.7 μm and a mode of 2.3 μm. The results are shown in Figure 4.4. The error bars indicate one standard deviation ($\pm$1 σ) from the average.

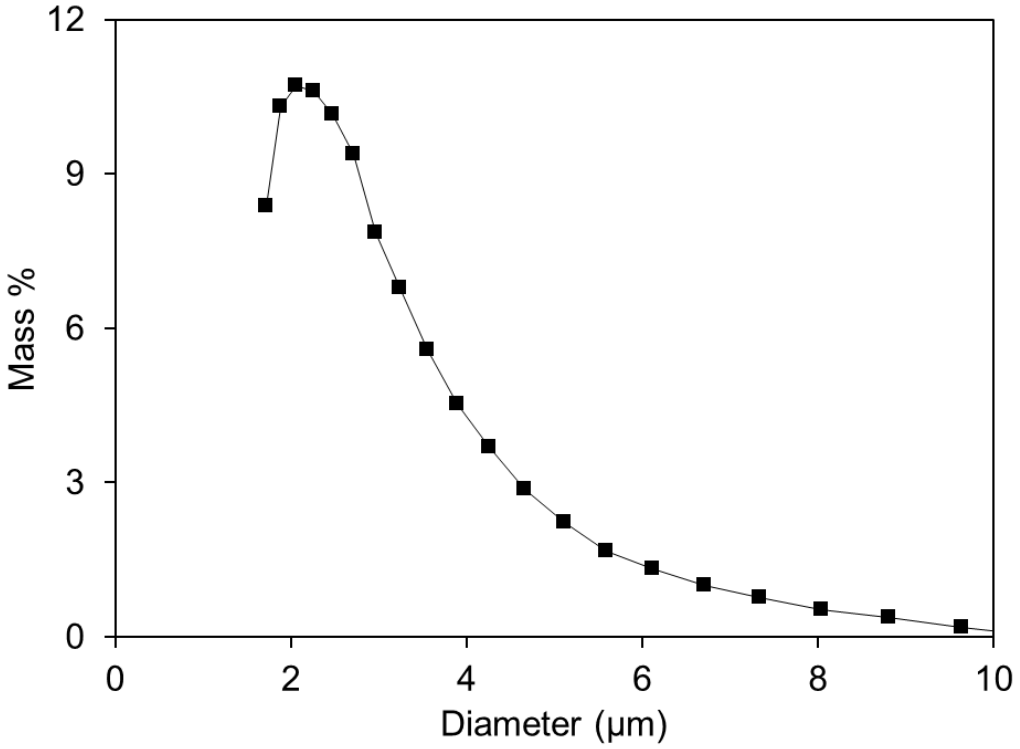


Figure 4.4: PSD of the Merseburg PCC

4.3.4. Raman spectroscopic analysis of PCC

There are 5 Raman peaks and 8 IR predicted active vibration modes for calcite (Mihailova, 2010) as defined by the irreducible representation in Equation 4.3:

$$\Gamma_{vib} = A_{1g}^{R} + 2A_{1u}^{inactive} + 3A_{2g}^{inactive} + 3A_{2u}^{IR} + 4E_{g}^{R} + 5E_{u}^{IR} \quad \text{.....(4.3)}$$

There are 30 predicted Raman active modes for aragonite (Mihailova, 2010) as defined by the irreducible representation in Equation 4.4:

$$\Gamma_{vib} = 9A_{1g}^{R} + 6A_{u}^{inactive} + 6B_{1g}^{R} + 8B_{1u}^{IR} + 9B_{2g}^{R} + 5B_{2u}^{IR} + 6B_{3g}^{R} + 8B_{3u}^{IR} \quad \text{.....(4.4)}$$

The Raman spectrum of the PCC formed in the modified Merseburg process is shown in Figure 4.5.

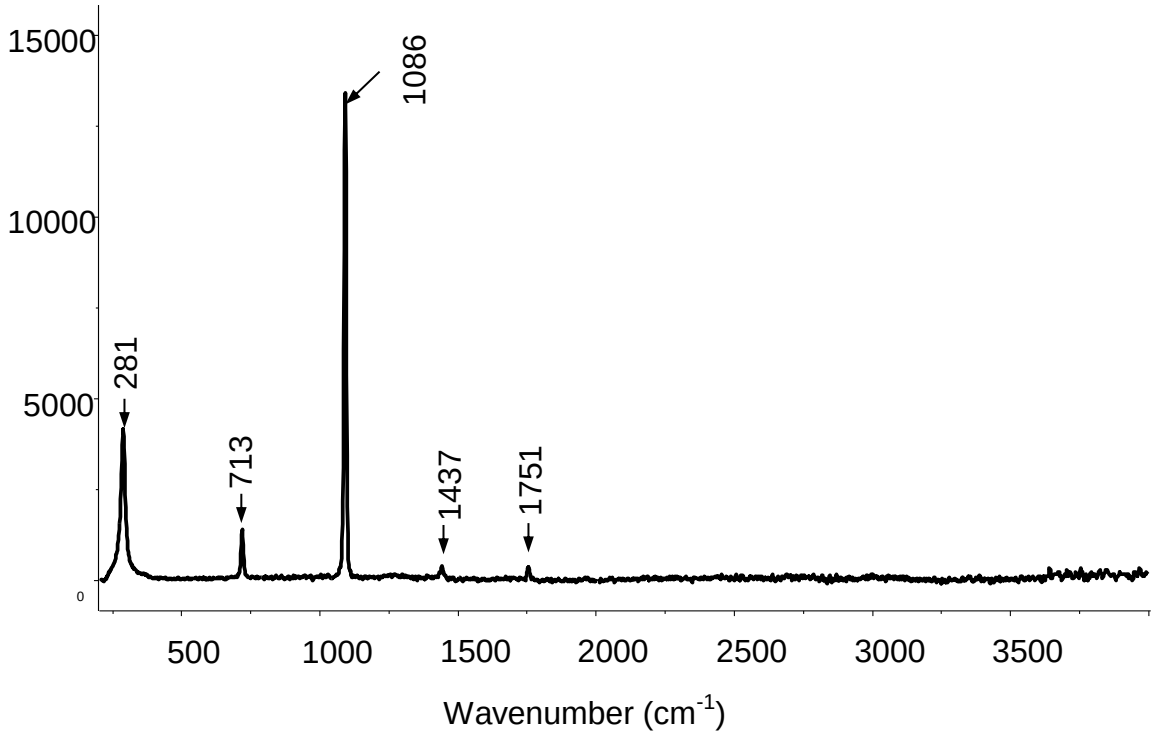


Figure 4.5: Raman spectrum of the modified Merseburg process PCC

The following Raman active bands are observed: 281 cm^{-1} ν_4CO_3; 713 cm^{-1} ν_4CO_3; 1086 cm^{-1} ν_1CO_3 and 1473 cm^{-1} ν_3CO_3. These Raman active bands for the stable polymorphs of $CaCO_3$ are reported in literature (Suito *et al*. 2001) at: ^{C}290 cm^{-1} or ^{A}207 cm^{-1} ν_4CO_3; ^{C}714 cm^{-1} and ^{C}715 cm^{-1} or ^{A}704 cm^{-1} ν_4CO_3; ^{C}1088 cm^{-1} and ^{C}1092 cm^{-1} ν_1CO_3 and ^{C}1415 cm^{-1} or ^{A}1462 cm^{-1} ν_3CO_3 where the superscripts A and C indicate aragonite and calcite respectively. These results confirm that the $CaCO_3$ produced in the modified Merseburg process is calcite as clearly distinguished by the Raman band at 281cm^{-1}. A non-fundamental shift is observed at 1751 cm^{-1}.

4.3.5. SEM analysis of PCC

The scanning electron microscopic (SEM) analysis of the PCC produced in the modified Merseburg process is shown in Figure 4.6. The results show formation of aggregates of primary rhombohedral crystals. The results show that the $CaCO_3$ precipitated under the current conditions is the scalenohedral polymorph of calcite, which is the industrially preferred form. The Merseburg PCC is comparable in crystal morphology to that produced by precipitation from lime, by Jung *et al*. (2000).

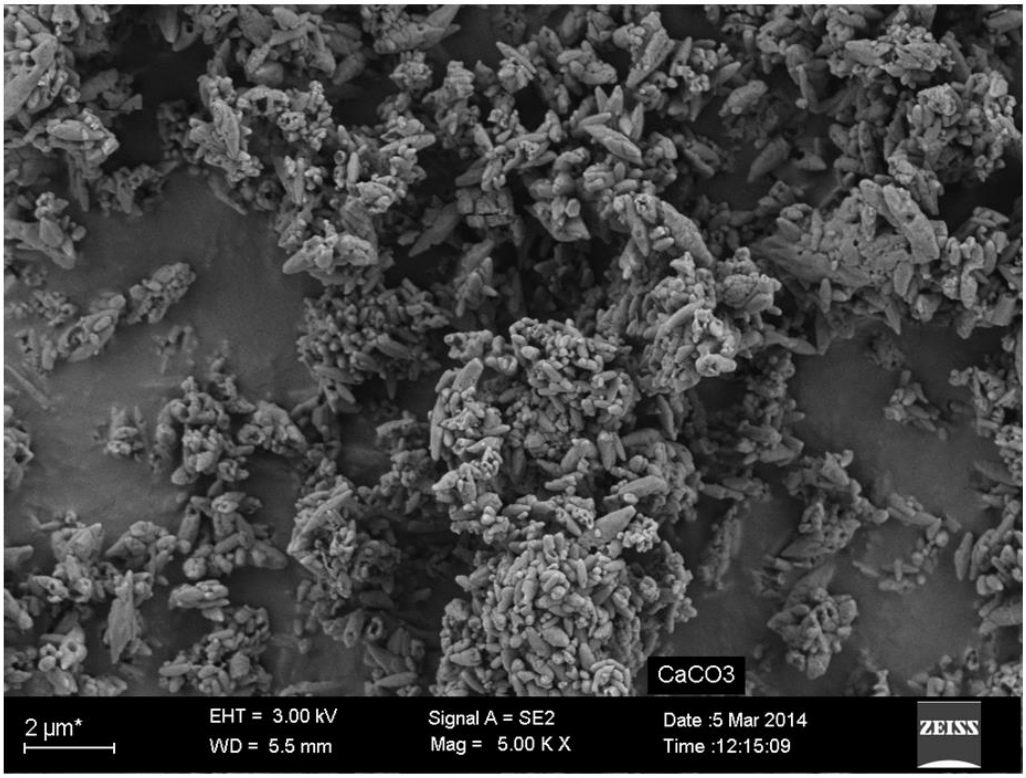


Figure 4.6: SEM image of the modified Merseburg PCC

4.3.6. Heavy metal analysis

The concentrations of the heavy metals in the phosphogypsum, the modified Merseburg process ammonium sulphate and PCC are given in Table 4.5. Low levels of lead and arsenic are observed in the phosphogypsum. These heavy metals partition during the Merseburg process, towards the PCC due to the low water solubility of lead sulphate and arsenic sulphate.

Table 4.5: ICP analysis of the phosphogypsum and the modified Merseburg process products

Heavy Metal	Phosphogypsum	Merseburg PCC	Merseburg ammonium
	mg/kg		
Cd	<1	<1	<1
Pb	41	56	10
As	17	21	7
Hg	<1	<1	<1
Ni	4	<1	<1

4.4. Conclusions

The omission of the CO_2 scrubbing towers will reduces the process capital layout, which in turn may mitigate the additional costs of installing a compaction unit for the production of granular ammonium sulphate. This study has demonstrated that 95% conversion efficiency of the phosphogypsum from the Lowveld of South Africa, is technical feasible in the modified Merseburg process. The efficiencies may be improved by minimising the ammonia gas loses in the gypsum conversion reactor. The ammonium sulphate produced is comparable in metal impurities to the commercially available grades. The PCC produced is the industrially preferred calcitic, scalenohedral polymorph with average diameter of 3.4 µm. These are important results in the quest for technologies for carbon capture and storage in South Africa and the world.

References

Abidin, V., Bouallou, C. and Clodic, D. (2011) Valorization of CO_2 emissions into ethanol by an innovative process. Chemical Engineering Transactions, vol. **25,** pp 1-6.

Alienov, D.P. *Fertilizer Manual*, Kluwer Academic Publishers, 1998, pp 246-248.

Al-Jundi, J., Al-Ahmad, N., Shehadeh, H., Afaneh, F., Maghrabi M. and Gerstmann, U. (2008), Investigation on The Activity Concentrations Of ^{238}U, ^{226}Ra, ^{228}Ra, ^{210}Pb and ^{40}K In Jordan Phosphogypsum And Fertilizers. *Radiation Protection Dosimetry,* vol. **131**, no. 4, pp 449-454.

Amaya, J.J., Doelle, K. and Mahmud, S. A comparative study of different fillers on uncoated eucalyptus digital printing paper properties: A pilot scale approach. *Paper Conference*, 2011. pp 2941. Available at http://www.tappi.org/content/events/11papercon/documents/Mahmud%20pptA.pdf. Accessed 1 March 2016

Atafar, Z., Mesdaghinia, A., Nouri, J., Homaee, M., Yunesian, M., Ahmadimoghaddam, M. and Mahvi, A.H. (2010) Effect of fertilizer application on soil heavy metal concentration. *Environmental Monitoring and Assessment*, vol. **160**, pp 83-89.

Boden, T.A., Marland, G. and Andres, R.J. (2015) Global, Regional, and National Fossil-Fuel CO_2 Emissions. Carbon Dioxide Information Analysis Center, Oak Ridge National Laboratory, U.S. Department of Energy, Oak Ridge, Tenn., U.S.A. doi 10.3334/CDIAC/00001_V2015

Boden, T.A., Marland, G., Andres, R.J. (2011) Global, Regional, and National Fossil-Fuel CO_2 Emissions. Carbon Dioxide Information Analysis Center, Oak Ridge National Laboratory, U.S. Department of Energy, Oak Ridge, Tenn., U.S.A. doi 10.3334/CDIAC/00001_V2011

Chou, M.I.M., Bruinius, J.A., Li, Y.C., Rostam-Abadi, M., Lytle, J.M. (1995) Manufacture of ammonium sulfate fertilizer from FGD-gypsum. *American Chemical Society Fuel Chemical division*. Chicago. Available online at http://web.anl.gov/PCS/acsfuel/files. Accessed 20 February 2016

Chou, M.I.M., Rosam-Abadi, M. and Lytle, J.M. (1996) Manufacture of ammonium sulfate fertilizer from gypsum-rich by-product of flue gas

desulfurisation – A prefeasibility cost estimate. Available online at https://web.anl.gov/PCS/acsfuel/preprint%20archive/Files/41_2_NEW%20ORLEANS_03-96_0579.pdf. Accessed 30 November 2015

Dawson, J.B., Steele, I.M., Smith, J.V. and Rivers, M.L. **(**1996) Minor and Trace Element Chemistry of Carbonates, Apatites and Magnetites in Some African Carbonatites**.** *Mineralogy Magazine,* vol. **60**, pp 415-425.

De Beers, M. *The production of precipitated calcium carbonate from industrial gypsum wastes*, PhD Theses, University of the North West, 2014.

De Villiers JPR (1971) Crystal structures of aragonite, strontianite, and witherite. *American Mineralogist*, vol. **56**, pp 758-767

Chemical Economic Handbook®, China Report https://www.ihs.com/products/phosphoric-acid-chemical-economics-handbook.html. Accessed 30 Jan 2016

Jarosch, D. and Heger, G. (1986) Neutron diffraction refinement of the crystal structure of Aragonite. *Mineralogische und Petrographische Mitteilugen*, vol. **35**, pp 27-131.

Jung, W.M., Kang, S.H., Kim, W. and Choi, C.K. (2000) Particle morphology of calcium carbonate precipitated by gas-liquid reaction in a Couette-Taylor reactor. *Chemical Engineering Science*, vol. **55**, pp 733-747.

Kanniche, M., Gros-Bonnivard, R., Jaud, P., Valle-Marcos, J., Amann, J-M. and Bouallou, C. (2010) Pre-combustion, post-combustion and oxy-combustion in thermal power plant for CO_2 capture. *Applied Thermal Engineering*, vol. **30**, pp 53-62.

Kontrec, J., Ukrainczyk, M., Babic-Ivancic, V. and Kralj, D. (2011) Synthesis of Calcium Carbonate by Semi-continuous Carbonation Method

in the Presence of Dextrans. *Croatica Chemica Acta*, vol. **84**, no. 1, pp 25-32

Kostov, I. and Kostov, R.I. (2006) Systematics and crystal genesis of carbonate minerals. *Geology and Geophysics*, vol. **49**, no. 1, pp 111-118

KPMG (2010) Carbon disclosure project available from http://www.cdproject.net. Accessed on 1 March 2016

Kubota, N., Yokota, M. and Mullin, J.W. (2000) Combined influence of supersaturation and impurity concentration on crystal growth. *Journal of Crystal Growth*, vol. **212,** pp 480-488.

Li, Y., Markley, B., Mohan, A.R., Rodriguez-Santiago, V., Thompson, D. and Niekerk, D.V. (2006) Utilization of carbon dioxide from coal-fired power plant for the production of value-added products, Penn State College of Earth and Mineral Sciences. Available at http://www.ems.psu.edu/~elsworth/courses/egee580/Utilization_final_report.pdf. Accessed on 1 March 2016

Liske, Y., Kapila, S., Flanigan, V., Nam, P. and Lorbert, S. (2001) Production of Feedstock Chemicals from Ammonium Sulfate and Ammonium Bisulfate. *Journal of Hazardous Substance Research*, vol. **2**, pp 8-11.

Loffelmann, M. and Mersmann, A. (2002) Prediction of crystallization coefficients of the population balance. *Chemical Engineering Science*, vol. **57**, pp 4301- 4310.

Mar, S.S. and Okazaki, M. (2012) Investigation of Cd contents in several phosphate rocks used for the production of fertilizer. *Microchemical Journal*, vol. **104**, pp 17-21.

Meck, M.L., Althopeng, J., Masamba, W.R.L., Ringrose, S. and Diskin, S. (2011) Minerals that Host Metals at Dorowa Rock Phosphate Mine, Zimbabwe. *The Open Mineral Processing Journal*, vol. **5**, pp 1-9.

Mendes, L., de Menderios, J.L., Alves, R.M.B. and Araujo, O.Q.F. (2014) Production of methanol and organic carbonates for chemical sequestration of CO_2 from an NGCC power plant. *Clean Technology and Environmental Policy*, vol. **16**, pp 1095-1105. DOI 10.1007/s10098-014-0712-0.

Michel-Sanchez, E. *Impact of particle morphology on the Rheology of PCC-Based coating*, PhD Theses, Georgia Institute of Technology, 2005.

Mihailova, B. Application of representations theory in solid state physics and chemistry: Vibrations in molecules and solids. *Summer School on Mathematical Crystallography*, France. 2010. available online at http://www.crystallography.fr/mathcryst/pdf/nancy2010/Mihailova.pdf (accessed 21 May 2016)

Orisakwe, O.E., Nduka, J.K., Amadi, C.N., Dike, D.O. and Bede, O. (2012) Heavy metals health risk assessment for population via consumption of food crops and fruits in Owerri, South Eastern, Nigeria. *Chemistry Central Journal*, vol. **6**, pp 77-84.

Robinson P (1953) US Patent 2631084A

Pereira, F. and Bilal, E. (2012) Phosphoric acid extraction and rare earth recovery from apatites of the Brazilian phosphatic ore. *Romanian Journal of Mineral Deposits*, vol. **85**, no. 2, pp 49-52.

Piskin, S. and Ozdemir, O.D. (2012) Effect of Process Conditions on Crystal Structure of Precipitated Calcium Carbonate ($CaCO_3$) From Fly Ash: Na_2CO_3 Preparation Conditions. *International Journal of Biological, Ecological and Environmental Sciences***,** vol. **1**, no. 6, pp 192-195.

Rajkovic, M.B. and Toskovic, D.V. (2002) Determination of Inorganic compounds in drinking water on the basis of household water heater scale. *Acta Periodica Technoligica,* vol. **33**, pp 71-92.

Reksten, K. (1990) Superstructures in calcite. *American Mineralogist*, vol. **75**, pp 807-812.

Savci, S. (2012) An agricultural pollutant Chemical fertilizer. International *Journal of Environmental Science and Technology*, vol. **3**, no. 1, pp 77-80.

Scheetz, B.E. and White, B. (1977) Vibrational spectra of the alkaline earth double carbonates. *American Mineralogist*, vol. **62,** pp 36-50.

Skinner, A.J., LaFemina, J.P. and Jansen, H.J.F. (1994) Structure and bonding of calcite, a theoretical study *American Mineralogist***,** vol. **79**, pp 205-214.

Smyth, J.R. (1997) The crystal structure of Calcite III*. Geophysical research letters*, vol. **24**, no. 13, pp 1595-1598.

Suito, K., Namba, J., Horikawa, T., Taniguchi, Y., Sakurai, N., Kobayashi, M., Onodera, A., Shimomura, O. and Kikegawa, T. (2001) Phase relations of $CaCO_3$ at high pressure and high temperature. *American Mineralogist*, vol. **86**, pp 997-1002.

Tutus, A., Cicekler, M., Ozdemir, A. and Okan, T.O. Effects of precipitated calcium carbonate (PCC) on optical properties of waste paper. *International Caucasian forestry Symposium*. Artvin, Turkey. 2013.

Unkrainczyk, M., Kontrec, J., Babic-Ivancic, V., Brecevic, L. and Kralj, D. (2007) Experimental design approach to calcium carbonate precipitation in a semi-continuous process. *Powder Technology*, vol. **171,** pp 192-199.

Vedantham, K. *Effect of operating parameters on the growth rate of solution grown crystals*, MSc Theses, Mississippi State University, 2004

CHAPTER 5

THERMAL REDUCTION OF PHOSPHOGYPSUM TO CALCIUM SULPHIDE USING GRAPHITE

5.1 High temperature X-Ray powder diffraction

The reports on the dehydration mechanism of gypsum vary widely depending on the experimental conditions and the analytical technique used. A review of these reports is given on Table 5.1. High temperature X-Ray Diffraction was performed in the temperature range 25 – 650 °C in order to understand the phase transformation that precedes the thermal reduction of sulphate in the mixture of phosphogypsum and graphite. Rietveld refinements were performed using TOPAS academic version 4.1.

Table 5.1: The review of studies on thermal dehydration of $CaSO_4.xH_2O$ over the period 1964 to 2009

Technique	Conditions	Summary of findings	Reference
	Controlled water vapour pressure dehydration	$CaSO_4.2H_2O \rightarrow CaSO_4.\ ½\ H_2O \rightarrow \gamma\text{-}CaSO_4$ E_a increased linearly with vapour pressure	McAdie, 1964
X-Ray diffraction, TGA & Optical microscopy	Dehydration of gypsum at 85 °C	$CaSO_4.2H_2O \rightarrow \gamma\text{-}CaSO_4$	Molony and Ridge, 1968

Technique	**Conditions**	**Summary of findings**	**Reference**
Autoclave	-	Conversion of gypsum to Hemihydrate is Linearly dependent on pressure	McConnell *et al.*, 1987
Neutron powder diffraction	Air or under hydrothermal and T<300 ºC	$CaSO_4.2H_2O$ →α-$CaSO_4$. ½ H_2O → β-$CaSO_4$. ½ H_2O →γ-$CaSO_4$	Bushuev *et al.*, 1983. Quoted by Ballirano & Mellis, 1996
In situ IR & TGA	Dry and constant gas flow N_2;	$CaSO_4.2H_2O$ → $CaSO_4$. ½ H_2O →γ-$CaSO_4$;E_a (63-106 ºC) = 90.3 kJ/mol	Putnis *et al.*, 1990
Variable Temperature Neutron diffraction	Vacuum 10^{-4} bar	$CaSO_4.xH_2O$ ($0.46 \leq x \leq 0.79$)	Abriel *et al.*, 1990
		Up to 100 ºC gypsum to $CaSO_4$. ½ H_2O dominant 1^{st} order. Above 100 °C dominated 2 phase boundary mechanism	Dos Santo, 1997. Quoted by Ballirano & Mellis, 1996
Single crystal Raman	115 °C – 147 °C and	$CaSO_4.2H_2O$ → $CaSO_4$. ½ H_2O →γ-	Sarma *et al.*, 1998

Technique	Conditions	Summary of findings	Reference
spectroscopy	%RH ca.60	$CaSO_4$ E_a 92.25 kJ/mol	
Variable Temperature Raman Spectroscopy	Stagnant air %RH ca. 50 25 ºC -300ºC	$CaSO_4.2H_2O$ →$CaSO_4$. ½ H_2O →γ-$CaSO_4$ Hemihydrate observed from 118 °C	Chang *et al.*, 1999
Micro Raman & FTIR	-264 ºC to -100 ºC; constant N_2 flow	$CaSO_4.2H_2O$ → $CaSO_4$. ½ H_2O →γ-$CaSO_4$	Chio *et al.*, 2004
Micro Raman & FTIR	27 °C – 127 °C	$CaSO_4.2H_2O$→γ-$CaSO_4$	Prasad *et al.,* 2005
EDXD	Dynamical reduced total pressure10^{-3} bar; 40 – 80 °C	JMAK model; E_a 75 kJ/mol $CaSO_4.2H_2O$→γ-$CaSO_4$	Carbone *et al.*,2008

5.1.1 Gypsum dehydration 25-650 °C

The diffractogram of the Phalaborwa phosphogypsum is shown in Appendix A. It has a monoclinic crystal structure and no other crystalline impurities detectable by XRD. The instruments set-up details are on Appendix B. The instrument peak positions were verified with a LAB_6 standard and diffractogram is shown in Appendix C. Figure 5.1 depicts the

2-d view of the 33 diffractogram taken during the heating from 25 °C to 650 °C and then cooling to 25 °C. The dotted line indicates approximate temperatures for the transitions from gypsum to hemihydrate(s) and from hemihydrate to anhydrite and the dominant phase in each region is indicated. The shift in peak positions is observed during the heating and the cooling of the reactant. This behaviour is attributed to crystal lattice expansion.

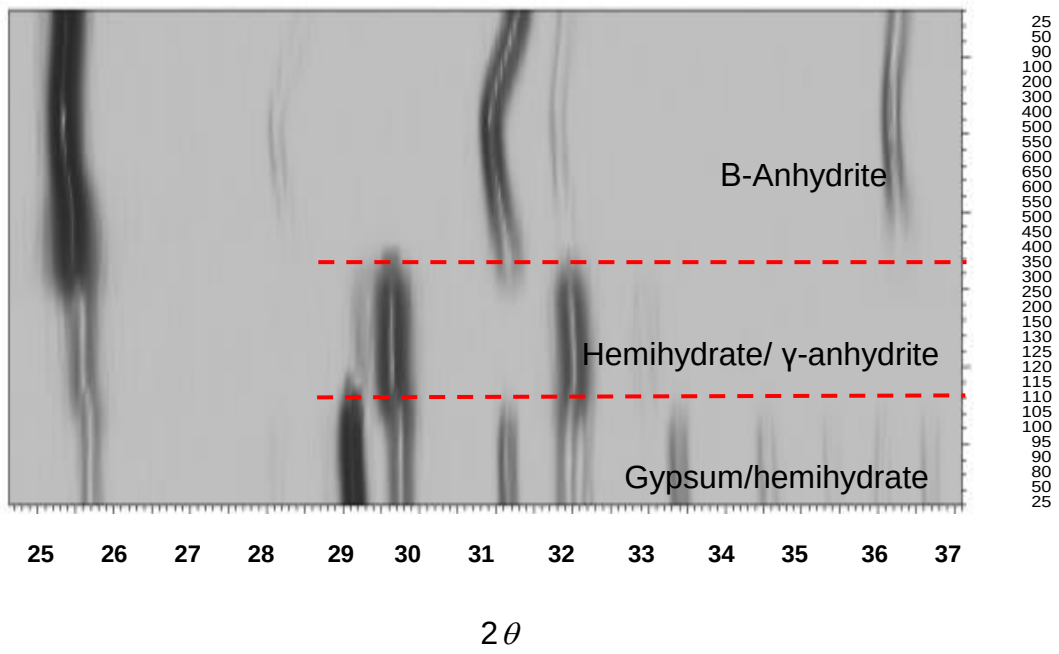


Figure 5.1: Reaction between gypsum and carbonaceous material 25-650 °C under nitrogen flow

Figure 5.2 shows the plot of the crystal lattice parameters for phosphogypsum during heating up to 650 ºC. The Rietveld refinement of the data was carried out on TOPAS Academic version 4.1. The data on the expansion of *a, b* and *c* lattice parameters obtained is compared and shows good agreement to that reported by Ballirano and Melis, (2009) but consistently lower than that reported by Schofield *et al.*, (1996). Ballirano and Melis argued that the difference observed between their data and that

of Schofield *et al.*, (1996) was due to difference in the temperature range of measurements and possible due to systematic errors in Schofield *et al*., (1996) experiments.

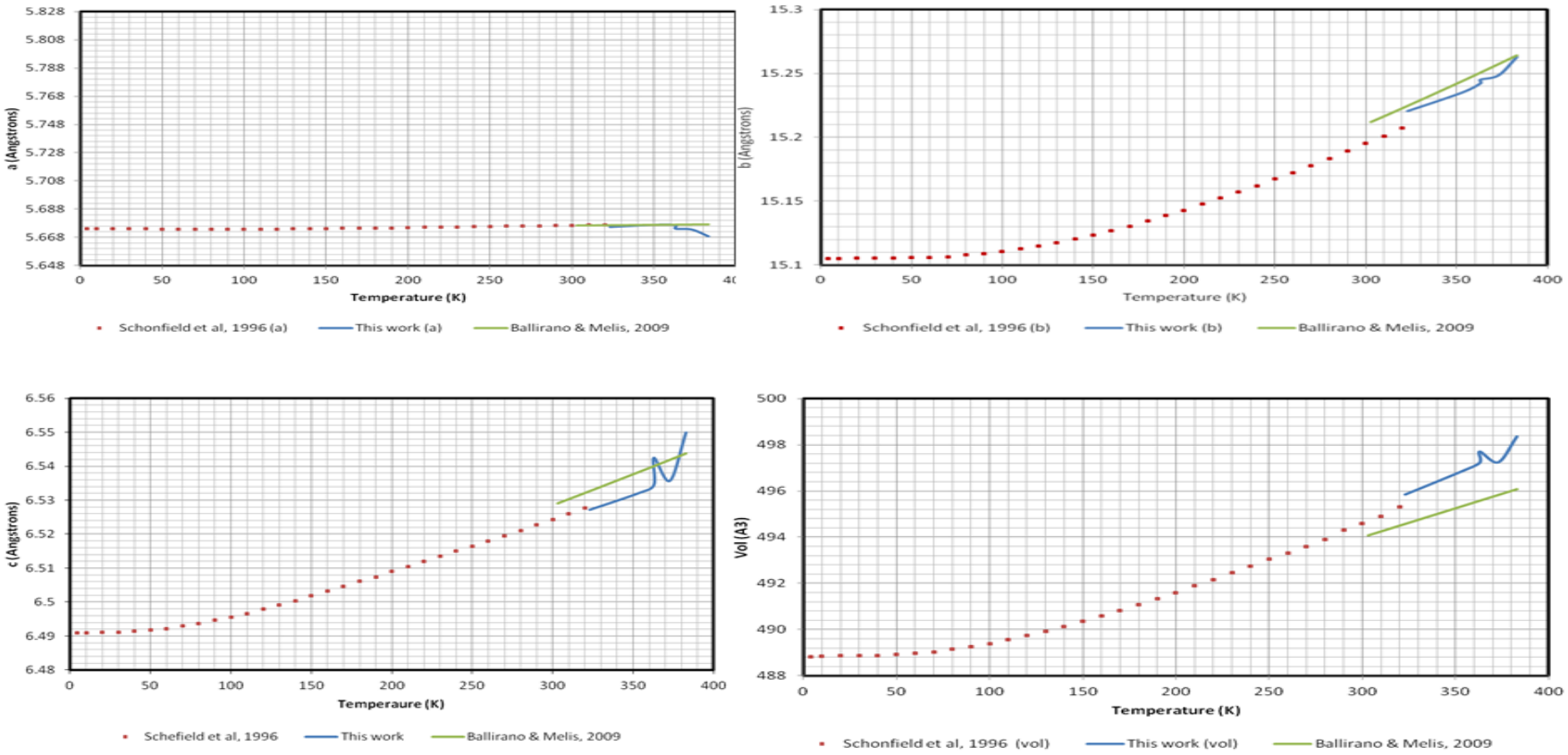


Figure 5.2: Evolution of lattice parameters and volumes of gypsum with temperature in the 25 – 650 °C range. Reference data of Schofield *et. al*., 1996 and Ballirano & Melis, 2009 are reported for comparison

Both these authors agreed that the expansion of gypsum is anisotropic along the *b*-axis and this was attributed to the weakening of the hydrogen bond (H-----O), acting along the *b*-axis, linking the adjacent polyhedral sheets as shown by the 010 plane in Figure 5.3.

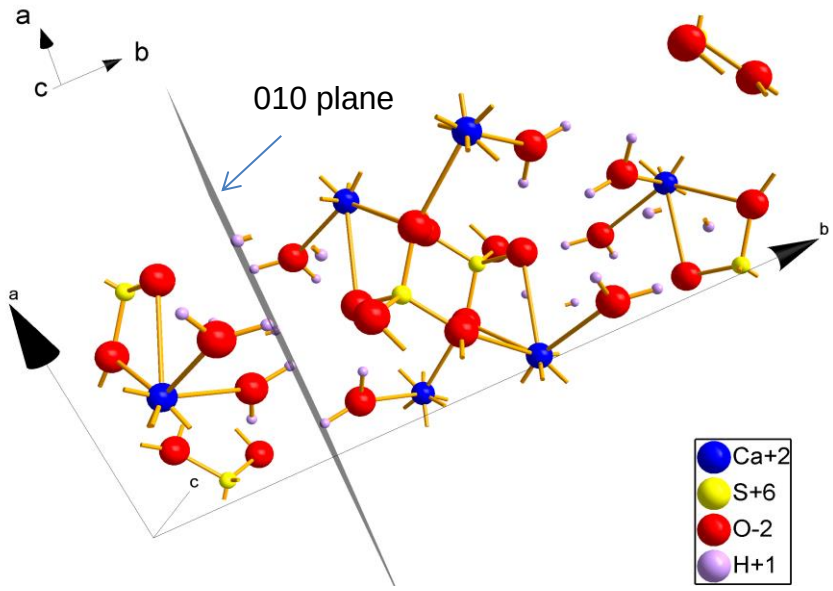


Figure 5.3: Ball and stick model of Gypsum showing the water layer in the 010 plane

Ballirano and Melis, 2009 studied the thermal behaviour of γ-$CaSO_4$. They reported that the thermal expansion is anisotropic along the *c*-axis. The transformation from γ→ β $CaSO_4$ begins at 182 °C and get to completion at 380 °C. Under the current experimental conditions γ-$CaSO_4$ is observed earlier at 117 ºC. The γ-$CaSO_4$ and β-$CaSO_4$ could be refined together up to temperatures of 500 °C. The space group $P6_222$ for γ-$CaSO_4$ was proposed by Ballirano *et al.*, 2005 and Ballirano and Melis, 2001 and confirmed by Christensen *et al.*, 2008, contrary to the *C*222 previously proposed by Bezou *et al.*, (1995). Therefore the Rietveld refinements were carried out in $P6_222$ space group and the refined lattice parameters *a*= 6.9757 Å and *c* = 6.3188 Å. Rietveld refinements β-$CaSO_4$ were carried out on space group, orthorhombic pseudo trigonal *AMMA* resulting

in the refined lattice parameters: *a*= 6.997 Å, *b*= 6.99 Å and *c*= 6.24 Å which are similar to those reported in the literature. Similar behaviour to that reported in Ballirano and Melis, 2009 and Ballirano and Melis, 2007 the thermal expansion of both γ-$CaSO_4$ and β-$CaSO_4$ is anisotropic along the *c*-axis.

In this chapter we discuss the reaction mechanism and the kinetic of the reduction of graphite with graphitic carbon.

5.2 Thermogravimetric analysis

The work covers the Thermogravimetric analysis of the reaction between phosphogypsum and graphite. The experiment was design by the main author and the analyses were performed by Benni Vilakazi at the thermal laboratory at NECSA. The lead author carried out the interpretation and wrote the manuscript for publication. The second and third authors supervised the work. The article has been re-submitted to the Journal of Thermal Analysis Calorimetry (Impact Factor 2.042). The referencing style has been changed from the publication journal in order to maintain consistency in this Thesis.

5.3 In situ Raman spectroscopy

The work covers the *in situ* Raman spectroscopic study of the reaction between phosphogypsum and graphite. The experiment was design by the lead author and the high temperature analyses were carried out at the WITS School of Physics, Nano laboratory by the main author under the guidance of Dr. Rudolf Erasmus. The ambient temperature analyses were performed by the second author at Sasol Technology (Dr. Werner Barnard). The main author interpreted the results and wrote the manuscript for publication. The second and third authors supervised the work. The outcome of this work is published in the journal: Spectrochimica

Acta A (Impact factor 2.098). The referencing style has been changed from the publication journal in order to maintain consistency in this Thesis.

5.4 Research Article: TG kinetics

TG-DSC analysis and kinetics of the reaction between phosphogypsum and graphite

Xolani Msila - Sasol Dyno Nobel, 486 Brandbach Road, Ekandustria, Bronkhorstspruit, 1021, South Africa; xolani.msila@sasol.com, +2713 933 6072, +2782 456 2468 (To whom correspondence should be addressed)

Werner Barnard - Sasol Technology R&D, 1 Klasie Havenga Road, Sasolburg, 1947, South Africa; werner.barnard@sasol.com, +2716 960 6219

David Gordon Billing - School of Chemistry, University of the Witwatersrand, Johannesburg, WITS 2050, South Africa; dave.billing@wits.ac.za, +2711 717 6759

Abstract

A kinetic study of the reaction between phosphogypsum and graphitic carbon was carried out using a TG-DSC analyser. The analyses were done under a nitrogen flow in the temperature range 25 to 1200 ºC. The results show that: (1) the increase in the nitrogen flow rate drives the thermal reduction of phosphogypsum forward, (2) after the dehydration of the phosphogypsum to anhydrite, the thermal reduction to calcium sulphide proceed via an intermediate compound formation of a mass loss of around 11%. The activation energy for the reduction of phosphogypsum

to calcium sulphide was obtained by the OFW and KAS methods to be in the 330-370 kJ/mol range. The reduction of phosphogypsum to calcium sulphide is a complex reaction with competing parallel independent reactions.

Key words: OFW, KAS, apparent activation energy, model-free methods, phosphogypsum

Introduction

For every ton of phosphoric acid produced from apatite ore, 1.7 tons phosphogypsum is produced as a by-product (Al-Jundi *et al*. 2008; Pereira and Bilal, 2012) as described by Equation 5.1. In turn elemental sulphur can be recovered from phosphogypsum by thermal reduction process followed by H_2S scrubbing using CO_2 and a PIPco or Fe process (Maree *et al*., 2005; Nengovhela, 2008; Mihara *et al*., 2008). The deterrent to such recovery of S is the high reduction temperature and the resultant cost. Thermal reduction of sulphate has been a subject of many studies, as reflected in the review by Machel (2001), specifically in relation to oil exploration.

$$Ca_{10}(PO_4)_6F_2 + 10H_2SO_4 + 20H_2O \rightarrow 10CaSO_4.2H_2O + 6H_3PO_4 + 2HF \quad (5.1)$$

$$CaSO_4.2H_2O + 2C \rightarrow CaS + 2CO_2 + 2H_2O \quad \text{.....(5.2)}$$

A sulphate ion is a tetrahedron, with S-O bond lengths of 1,47Å and O-S-O bond angle of 109° (Ma *et al*., 2008; Ellis *et al*., 2007). This molecular symmetry results in high activation energy (E_a): 234 kJ/mol (Ellis *et al*., 2007), 354 or 324 kJ/mol (Goldstein and Aizenshtat, 1994), for the

thermal sulphate reduction (TSR) by the electron donors such as hydrocarbons. In laboratory evaluation of the thermal reduction of calcium sulphates (anhydrite and gypsum) with C_1, C_2 and C_3 hydrocarbons, the E_a of 152.9 kJ/mol, 131.0 kJ/mol and 120.6 kJ/mol were obtained respectively (Yue *et al*., 2006); 96.8 kJ/mol using natural gas containing inclusively C_1-C_6 hydrocarbons (Ding *et al*., 2007). The common trend in these studies were reaction temperature $\leq$ 200 ºC and presence of moisture. The thermal reduction studies carried out on Flue Gas Desulphurization (FGD) gypsum using activated carbon by Nengovhela (2008) at elevated temperature concluded that the reduction proceeds via complex reaction. Following the Raman spectroscopic study of phosphogypsum reduction with graphite by Msila *et al.* (2015) we use the TG-DSC to evaluate the kinetics parameter (E_a) of phosphogypsum reduction with graphitic carbon Equation 5.2, by following the Ozawa-Flynn-Wall- (OFW) method (Flynn and Wall, 1966) and Kissinger-Akahira-Sunose (KAS) methods (Akahira and Sunose, 1971).

Kinetics

Kinetics of solid reactions is based on assumption that they are a function of temperature and conversion as described by the Equation 5.3.

$$d\alpha/dt = k(T) \cdot f(\alpha) \quad \text{.....(5.3)}$$

where f(α) is the reaction model (Apaydin-Varol, 2014), k is the reaction constant and α is the conversion defined by: $\alpha = (m_i - m_a)/(m_i - m_f)$

where m_i is the initial mass,

m_a is the actual mass at time t and m_f is the final mass.

The Arrhenius equation, Equation 5.4, describes the dependence of the constant k on temperature as follows:

$$k = Ae^{-E_a/RT} \quad \text{.....(5.4)}$$

where, A is the pre-exponential factor, E_a is the activation energy, R is the gas constant with the value 8.314 $J.K^{-1}.mol^{-1}$ and T is the absolute temperature in K.

Combining Equations 5.3 and 5.4 we get Equation 5.5:

$$d\alpha/dt = A \cdot f(\alpha) \cdot e^{-E_a/RT} \quad \text{.....(5.5)}$$

Reaction models can be reduced into 3 major types: accelerating, decelerating and autocatalytic (Vyazovkin *et al*., 2011). For accelerating models, the dependence of the reaction model to the conversion is expressed in a power model Equation 5.6.

$$f(\alpha) = (1-\alpha)^n \quad \text{.....(5.6)}$$

where n is the reaction order.

If we substitute for $f(\alpha)$ in Equation (5.5) we get Equation 5.7:

$$d\alpha/dt = A \cdot (1-\alpha)^n \cdot e^{-E_a/RT} \quad \text{.....(5.7)}$$

For linear heating non-isothermal TGA the heating rate (β) is expressed as: $\beta = dT/dt$ and therefore Equation 5.7 for linear heating TGA can be expressed as Equation 5.8:

$$d\alpha/dT = A/\beta \cdot (1-\alpha)^n \cdot e^{-E_\alpha/RT} \quad \text{.....(5.8)}$$

For condensed phase kinetics, the model-free Isoconventional methods represent a simple, way to treat kinetic data and enable process modelling without insight into the mechanism and use the activation parameters for temperatures regimes outside those applied in the measurements (Simon, 2004). Two of such model-free methods are known as OFW and KAS methods. The OFW method is derived from Equation 5.9.

$$\ln(\beta) = \ln\left(A_\alpha E_\alpha / Rg(\alpha)\right) - 5.331 - 1.052\, E_\alpha / RT_{\alpha i} \quad \text{.....5.9}$$

where g(α) is a constant at a given value of conversion. The subscript α and i are a value of conversion and heating rate respectively. The plot of ln (β) *vs* $1/T$ should yield a straight line with the slope equals $-1.052\, E_\alpha/R$ and the Y-intercept that equals $\ln\left(A_\alpha E_\alpha / Rg(\alpha)\right) - 5.331$. In this study the kinetic parameter E_a for the reduction of phosphogypsum with graphite obtained from the OFW method will be compared to that obtained by following the KAS method. The E_a in the KAS method is derived from the slope of the plot of $\ln\left(\beta/T_{\alpha i}^2\right)$ *vs* $1/T_{\alpha i}$ for a given value of conversion (α).

This plot should yield a straight line with the slope equals $-E_\alpha/R$ and it is derived from Equation 5.10. The Y intercept equals $\ln\left(AR/Eg(\alpha)\right)$ from which the pre-exponential factor, A, can be calculated

$$\ln\left(\beta/T^2\right) = \ln\left(A_\alpha R/E_\alpha g(\alpha)\right) - E_\alpha/RT \quad \text{..... 5.10}$$

Experimental

Non-isothermal reaction of phosphogypsum (PG) reduction with graphite was carried out using the TG-DSC analyser SDT Q600. About 6 mg of sample was heated under ultrapure nitrogen in the temperature range 25-1200 ºC. The nitrogen flow rates and the heating rates applied at different molar ratios are summarised on Table 5.2.

Table 5.2: Experimental setting for kinetic studies

PG: C Molar ratio	Heat rate (°C/min)	N_2 Flow rate (ml/min)
1:2	20	100
1:3	15	100
1:3	20	100
1:3	25	100
1:3	30	100
1:3	20	75
1:3	20	125
1:3	20	150
1:4	20	100

Results and discussion

Effect of molar ratio

Figure 5.4 shows the thermograph (TG) for the molar ratios of PG:C ratios of 1:2, 1:3, and 1:4. The thermal event at 80-150 ºC is associated with the dehydration of gypsum to anhydrite via hemihydrate. The low resolution of the TG makes the clear distinction of the two dehydration step unclear. These dehydration steps indicated as (A) on the thermograph are followed by a gradual mass loss (B) up to the onset temperature of the next thermal event around 800 ºC indicated on the thermograph as (C). The stoichiometric calculated residual mass reduction of PG with C to calcium sulphide, based on Equation 5.2 is 34.7%. The molar ratio of C/PG =3 gives a residual mass value 35.7%, the closest to the theoretically calculated, compared to the 32.3% and 37.5% obtained for the ratios 2 and 4 respectively.

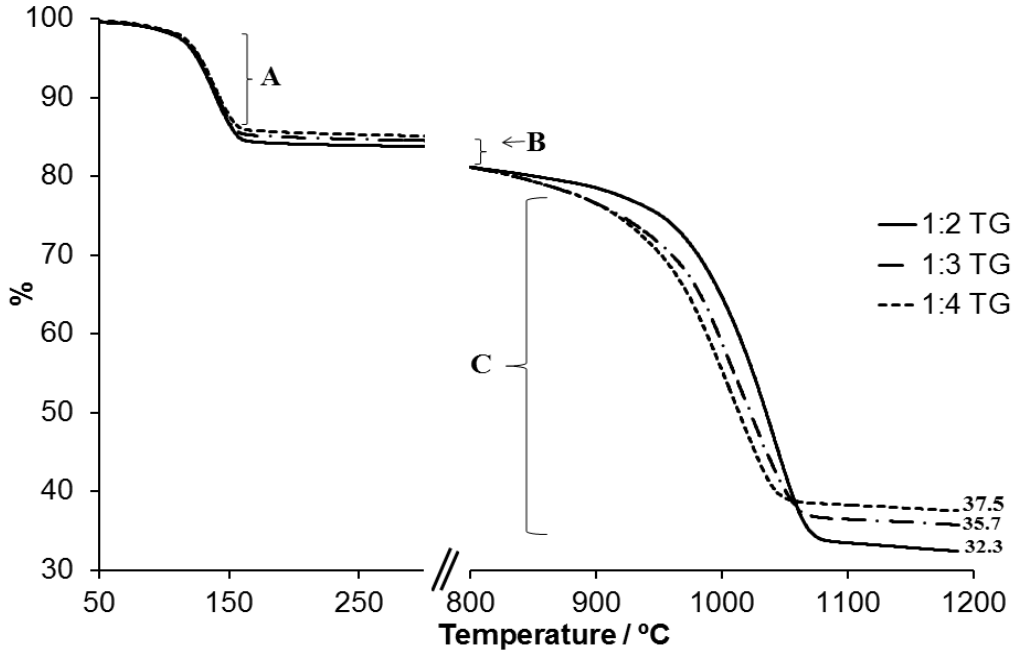


Figure 5.4: Thermographs of phosphogypsum reaction with graphite in molar ratios (PG:C) of 1:2, 1:3 and 1:4

Effect of N_2 gas flow rate

Figure 5.5 shows the TG for the N_2 flow rates of 75; 100, 125 and 150 m//min for the C/PG molar ratio of 3. The thermal event associated with the dehydration of gypsum to anhydrite is observed in similar temperature range for all the N_2 flow rates applied. The increase in N_2 flow rate from 75 to 125 m//min resulted in no observable effect on the onset temperature of around 800 ºC and the maximum reaction temperature of around 1090 ºC. The N_2 flow increase to 150 ml/min slowed down the conversion rate and the overall residual mass at the end of the reaction.

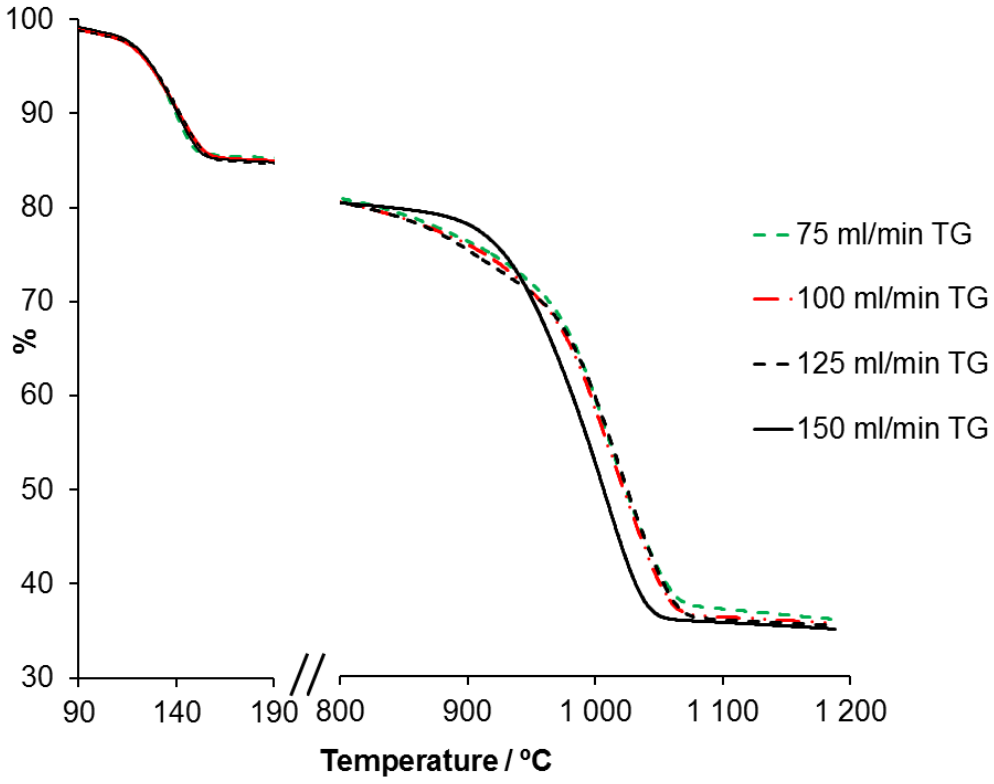


Figure 5.5: TG analysis of the reaction between phosphogypsum and graphite at molar ratio (1:2) at varying N_2 flow rates

The residual mass (M_R) is plotted against the N_2 flow rate in Figure 5.6. The dependency of the overall conversion of phosphogypsum on the N_2 flow rate can be described by the logarithmic function y = -0.0135

x+37.161, where y is the residual mass % and x is the N_2 flow rate with a regression coefficient (R^2) of 97%. The observed decrease in the residual mass towards the expected (theoretical) value with the increase in the N_2 flow rate suggests the formation of gaseous reaction products whose removal drives the phosphogypsum reduction reaction forward.

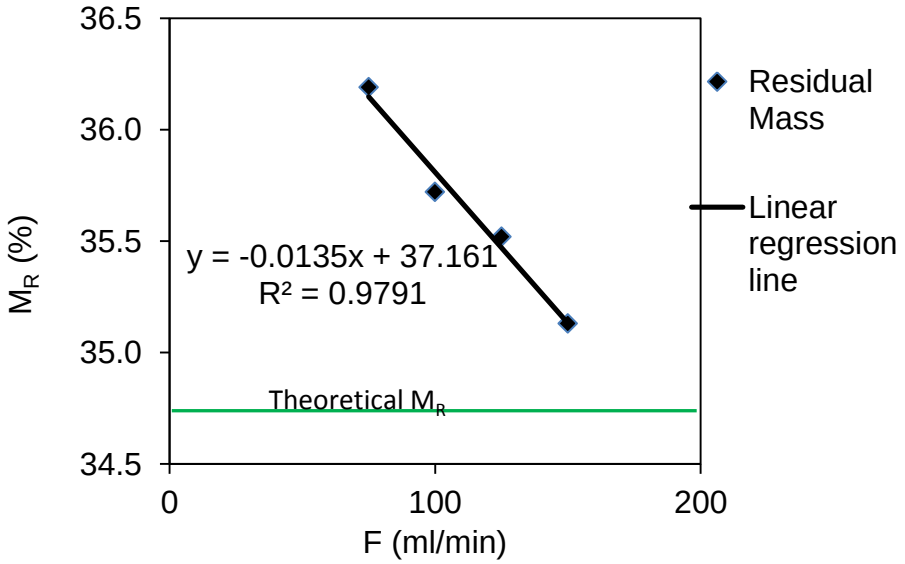


Figure 5.6: Dependency of residual mass (M_R) on the N_2 Flow rate (F)

Based on these results, the reaction conditions for studying the reaction kinetics were optimised to a molar ratio of PG:C (1:3) and the nitrogen flow rate of 100 m//min. This flow rate is in line with that applied for the in situ Raman spectroscopic study in section 5.5.

Effect of heating rate

The reaction conditions for studying the reaction kinetics were: a molar ratio of PG:C (1:3) and the nitrogen flow rate of 100 m//min. Figure 5.7 shows the normalized mass loss in the temperature range 25-1200 ºC under the heating rates 15, 20, 25 and 30 ºC/min. The thermal event below 200 ºC, resulting in mass loss of approximately 23% is attributed to the loss volatiles and the of gypsum crystal water to form hemihydrate

(Ballirano and Melis, 2009a), then anhydrite (Ballirano and Melis, 2009b) as described by Equation 5.11.

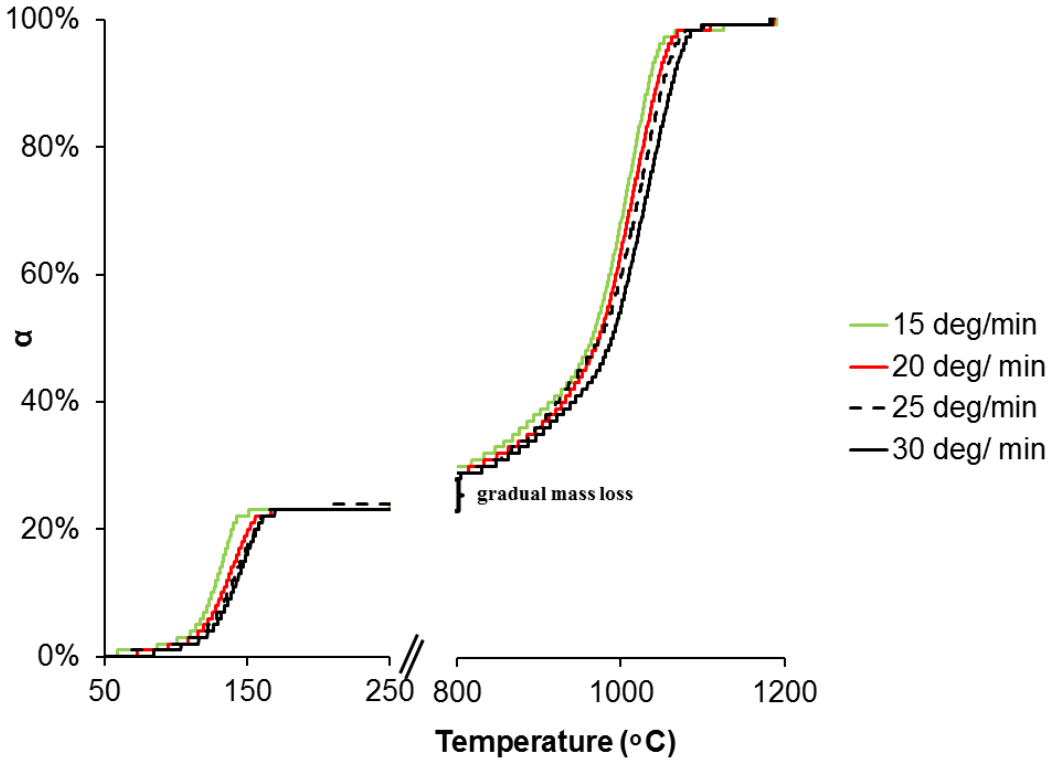


Figure 5.7: Normalised mass loss for the reaction between phosphogypsum and graphite

There is a gradual mass loss between 600 ºC and 800 ºC that has been explained by the Ellingham Diagram as the combustion of graphite to a mixture of carbon monoxide and carbon dioxide (Nengovhela, 2008). This event is followed by the thermal reduction of anhydrite to calcium sulphide as described by Equation 5.12.

$$CaSO_4.2H_2O(s) \xrightarrow{80^{\circ}C} CaSO_4.0.5H_2O \xrightarrow{142^{\circ}C} \gamma - CaSO_4(s) + 2H_2O(g) \quad (5.11)$$

$$CaSO_4(s) + 4CO(g) \rightarrow CaS(s) + 4CO_2(g) \quad (5.12)$$

Figure 5.8 depicts the first derivatives of the thermographs (dTG) of the mass loss at the heating rates 15, 20, 25 and 30 ºC/min. Two events not evident in Figure 5.7 are indicated with letters A & B in Figure 5.8. The thermal A is the dehydration of gypsum to hemihydrate as shown in Equation 5.11 followed by the dehydration to anhydrite. Around 900 ºC, the event B that results in a 11% mass loss and is attributed to the formation of an intermediate compound before the formation of CaS. This intermediate has been reported by Msila *et al* (2015) as a dehydrated orschallite type compound.

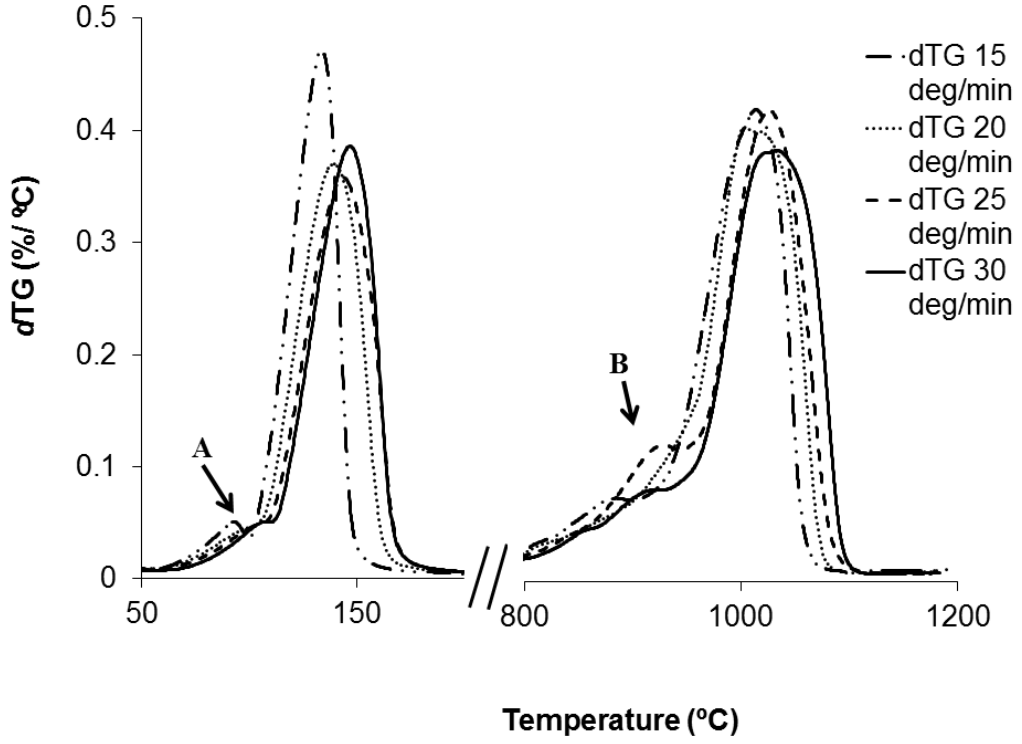


Figure 5.8: First derivative of the thermographs of phosphogypsum reduction with graphite at heating rates 15, 20, 25 and 30 ºC/min; A indicates the dehydration of gypsum to hemihydrate and B indicates the formation of an intermediate compound

The OFW and KAS plots were constructed according to Equations 5.9 and 5.10 are plotted Figures 5.9 and 5.10 respectively. The linear plots fit the OFW and the KAS models (R^2>0.9) in the conversion range 0-30% and the conversion range >60%.

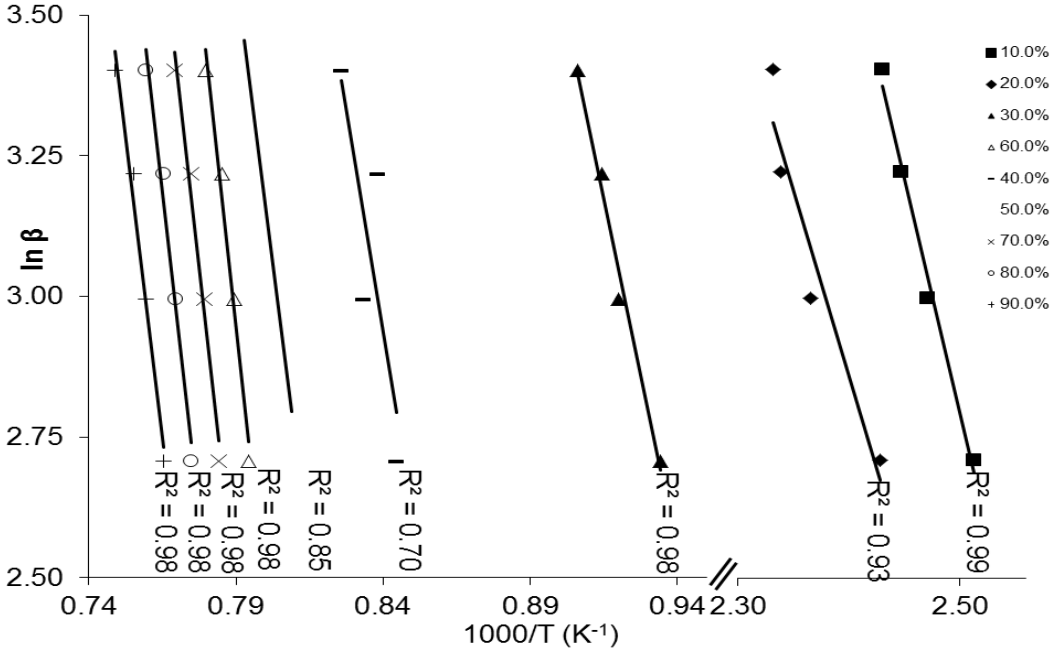


Figure 5.9: Plot according to Ozawa-Flynn-Wall method (OFW)

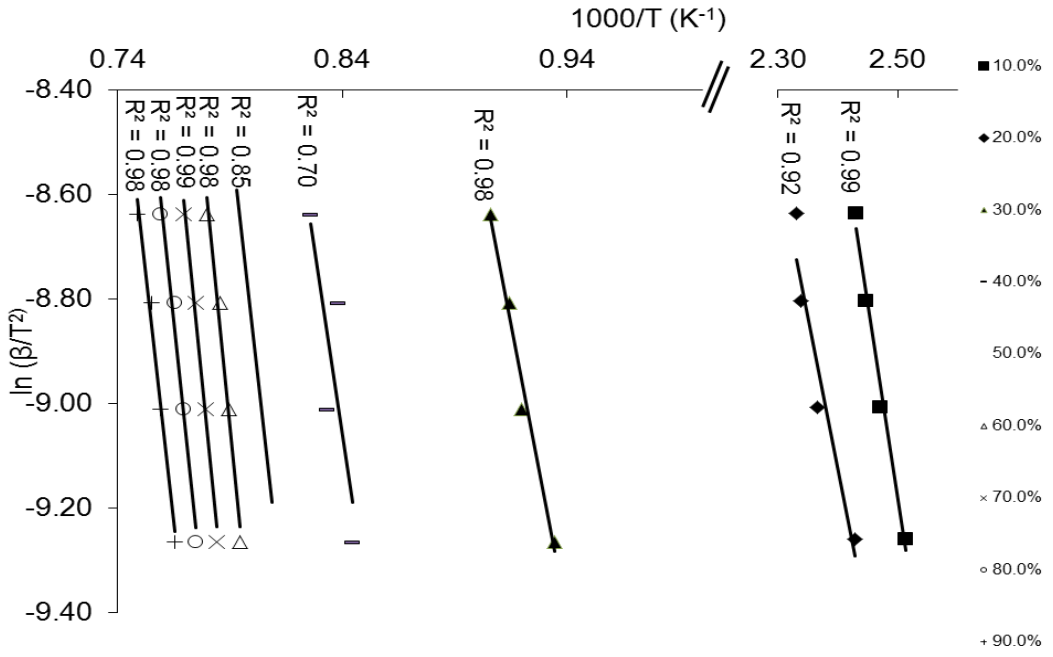


Figure 5.10: Plot according to Kissinger-Akahira-Sunose Method (KAS)

From the slopes of the linear curves in Figures 5.9 and 5.10, the apparent activated energies were calculated as per Equations 5.9 and 5.10. The calculated apparent activation energies are depicted in Figure 5.11. Three regions are evident in both the OFW and the KAS plot. Region 1 with the apparent E_a, 47-62 kJ/mol is in the conversion region $\alpha \leq 20\%$, is related to the thermal dehydration of gypsum to anhydrite; regions 2 with apparent E_a, 190-326 kJ/mol is related to the CO/CO_2 evolution in the region α=20-50%; Region 3: α>60% where the apparent E_a ranges 330-370 kJ/mol relates to the reduction of anhydrite. Following Vyazovkin and Lesnikovich (Vyzovkin and Lesnikovich, 1990) interpretation of the TG curve, the reduction of gypsum with graphite is a complex reaction composed of a series of independent parallel reactions.

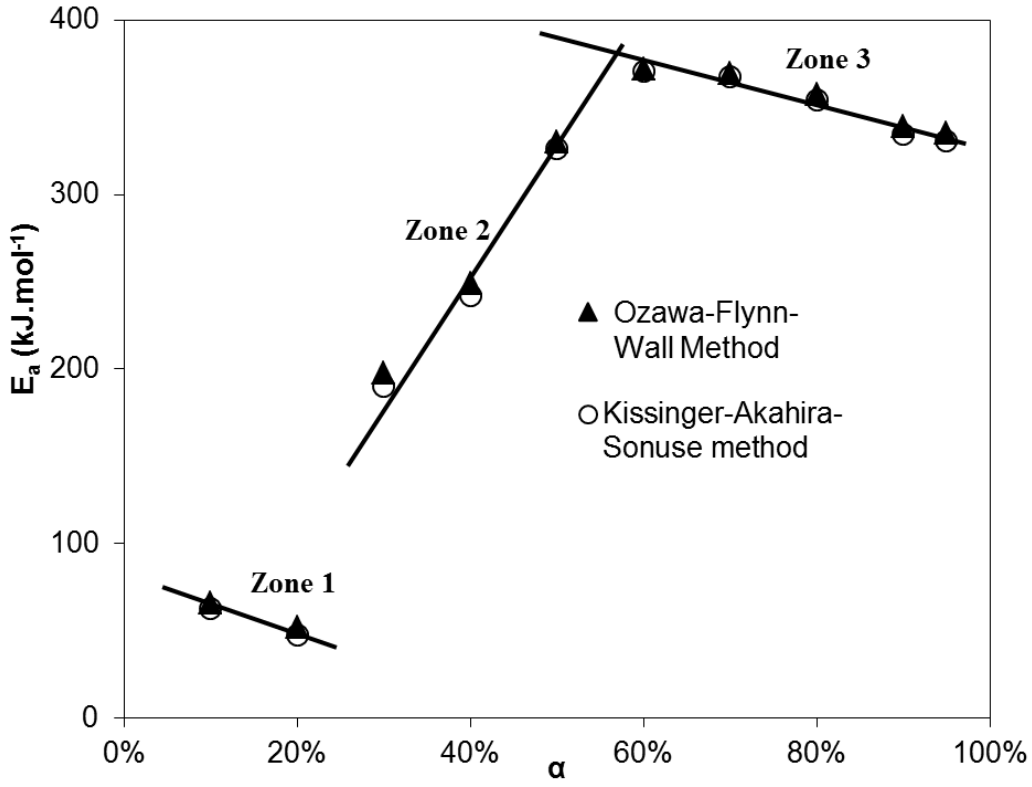


Figure 5.11: Activation energies calculated according to the OFW and KAS methods

Conclusions

The phosphogypsum reduction was preceded by a parallel dehydration to hemihydrate and anhydrite at temperatures below 200 ºC. The TSR was complete just above 1000 ºC, preceded by formation of an intermediate compound characterized by an 11% mass loss. The increase in the flow rate of N_2 is accompanied by the increase in the residual mass towards the theoretical value. Due to the increase of the calculated activation energy with the increase in conversion, the phosphogypsum reduction with graphite is determined to follow a complex mechanism with apparent activation energy determined by the OFW and KAS methods to be in the range 330-370 kJ/mol.

References

Akahira, T., Sunose, T. (1971) Method of determining activation deterioration constant of electrical insulating material, Res Report Chiba Institute of Technology, Sci Technol, vol.**16**, pp 22-31.

Al-Jundi, J., Al-Ahmad, N., Shehadeh, H., Afaneh, F., Maghrabi M. and Gerstmann, U. (2008), Investigation on The Activity Concentrations Of ^{238}U, ^{226}Ra, ^{228}Ra, ^{210}Pb and ^{40}K In Jordan Phosphogypsum And Fertilizers. *Radiation Protection Dosimetry,* vol. **131**, no. 4, pp 449-454.

Apaydin-Varol, E. (2014) Pyrolysis kinetics and thermal decomposition behaviour of polycarbonate – a TGA-FTIR study. *Thermal Science*, vol. **18**, no. 3, pp 833-942.

Ballirano, P. and Melis, E. (2009) Thermal behaviour and kinetics of dehydration in air of basanite, calcium sulphate hemihydrate ($CaSO_4.0.5H_2O$), from X-ray Powder diffraction. *European Journal of Mineralogy*, vol. **21**, pp 985-993.

Ballirano, P. and Melis, E. (2009) Thermal behaviour and kinetics of gypsum in air of basanite from in situ real-time laboratory parallel-beam X-ray Powder diffraction. *Physics and Chemistry of Minerals*, vol. **36**, pp 391-402.

Ding, K., Li, S., Yue, C. and Zhong, N. (2007) Simulation Experiments on Thermochemical Sulfate Reduction Using Natural Gas. *Journal of Fuel Chemistry and Technology*, vol. **35**, pp 401-406.

Ellis, G.S.**,** Zhang, T.**,** Ma, Q. and Tang, Y. (2007) Theoretical study on the reactivity of sulfate species with hydrocarbons: *Geochimica et Cosmochimica Acta,* vol. **72**, no. 18, pp 4565-4576.

Flynn, J.H., Wall, L.A. (1966) General treatment of the thermogravimetry of polymers. J Res Nat Bur Standards, Part A, vol. **70**, pp 487

Goldstein, T.P. and Aizenshtat, Z. (1994). Thermal sulphate reduction: A review. *Journal of Thermal Analysis*, vol. **42**, pp 241-290.

Ma, Q., Ellis, G.S., Amrani, A., Zhang, T. and Tang, Y. (2008) Theoretical study on the reactivity of sulfate species with hydrocarbons. *Geochimica et Cosmochimica Acta*, pp 4565-4576.

Machel, H.G. (2001) Bacterial and thermochemical sulfate reduction in diagenetic settings. *Sedimentary Geology*, vol. **140,** pp 143–175.

Maree, J.P., Theron, D., Nengovhela, N.R. and Hlabela, P.S. (2005) Sulphur from smelter gases and sulphate-rich effluents. *Journal of South African Institute of Mining and Metallurgy*, vol. **105**, pp 1-4.

Mihara, N., Soya, K., Kuchar, D., Fukuta, T. and Matsuda, H. (2008) Utilisation of calcium sulfide derived from waste gypsum boards for metal-containing wastewater treatment. *Global NEST Journal*, vol. **10**, no. 1, pp 101-107.

Msila, X., Barnard, W. and Billing, D.G. (2015) Raman spectroscopic study of phosphogypsum thermal reduction with the carbonaceous material. *Spectrochimica Acta A*, pp 317-322.

Nengovhela, R.N. *The recovery of sulphur from waste gypsum*, PhD Theses, University of Pretoria, 2008.

Pereira, F. and Bilal, E. (2012) Phosphoric acid extraction and rare earth recovery from apatites of the Brazilian phosphatic ore. *Romanian Journal of Mineral Deposits*, vol. **85**, no. 2, pp 49-52

Simon, P. (2004) Isoconventional methods: fundamental, meaning and application. *Journal of Thermal Analysis*, vol. **76**, no.1, pp 123-132.

Vyazovkin. S.V. and Lesnikovich, A.L. (1990) An approach to the solution of the inverse kinetic problem in the case of complex processes. Part 1. Methods employing a series of thermoanalytical curve. *Thermochimica Acta*, vol. **165**, pp 273-280.

Yue, C., Li, S., Ding, K. and Zhong, N. (2006) Thermodynamics and kinetics of reactions between C1-C3 hydrocarbons and calcium sulfate in deep carbonate reservoirs. *Geochemical Journal*, pp 87-94.

5.5 Published Research Article: Raman spectroscopy

Raman spectroscopic study of phosphogypsum thermal reduction with carbonaceous material

*Xolani Msila[1], Werner Barnard[2], Dave G. Billing[3]

[1]Sasol Dyno Nobel, 486 Brandbach Road, Ekandustria, Bronkhorstspruit, 1021. xolani.msila@sasol.com;

[2]Sasol Technology R&D, 1 Klasie Havenga Road, Sasolburg, 1947. werner.barnard@sasol.com.

[3]School of Chemistry, University of the Witwatersrand, Johannesburg, WITS 2050, South Africa

Abstract

Elemental sulphur (S) can be produced from hydrogen sulphide (H_2S) in a PIPco or Iron process. In turn H_2S can be stripped with carbon dioxide (CO_2) from calcium sulphide (CaS) obtained from the thermal reduction of phosphogypsum with carbon. The reaction pathway for the thermal reduction of the phosphogypsum with graphite was studied using Thermogravimetric analysis and *in situ* Raman spectroscopy. The dehydration of the phosphogypsum to anhydrite was completed at about 142 °C. The dehydration was followed by the formation of the intermediate compound at about 860 °C which is characterised by a mass loss of about 11%. The intermediate compound, identified using *in situ* Raman spectroscopy to be a dehydrated Orschallite-type compound ($Ca_3[SO_4][SO_3]_2$), converted to CaS at about 935 °C. The presence of the metal impurities in the phosphogypsum: Ni^{2+}(4 $mg.kg^{-1}$); Co^{2+}(2 $mg.kg^{-1}$); Mn^{2+}(5 $mg.kg^{-1}$); Cu^{2+}(14 $mg.kg^{-1}$); Fe^{2+}(200 $mg.kg^{-1}$) and Mg^{2+}(300

mg.kg^{-1}) showed no influence the onset temperature for the reduction reaction.

Key Words: Phosphogypsum, *in situ* Raman spectroscopy, thermal sulfate reduction.

Introduction

The association of the dissolved sulphate and hydrocarbons is thermodynamically unstable in virtually all diagenetic environments (Machel, 2001). Hence redox reaction occurs where sulphates are reduced by the hydrocarbons either bacterially (bacterial sulphate reduction- BSR) or inorganically (thermal sulphate reduction – TSR). Although TSR is thermodynamically possible at temperatures as low as 25 °C; there is evidence that BSR and TSR occur in two mutually exclusive thermal regimes. BSR predominantly occurs at shallow depth (T < 100 °C) and TSR in deeper evaporatic or carbonate reservoirs (T > 100 °C) (Machel, 2001). BSR by various electron donors is documented in the literature by Bijmans, 2008 and Kleikemper, 2003. The electron donors include hydrogen gas, synthetic gas, methane, methanol, ethanol, glycerol, acetate, lactate and organic waste (Bijmans, 2008). In addition to these, other e-donors have been evaluated in the laboratory studies of reduction of solid calcium sulphates (anhydrite and gypsum): C_1-C_3 hydrocarbons (Ellis *et al.,* 2007), CO and coal dust (Nengovhela *et al.*, 2007) and C_1-C_6 hydrocarbons (Ding *et al.*, 2007). Yue *et al.*, 2006, reported methane as the most non-reactive hydrocarbon in the TSR reaction in the range of hydrocarbons tested. This is in line with the finding by Machel, 2001. Machel suggested that the order of reactivity in hydrocarbons is: branched alkanes + *n*-alkanes > cyclic + mono aromatic compounds > methane. A common challenge in all the work carried out so far on TSR has been to reduce the activation energy of the redox reactions involved.

There have been many attempts to explain the redox reaction mechanism involved in the reduction of sulphate. Machel, 2001 singled out temperature to be the most important factor that governs the redox reactions involved in the TSR. However, there are other potential factors that enhance or reduce the rate of TSR in a natural environment such as: (i) initial total sulphur concentration; (ii) pH; (iii) salts (soaps) of inorganic acids; (iv) organic acids; (v) metal complexes; (vi) catalytic action of Ni^{2+}, Co^{2+}, Mn^{2+}, Cu^{2+}, Fe^{2+}, Ca^{2+} and Mg^{2+}; (vii) organic compounds such as phenols, aldehydes aniline, urea, and vanillin; and (viii) clay minerals particularly montmorillonite; and silica gel. The effect of the many of these factors is not well understood but it is clear that the increase in temperature and the initial concentration of H_2S enhances the rate of TSR (Ellis *et al.*, 2007).

Ma *et al.*, 2008 in the theoretical study of the mechanism of TSR, elucidated the catalytic function played by the H_2S in reduction of sulphate. Sulphate anions are symmetric tetrahedrons with S-O bond lengths of 1,47 Å and O-S-O bond angle of 109° (Ma *et al.*, 2008; Ellis *et al.*, 2007). This makes sulphate extremely unreactive to reduction by hydrocarbons with the activation energy of 234 - 354 $kJ.mol^{-1}$ (Ellis *et al*., 2007; Goldstein and Aizenshtat, 1994) H_2S dissociates in water to form HS^- and H^+. The acidification of water by the dissociation of H_2S encourages the formation of protonated sulphate (HSO_4^-). The more acidic the water is the more bisulphate forms. The resulting protonated S-O bond is longer (weaker); 1,71 Å and the resulting molecule is polar with a total dipolar moment of 3,02 Debye. The presence of H_2S therefore lowers the activation energy for sulphate reduction to 222 $kJ.mol^{-1}$. This mechanism required H_2S to dissociate for the H^+ to protonate the sulphate, which in turn has to be in its dissolved anionic form. The wettability of calcium sulphate therefore becomes an important parameter to be considered.

Ellis *et al.*, 2007 carried out experiments that confirmed catalysis of TSR by H_2S. They further suggested that magnesium played a significant role in a two-stage reduction of sulphate. Therefore they proposed that the mechanism involved the formation of contact ion-pairs between Mg^{2+} and SO_4^{2-} ions in solution. The formation of $MgSO_4$ contact ion-pairs by Mg^{2+} bidentate coordination changed the symmetry of the SO_4^{2-} ion from T_d to $C_{2v.}$ This coordination results in an increased S-O bond length. The longer S-O bond is weaker and easier to reduce.

Ding *et al.*, 2007 studied the role of labile sulphur compounds in TSR, and proposed a different mechanism. They proposed that the mechanism occurs via the formation of sulphur radicals that enhances the formation of alkene compounds. The alkenes are easier to oxidise than alkanes. Prior to 1991 it was believed that the oxidation of hydrocarbons under geological conditions would not proceed unless the lower oxidation state sulphur, such as H_2S, is present (Goldstein and Aizenshtat, 1994). The geological conditions are characterised by, amongst other factors, the dissociated SO_4^{2-} salts in aqueous solution (Ellis *et al.*, 2007; Zhang *et al.*, 2008; Amrani *et al.*, 2008). The presence of initial low oxidation state sulphur has been shown to increase the rate of TSR and lower the activation energy of the S-O bond rupture (Zhang *et al.*, 2008). Amrani *et al.*, 2008 carried out experiments to understand the role of labile sulphur compounds in TSR. Their findings disputed the mechanisms via (a) the thermal release of H_2S from the thiols; (b) generation of alkenes by leaving H_2S compounds; and (c) the radical formation followed by chain reaction of active compounds formation. They instead suggest that the thiols react directly with the sulphate resulting in the formation of sulphate ester. The ester formation results in the lower activation energy for the rupturing of the S-O bond.

But the conditions required for TSR in a geological environment have been shown not to be essential for the solid/liquid or the solid/gas such as in the reaction with C_1-C_6 hydrocarbons (Ding *et al.*, 2007); or with C_1-C_3

hydrocarbons under pressure (Yue *et al.* 2006); and solid-solid reaction such as coal dust and CO at ambient pressure (Nengovhela, *et al.*, 2007, Nengovhela *et al.*, 2008). These studies reported no dissociation of sulphate, acidification or H_2S initiation but showed that different carbon sources required different amount of energy to reduce the sulphate. The activation energy (E_a) for the reactions between solid gypsum and C_1-C_3 hydrocarbon were 152.9 kJ.mol^{-1}, 131.0 kJ.mol^{-1} and 120.6 kJ.mol^{-1} for C_1, C_2 and C_3 respectively, whereas the reaction of coal and carbon monoxide with gypsum the E_a was 14340 kJ.mol^{-1} and 28680 kJ.mol^{-1}.

It is evident from literature reports that the reaction mechanism of TSR in aqueous solution is not the same as those in solid/solid reaction. The study by Nengovhela *et al.*, 2008, which focused on the reaction of gypsum with coal dust and CO, proposed that the mechanism is complex and it results in the formation of CaS. In this study the authors follow the reaction mechanism pathway between graphite and phosphogypsum, a by-product from a phosphoric acid facility in the Lowveld region of South Africa. Thermogravimetric analysis and *in situ* Raman spectroscopy will be used under similar reaction conditions to those previously described by Mihara *et al.*, (2008) and optimised by Nengovhela, (2008).

Materials and methods

The concentrations of inorganic impurities in phosphogypsum were determined using an Inductively Coupled Plasma_Optical Emission Spectroscopy (ICP_OES). A stoichiometric carbon rich mixture of gypsum and the carbonaceous material (1:3 molar ratio) was prepared by mixing 17.2 g of gypsum with 3.6 g of carbon. The mixture was finely ground with the mortar and pestle. Thermogravimetric measurements were done using a TG-DSC analyser SDT Q600 instrument. About 6 mg of sample was heated from ambient temperature to 1200 °C at 20, 25 and 30 °C.min^{-1}, under constant flow of nitrogen (100 cm^3.min^{-1}).

In situ Raman measurements were carried out in a Linkam™ TS 1500 reactor controlled by the TMS 94. A stoichiometrically carbon-rich mixture of graphite: gypsum (3:1 molar ratio) was reacted up to 1080 °C, under a 100 $cm^3.min^{-1}$ continuous nitrogen flow. The mixture was heated up at the rate of 20 $°C.min^{-1}$ to set temperatures then quenched before Raman scans were taken on the Bruker Raman spectrometer equipped with charge-coupled device detector and a green laser (λ = 532 nm). Blank runs for gypsum and the carbonaceous material were also carried out under the same conditions. The commercial grades of likely products of gypsum decomposition and gypsum reduction with carbon such as calcium sulphite in the form of hannebachite $(CaSO_3)_2.H_2O$ and calcium oxide were analysed under ambient conditions.

Results and discussion

Raman characterisation of the reactants: phosphogypsum and the carbonaceous material - before and after heating

Gypsum crystallises in monoclinic crystal system, space group *C*2/*c* (Ray *et al.*, 2010). Each sulphate is tetrahedrally bonded to the calcium ion although a distinct distortion of the shape commonly occurs which gives rise to band splitting in Raman spectroscopy (Sama *et al.*, 1998). Factor group analysis predicts 72 vibration modes for gypsum belonging to the irreducible representations: $17A_g^R$ +17 A_u^{IR} + $19B_g^R$ + 19 B_u^{IR} (Sama *et al.*, 1998 and Berenblut *et al.*, 1973). In this study 8 peaks are observed). The observed Raman bands are assigned and compared to the published data in Table 5.3.

Table 5.3: Band positions (cm^{-1}) for phosphogypsum before and after heating to 1080 °C and assignments

This work		Sama *et al*., 1998; Compton, 2003	Berenblut *et al.,* 1973	Assignment
Before heat	After heat			
415	417	420	416	ν_2 SO_4 B_{3g}
495	500	494	498	ν_2 SO_4 A_g
620	610,630 (d)	623	626	ν_4 SO_4 B_{2g}
673	677			
1009	1019	1008	1016	ν_1 SO_4 A_g
1139	1114,1130,1162	1139(triplet)	1128	ν_3 SO_4 B_{1g}
-		3264		ν_2 (H_2O)
3407		3345		ν_1 (H_2O)
3496		3452		ν_3 (H_2O)

No reaction or breakdown of phosphogypsum was observed when it was heated under continuous flow of N_2 up to a temperature of 1080 °C. The dehydration of phosphogypsum under continuous N_2 flow is characterised by the shift in the ν_1 SO_4 shift from 1009 cm-1 to the higher wave numbers, 1019 cm^{-1}. The v_3 SO_4 band is resolved into a triplet at 1124 cm^{-1}, 1130 cm^{-1} and 1162 cm^{-1}. Sama, *et al.*, (1998) attributes this behaviour

to the symmetry changes as the gypsum dehydrates. A large shift of the SO4 modes in gypsum from the free T_d symmetry also corroborates the distortion. They argued that all internal modes splitting of SO_4 in gypsum could be explained using $T_d \rightarrow C_2 \rightarrow C_{6h}^2$ correlations. Furthermore, the internal modes also showed non-uniform splitting, which was attributed to the distortion of SO_4 tetrahedral.

Characterisation of carbonaceous material and its heating product

The carbon D shift is observed at 1360 cm^{-1}, the G shift or E_{2g} of graphite carbons is observed at 1597 cm^{-1}. These observations are in good agreement with those reported in literature (Nakamizo *et al.*, 1974; González *et al.*, 2003 and Sadesky *et al.*, 2005) for the deformed graphitic structure and sp^3 carbon shift. The band at 2914 cm^{-1} are the combination of the D and the G band (D+G) whereas the band at 3177 cm^{-1} is the G band overtone (G+G) A broad shoulder around 2700 cm^{-1} is visible. This can be attributed to the D band overtone (D+D) or 2D.

The Raman spectra of graphite used before and after heating to 1080 °C under continuous N_2 flow are shown in Figure 5.12 and Figure 5.13 respectively.

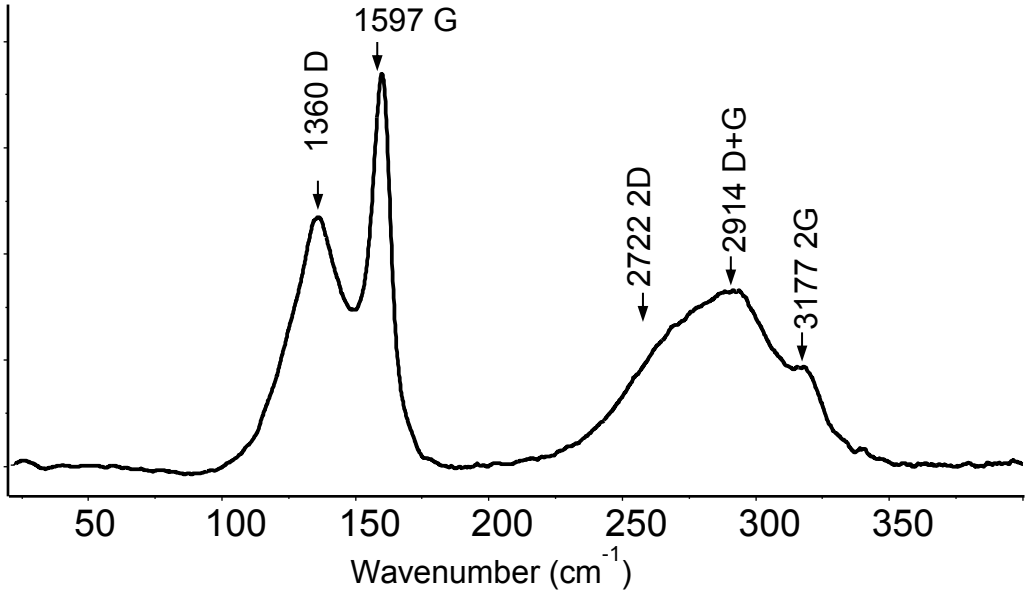


Figure 5.12: Room temperature Raman spectrum of the carbonaceous materials before heating

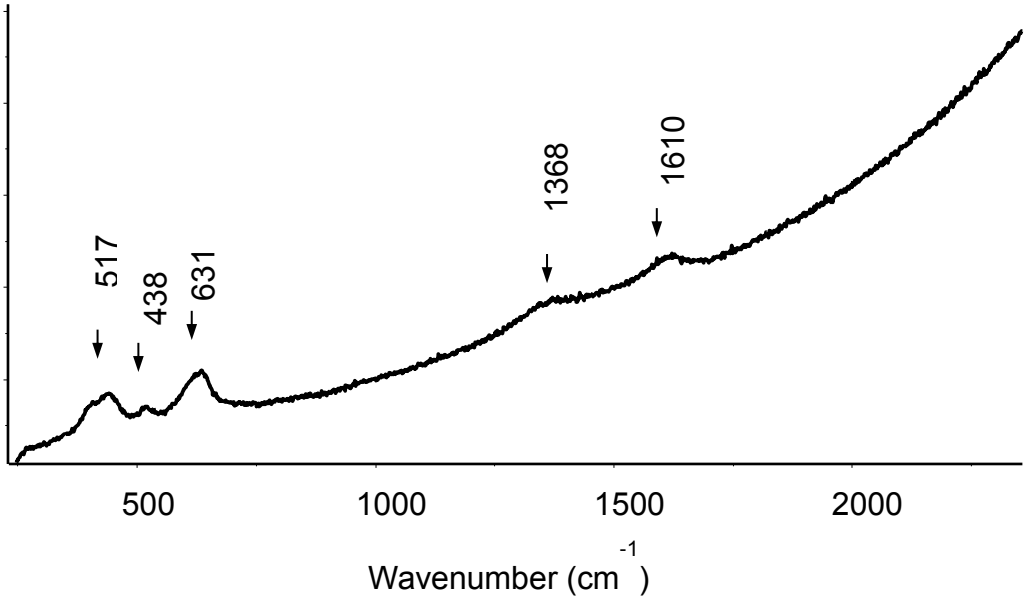


Figure 5.13: Room temperature Raman spectrum of graphite heated under continuous N_2 flow to 1080 °C

The carbonaceous material type used was therefore confirmed to be a disordered graphitic carbon. After heating to 1080 °C the D and the G Raman shifts at 1368 cm^{-1} and 1610 cm^{-1} are still weakly visible as shown in Figure 5.13. Non-fundamental Raman shifts are observed at 438 cm^{-1}, 517 cm^{-1} and 631 cm^{-1}. These Raman shift are attributed to the presence of impurities in the carbon analysed. The lower intensities of the D and G

bands after heating as well as the frequency change of the G band is an indication of structural changes in the carbonaceous material.

Reaction between gypsum and the graphitic carbon under continuous N_2 flow

Thermogravimetric analysis of phosphogypsum + graphite reaction mix

Figure 5.14 shows the first derivative of the thermograph of graphite mixed with phosphogypsum. Five thermal events observed are indicated as E1, E2…E5. E1 occurs around 80 °C and E2 begins around 142 °C and it was previously described by Nengovhela (2008) as associated with the loss of gypsum's crystal water as described by the Equation 5.13.

$$CaSO_4 \cdot 2H_2O(s) \rightarrow CaSO_4 \cdot 0.5H_2O \rightarrow \gamma\text{-}CaSO_4(s) + 2H_2O(g) \quad (5.13)$$

These events result in a loss of 16.9% mass, a very close estimation to the expected 17% if an assumption is made that only the crystal water is released and no graphite has oxidised up to around 180 °C. The third thermal event (E3) is gradual mass loss of approximately 2%, between 600 °C – 850 °C. Nengovhela (2008) attributed this event to oxidation of graphite to carbon dioxide due to presence of trace amounts oxygen, possibly in the N_2 gas used. The carbon oxidation reaction is shown in Equation 5.14.

$$C(s) + O_2(g) \rightarrow CO_2(g) \quad (5.14)$$

This oxidation event leaves enough graphite to react with the phosphogypsum. Nengovhela (2008) described one more event at 900 °C

-1100 °C, described in the thermograph as (E5). The reaction can be represented by Equation 5.15.

$$CaSO_4(s) + 2C(s) \rightarrow CaS(s) + 2\,CO_2(g) \quad (5.15)$$

The formation of calcium sulphide as the end product would result in a calculated residual percentage of 35%. According to Kato *et al*., (2012) there is one more transformation after the calcium sulphide, which is the formation of calcium oxide (CaO). The CaO formation would lead to a theoretical residual value of 27%. This value is far from the actual 35% observed in this study and therefore calcium sulphide is the more likely product of the reaction under current conditions and not the CaO.

The onset temperature for the formation of calcium sulphide, measured to be 937 °C, in this study is comparable to that reported by Nengovhela for FGD gypsum. The catalytic behaviour of Ni^{2+}(4 $mg.kg^{-1}$); Co^{2+}(2 $mg.kg^{-1}$); Mn^{2+}(5 $mg.kg^{-1}$); Cu^{2+}(14 $mg.kg^{-1}$); Fe^{2+}(200 $mg.kg^{-1}$) and Mg^{2+}(300 $mg.kg^{-1}$) reported by Ellis *et al.*, 2007 to lower the activation energy of sulphate reduction could not be confirmed at the concentration level of impurities measured in this study.

The thermal events indicated by E4 around 869 ºC in the 1st derivative of the thermograph have not previously been reported. These thermal events, which precedes and overlaps with the formation of the calcium sulphide are characterised by mass loss of approximately 11% and is an indication of the formation of intermediate compound.

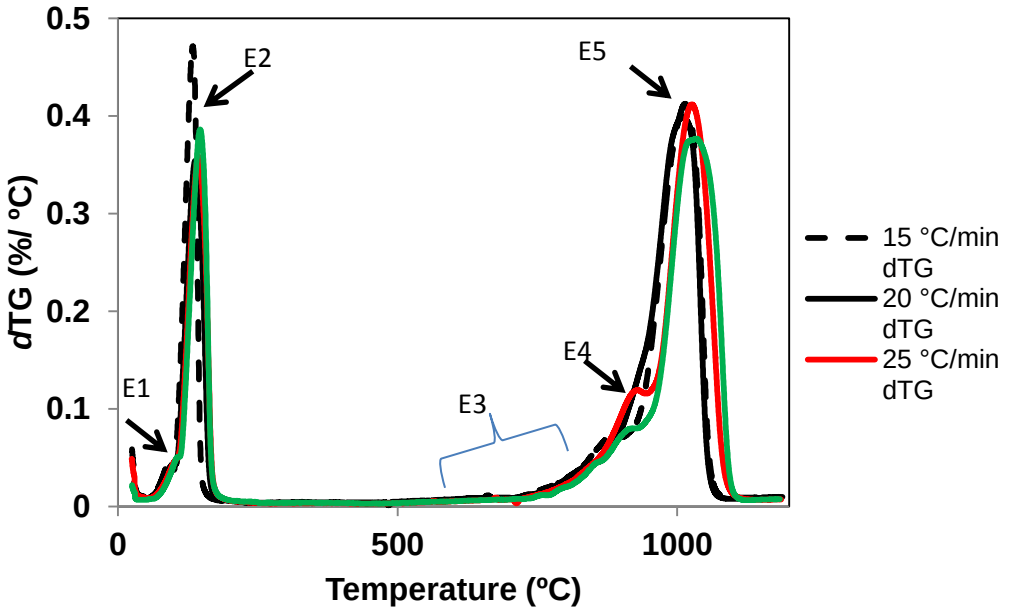


Figure 5.14: First derivatives of the thermographs of phosphogypsum + carbonaceous material (1:3 molar ratio)

Elimination of possible dehydration, decomposition and thermal reduction products

There are several possible transformations when phosphogypsum is heated from ambient to above 1080 °C. When gypsum is reacted with different electron donors such as C or CO the products vary depending on whether the environment in oxidative or inert. The possible reactions are shown Equation 5.16 - 5.18, CaO is the most likely decomposition product of anhydrite decomposition:

Decomposition of anhydrite to CaO

$CaSO_4(s) \xrightarrow{1227^{\circ}C} CaO(s) + SO_3(g)$ (Tian *et al.*, 2008) ..... (5.16)

$CaSO_4(s) + CO \rightarrow CaO(s) + SO_2(g) + CO_2$ (g) (Mihara *et al.*, 2008) ..... (5.17)

$3CaSO_4(s) + CaS \rightarrow 4CaO(s) + 4SO_2(g) + CO_2(g)$ (Mihara *et al.*, 2008) …..(5.18)

Tian *et al.*, 2008 reported the activation energy for decomposition of $CaSO_4$ to CaO to be 992 $kJ.mol^{-1}$. They further suggest that although the decomposition of $CaSO_4$ to CaO occurs around 1227 °C, the activation energy is greatly reduced in inert conditions and the rate of decomposition is increased which makes the possibility of CaO formation at 1000 °C under N_2 flow a possibility. CaO crystallises in a cubic space group *Fd* $\bar{3}$ *m* Although factor group analysis predicts no Raman active bands for CaO, a weak non-fundamental band was observed at 360 cm^{-1} (Figure 5.15). This band has previously been observed by Chang (1996) at 352 cm^{-1}. Other non-fundamental shifts are observed at 650 cm^{-1}, 1126 cm^{-1}, 1354 cm^{-1}, 1544 cm^{-1}, 1626 cm^{-1}, 1819 cm^{-1} and 2020 cm^{-1} possible due to structural defects on CaO.

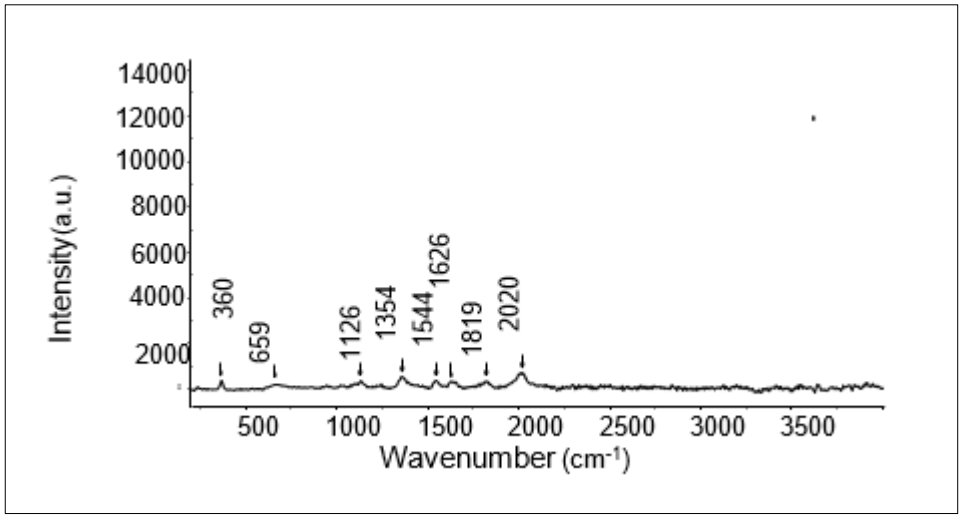


Figure 5.15: Raman spectrum of CaO

Raman identification of the intermediate compound

CaS crystallises in the cubic crystal system, space group $Pm\bar{3}m$ Wyckoff positions 4a (George *et al.*, 1963). Using the online method of Kroumova *et al.*, (2003) predicts CaS to have no Raman active and one IR active vibration modes. *In situ* analysis of the gypsum and graphite reaction is expected to be accompanied by the disappearance of anhydrite bands (Figure 5.16).

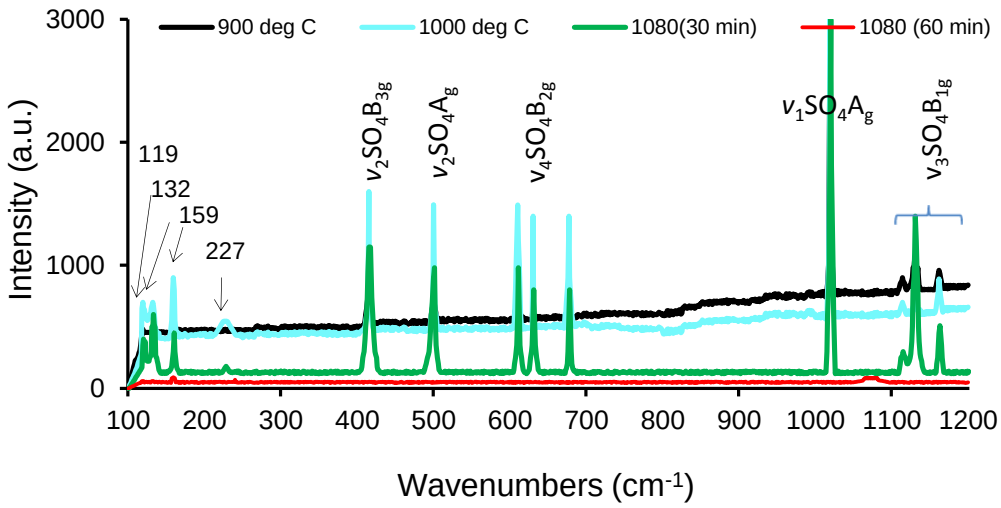


Figure 5.16: Raman spectra of graphite: gypsum reaction at 900 °C- black; 1000 °C - turquoise, 1080 °C (30min)-green & 1080 °C (60min)- red

In the reaction between gypsum and the graphitic carbon Raman bands at 119 cm^{-1}; 132 cm^{-1}; 159 cm^{-1}; 167 cm^{-1} and 227 cm^{-1} are observed at temperatures above 900 °C (Figure 5.15). Frost and Keeffe, (2009) reported bands for hannebachite $(CaSO_3)_2.H_2O$ at 1000 cm^{-1}, 969 cm^{-1}, 655 cm^{-1} with multiple bands for the ν_4 (E) mode at 444 cm^{-1}, 492 cm^{-1} and 520 cm^{-1}. In this study the bands for hannebachite were measured at: $\nu_1(A_1)$ symmetric stretching mode at 993 cm^{-1} and $\nu_4(E)$ bending modes at 472 cm^{-1} and 442 cm^{-1}. Lower wavenumbers bands are observed at 149 cm^{-1} and 218 cm^{-1}. These bands are attributed to lower symmetry SO_3^{-2}

bending modes. Ross (1972) reported $CaSO_3.2H_2O$ to have Raman active bands at 972 cm^{-1} $\nu_1(A_1)$; 937 cm^{-1} $\nu_3(E)$; 634 cm^{-1} $\nu_2(A_1)$ and 457 cm^{-1} $\nu_4(E)$. Frost and Keeffe (2009) explained the difference between the hannebachite and calcium sulphite, band positions to be due to the SO_3^{2-} anion bonding to Ca^{2+} through the sulphur atom as opposed to the oxygen atom. The low frequency Raman bands at 119 cm^{-1}; 132 cm^{-1}; 159 cm^{-1}; 167 cm^{-1} and 227 cm^{-1} observed in Figure 5.16 cannot be explained by formation of hannebachite or a $CaSO_3$ type of a compound as an intermediate before the formation of CaS.

The structure of orschallite is shown in Figure 5.17. It shows two distinct environments for S^{+6} and the S^{+4} where the SO_3^{2-} appears to be bonded to the Ca^{2+} ion and SO_4^{2-} appears in discrete octahedrals.

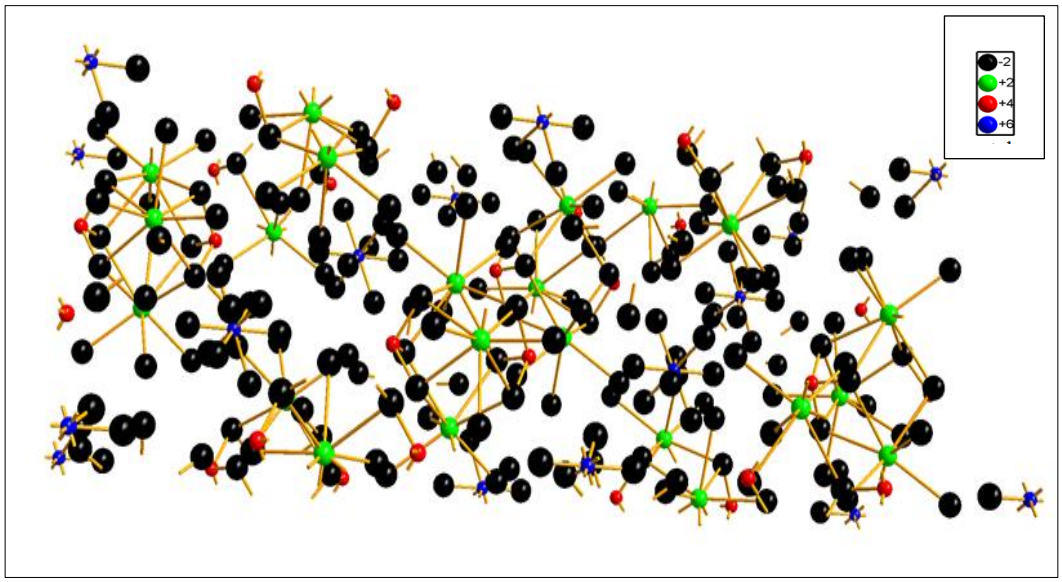


Figure 5.17: Wire or sticks model of Orschallite ($Ca_3[SO_4][SO_3]_2 \cdot 12H_2O$) from Diamond crystal visualisation software [black - O^{2-}; green - Ca^{2+}; red - S^{4+}; blue - S^{6+}]

Frost and Keeffe (2009) further report the observation of Raman bands at 119 cm^{-1}, 148 cm^{-1}, 173 cm^{-1}, 194 cm^{-1} and 264 cm^{-1}. These bands are associated with the lower symmetry SO_3^{2-} bending modes in orschallite. These bands observed in the current study can be associated with those

described for SO_3^{2-} bending mode in orschallite. It is proposed that the transformation of $CaSO_4$ to CaS goes through a rearrangement to dehydrated orschallite-type compound. The oxygen is lost in the formation of CO which is driven off by the N_2 flow. The proposed reaction pathway is described by Equation 5.19

$$3CaSO_4 \cdot 2H_2O(s) + 6C \rightarrow 3CaSO_4(s) + 6C(s) \rightarrow Ca_3[SO_4][SO_3](s) + 4C + 2CO_2(g) \rightarrow 3CaS(s) + 4CO_2(g) \quad (5.19)$$

The reaction after the dehydration of gypsum will therefore proceed in at least two steps as proposed by the balanced equation. The loss of 11% mass in E4 during the TGA accounts for half of the expected mass loss from the proposed reaction pathway. This implies that the transformation to CaS overlaps with the formation of the $Ca_3[SO_4][SO_3]_2$ type compound and evolution of carbon monoxide.

Conclusions

Gypsum does not decompose under N_2 or air blanket up to the temperature of 1080 °C, but dehydrates to anhydrite. When phosphogypsum is reacted with graphite under N_2 blanket, it dehydrates to hemihydrate around 80 °C then to anhydrite at around 142 °C. An intermediate compound forms around 869 °C. This intermediate compound is identified by Raman spectroscopy to be a dehydrated orschallite-type compound, accompanied by the evolution of carbon monoxide. The orschallite-type compound transforms to CaS. The transformation to CaS was complete at the temperature of around 1080 °C.

References

Amrani, A., Zhang, T., Ma, Q., Ellis, G.S., Tang, Y. (2008). Theoretical study on the reactivity of sulfate species with hydrocarbons. *Geochimica et Cosmochimica* Acta, vol. **72**. no.18, pp 4565-4576.

Berenblut, B.J., Dawson, P., Wilkinson, G.R. (1973) A comparison of the Raman spectra of anhydrite ($CaSO_4$) and gypsum ($CaSO_4 \cdot 2H_2O$), *Spectrochimica Acta*. vol. **29**, pp 29-36.

Bijmans, M.F.M. *Sulfate Reduction under Acidic Conditions for Selective Metals Recovery,* PhD Theses, Wageningen Universiteit, 2008.

Chang, H. (1996) The Role of HgO in Synthesizing Hg-Compounds. *Chinese Journal of Physics*, vol. **34**, no.2, pp 310-314.

De Villiers, J.P.R. (1971) Crystal structures of Aragonite, Strontianite and Witherite. *American Mineralogist*, vol. **56**, pp 758-767.

Ding, K., Li, S., Yue, C. and Zhong, N. (2007) Simulation Experiments on Thermochemical Sulfate Reduction Using Natural Gas. *The Journal of Fuel Chemistry and Technology*, vol. **35**, no. 4, pp 401-406.

Ellis, G.S.**,** Zhang, T.**,** Ma, Q. and Tang, Y. (2007) Theoretical study on the reactivity of sulfate species with hydrocarbons: *Geochimica et Cosmochimica Acta,* vol. **72**, no. 18, pp 4565-4576.

Emeleus, H.J. and Sharpe, A.G. *Advances in Inorganic Chemistry and Radiochemistry,* vol. ***18***, 1977. pp 287. (Academic press Incorporated).

Frost, R.L., Keeffe, E.C. (2009) Raman spectroscopic study of the sulphite bearing minerals scotlandite, hannebachite and orschallite –implications for the desulphation of soils. *Journal of Raman Spectroscopy*, vol. **40**, no. 3, pp 244-248.

Goldstein, T.P. and Aizenshtat, Z. (1994). Thermal sulphate reduction: A review. *Journal of Thermal Analysis*, vol. **42**, pp 241-290.

González, D., Miguel, A.M-M. and Garcia, A.B (2003) Graphite materials prepared from anthracite; a structural characterisation. *Energy Fuel*, vol. **17**, pp 1324 -1329.

http://www.cryst.ehu.es/rep/sam.html {Free online solid state vibrational mode analysis} cited as Kroumova *et al.*, (2003) Phase transitions. Vol. **76**, no.1-2, pp 155

Jarosch, D. and Heger, G. (1986) Neutron diffraction refinement of the crystal structure of Aragonite. *Mineralogische und Petrographische Mitteilugen*, vol. **35**, pp 27-131.

Kleikemper, J. *Activity and Diversity of Sulfate-Reducing and Methanogenic Microorganisms in a Petroleum- Contaminated Aquifer,* PhD Theses, University of Bayreuth, 2003.
Klinowski, J. *High resolution spectroscopy (Raman)*, University of Cambridge, 2003.

Kontrec, J., Ukrainczyk, M., Babic-Ivancic, V. and Kralj, D. (2011) Synthesis of Calcium Carbonate by Semi-continuous Carbonation Method in the Presence of Dextrans. *Croatica Chemica Acta*, vol. **84**, no. 1, pp 25-32.

Ma, Q., Ellis, G.S., Amrani, A., Zhang, T. and Tang, Y. (2008) Theoretical study on the reactivity of sulfate species with hydrocarbons. *Geochimica et Cosmochimica Acta*, pp 4565-4576.

Machel, H.G. (2001) Bacterial and thermochemical sulfate reduction in diagenetic settings – old and new insight. *Sedimentary Geology,* vol. **72**, pp 143-175.

Maree, J.P., Theron, D., Nengovhela, N.R. and Hlabela, P.S. (2005) Sulphur from smelter gases and sulphate-rich effluents. *Journal of South African Institute of Mining and Metallurgy*, vol. **105**, pp 1-4.

Mihara, N., Soya, K., Kuchar, D., Fukuta, T. and Matsuda, H. (2008) Utilisation of calcium sulfide derived from waste gypsum boards for metal-containing wastewater treatment. *Global NEST journal,* vol. **10**, no. 1, pp 101-107.

Nakamizo, N., Kammereck, R. and Walker P.L. (1974) Laser Raman studies on carbons. *Carbon*, vol.**12**, pp 259-267.

Nengovhela, N.R, Strydom, C.A., Maree, J.P., Oosthuizen, S. and Theron, D.J. (2007) Recovery of sulphur and calcium carbonate from waste gypsum. *Water SA*, vol. **33**, no. 5, pp 741-748.

Nengovhela, R.N. *The recovery of sulphur from waste gypsum*, PhD Theses, University of Pretoria, 2008.

Prasad, P.S.R., Pradhan, A. and Gowd, T.N. (2001) *In situ* micro-Raman investigation of dehydration mechanism in natural gypsum. *Current Science,* vol. **80**, no. 9, pp 1203.

Ratlabala M.E. 2003. An overview of South Africa's mineral based fertilizers. Department of Minerals and Energy. The Republic of South African government.

Ray, C., Landqvist, J., Johansson, J.N. and Berg, S. *Raman Spectroscopy: Analytical methods in earth science,* UPPSALA Universiteit, 2010.

Reksten, K. (1990) Superstructures in Calcite. *American Mineralogist*, vol. **75**, pp 807-812.

S.D. Ross, *Inorganic Infrared and Raman Spectra,* McGraw-Hill: London 1972.

Sadezky, A., Muckenheber, H., Grothe, H., Neissner, R., & Poschi, U. 2005 Raman microspectroscopy of soot and related carbonaceous materials: Spectral analysis of structural information. *Carbon*, vol. **43**, pp 1731-1742.

Sarma, L.P., Prasad, P.S.R. and Ravikumar N. (1998). Raman Spectroscopic Study of Phase Transitions in Natural Gypsum. *Journal of Raman spectroscopy*, vol. **29**, pp 851-856.

Scheetz, B.E. and White, B. (1977) Vibrational spectra of the alkaline earth double carbonates. *American Mineralogist*, vol. **62,** pp 36-50.

Skinner, A.J., LaFemina, J.P. and Jansen, H.J.F. (1994) Structure and bonding of calcite, a theoretical study *American Mineralogist***,** vol. **79**, pp 205-214.

Smyth, J.R. (1997) The crystal structure of Calcite III. *Geophysics research letter*, vol. **24**, no. 13, pp 1595-1598.

Tian, H., Guo, Q. and Chang, J. (2008) Investigation into decomposition behavior of $CaSO_4$ in chemical-looping combustion. *Energy and Fuels,* vol*.* **22**, no. 6, pp 3915-3921.

Wopenka, B. and Pasteris, J.D. (2005) A mineralogical perspective on the apatite in bone. *Material science and engineering*, **C25**, pp 131-143.

Yue, C., Li, S., Ding, K. and Yhong, N. (2006) Thermodynamics and Kinetics of reactions between C1-C3 hydrocarbons and calcium sulfate in deep carbonate reservoirs. *Geochemical Journal*, vol. **40**, no.1, pp 87-94.

Zhang, T., Amrania, A., Ellis, G.S., Ma, Q. and Tang, Y. 2008 Experimental investigation on thermochemical sulfate reduction by H_2S initiation. *Geochimica et Cosmochimica Acta*, pp 3518-3530.

Zhang, T., Ellis, G.S., Waters, C.C., Kelemen, S.R., Wang, K and. Tang, Y. (2008) Geochemical signatures of thermochemical sulfate reduction in

controlled hydrous pyrolysis experiments. *Organic Geochemistry,* vol. 39, no. 3, pp 308-328.

CHAPTER 6

CONCLUSIONS AND RECOMMENDATION

6.1 Suitability of the Lowveld phosphogypsum for use in building materials

The South African Nuclear Regulator Act 47 of 1999 is intended to control the use, storage and disposal of radiation sources. The Act exempts from regulation materials of low exposure or potential exposure. The suitability of the phosphogypsum from the Lowveld of South Africa for possible use in building materials was evaluated against the requirements of this Act.

The Lowveld phosphogypsum contains low to appreciable activity concentrations of the radioactive nuclides: U-238; U-235; Th-232 and their progenies. The average concentrations of these radioactive nuclides are below the maximum limit of 500 Bq/kg each, set for regulation by the Act. The phosphogypsum is therefore exempted from regulation control. The concentration of K-40, is below the minimum detectable amount, of 100 Bq/kg, by the γ-spectrometer used and therefore also well within the 10 000 Bq/kg maximum limit set for building materials by the Act. The phosphogypsum is therefore suitable for use as building material in South Africa. Based on the results obtained in this study, the concentration index ($I\gamma$) is in the range $1<I_{\gamma}<6$, it is recommended that the phosphogypsum be utilised for in building materials with restrictions such as in prefabrication of gypsum boards or be diluted before use. An assessment should be done for decision making with the consideration of scenario of use.

The U-238; U-235; Th-232 and their progenies are in disequilibria in the phosphogypsum. The distribution of their concentration showed that concentration of U-238 and its decay products Pb-210 and Ra-226 originating from the apatite ore are partitioned during processing in such a

way that U-238 accumulates in the phosphoric acid while Ra-228 and Ra-226 accumulates in the phosphogypsum. The majority of phosphoric acid is used in the manufacturing of fertilizers. Therefore the accumulation of radioactive progenies in phosphoric acid may lead to their accumulation in food grown where the fertilizer is applied.

The partitioning behaviour can be attributed to the very low aqueous solubility of radium sulphate and lead sulphate relative to that of uranium sulphate. The concentrations of the progenies whose sulphate are low in solubility are also Gaussian distributed in the phosphogypsum.

6.2 Conversion of the Lowveld phosphogypsum to ammonium sulphate and precipitated calcium carbonate

The production of ammonium sulphate and precipitated calcium carbonate was carried out in a Merseburg process that had been modified by forming the ammonium carbonate in the gypsum conversion reactor. The formation of ammonium carbonate from carbon dioxide and ammonia is an exothermic reaction, ΔH = -101 kJ/mol. On average the temperature in the gypsum conversion reactor increased by a 35 ºC during the ammonium carbonate formation. The addition of carbon dioxide to the gypsum conversion reactor would result in the reduction of the heating requirement to reach the reaction temperature of 70 ºC.

The optimal reaction time to convert the phosphogypsum and precipitate the calcium carbonate has previously been determined to be between in 5-7 hours.

The morphology of the precipitated calcium carbonate crystal produced under the current conditions was determined to be a scalenohedral calcite polymorph with average diameter of 3.4 $\pm$ 0.1 µm. This is polymorph of calcium carbonate that is most preferred by paper industry due to the superior optical quality achieved when it is used.

Sulphuric acid addition was necessary to lower the pH. At the end point of ammonium carbonate formation. The pH of the solution was about 8.5. Ammonium sulphate precipitation is optimal at pH of about 3.5. Sulphuric acid was therefore used to lower this pH before concentrating the solution for the precipitation of ammonium sulphate.

The heavy metal content of the $(NH_4)_2SO_4$ is comparable to the commercially available grades.

The economic feasibility of converting phosphogypsum to precipitated calcium carbonate and ammonium sulphate is dependent on the proximity of the available carbon dioxide and ammonia to the phosphogypsum, the size of the plants as well as the ammonia prices.

6.3 Thermal sulphate reduction of the Lowveld phosphogypsum using carbonaceous material to calcium sulphide

6.3.1 Reaction mechanism pathway

6.3.1.1 X-ray powder diffraction

The phosphogypsum dehydrated to hemihydrate then to anhydrite when heated in the mixture with graphite under nitrogen. Prior to dehydration the anisotropic lattice expansion along the b-axis of the gypsum crystal is observed by the change in diffraction peak positions. No further phase transformation beyond anhydrite formation is observed in the temperature range 25–650 ºC. The anhydrite partially rehydrates to gypsum after cooling down when the reaction is carried out under air but no rehydration when the reaction is carried out under continuous nitrogen flow of 100 ml/min.

6.3.1.2 TG-DSC kinetics

The phosphogypsum reduction was preceded by a parallel dehydration to hemihydrate at 96 ºC and anhydrite at temperatures below 170 ºC. A gradual mass loss is observed from about 650 ºC which could be attributed to partial oxidation of graphite to carbon mono/dioxide. The thermal sulphate reduction was complete just above 1000 ºC, proceeded by formation of an intermediate compound at about 900 ºC, characterised by a 11% mass loss. The phosphogypsum reduction with graphite follows a complex mechanism with average activation energy as determined by the OFW and KAS kinetic methods to be 330-370 kJ/mol.

6.3.1.3 In situ Raman Spectroscopy

The gypsum does not decompose under N_2 or air blanket up to the temperature of 1080 ºC, but dehydrates to anhydrite. This is characterised by the shift in the ν_1 SO_4 vibrational band in the Raman spectrum. When the gypsum is reacted with graphite under continuous air flow, no reaction other than the dehydration to anhydrite occurred. When gypsum is reacted with graphite under N_2 blanket, it converts to CaS with onset temperature of the redox reaction around 900 ºC. An intermediate, dehydrated Orschallite-type compound forms accompanied by the evolution of carbon monoxide. The intermediate transforms to CaS as per the proposed mechanism is give in Equations 6.1:

$$\begin{aligned} &3CaSO_4.2H_2O(s) + 6C \\ &\rightarrow 3CaSO_4(s) + 6C(s) \rightarrow Ca_3[SO_4][SO_3](s) + 4C + 2CO_2(g) \\ &\rightarrow 3CaS(s) + 4CO_2(g) \end{aligned} \quad \text{.....(6.1)}$$

The onset temperature for such a transformation has been measured to be around 900 ºC when graphite is used as an electron donor. This onset temperature was not influenced by the heavy metal impurities present in phosphogypsum at the present concentration.

6.4 Recommended future research

6.4.1 Radioactive nuclides in phosphogypsum

The current study was based on samples taken during the production process. A study on the phosphogypsum dug out samples may reveal the current concentrations after decades of decay. A modelling study can be carried out to map activity concentrations in the different areas of the phosphogypsum dams.

6.4.2 Modified Merseburg process

The technical feasibility of the modified Merseburg process has been proven in this Thesis. In order to ascertain that the goal of reducing the capital layout, it is recommended that a comparative Economical feasibility study be carried out.

6.4.3 Thermal reduction of phosphogypsum

The high temperature requirement for the thermal reduction of phosphogypsum is the deterrent to sulphur recovery in this manner, considering the current low price of sulphur. Although sulphur is cheap its price can be volatile and its transportation and supply can be dependent on world's political stability as was seen in 2008. Further investigation of alternative electron donors that may lower the activation energy for the reduction reaction would add value to the scientific knowledge base.

Publications and papers under review

Reference: SAA13568

Msila X, Barnard W, Billing DG (2015) Raman spectroscopic study of the thermal reduction of phosphogypsum with a carbonaceous material. Spectrochimica Acta Part A: Molecular and Biomolecular Spectroscopy: 317-322 DOI: 10.1016/j.saa.2015.04.017

Reference: SAJS-2015-0102

Msila X, Labuschagne F, Barnard W, Billing, DG (2016) Radioactive nuclides in phosphogypsum from the Lowveld region of South Africa. South Africa Journal of Science 112(1): 98-102 http://dx.doi.org/10.17159/sajs.2016/20150102.

Reference: CTEP-D-15-00625R3

Msila X, Billing D, Barnard W (2016) Capture and storage of CO_2 in phosphogypsum – the modified Merseburg process. Clean technology and environment policy. Published on line 26-03-2016. DOI: 10.1007/s10098-016-1157-4.

Reference: JTAC-D-15-01694

Msila X, Billing DG, Barnard W,. TG-DSC analysis and kinetics of the reaction between phosphogypsum and graphite". JTAC (under review)

REFERENCES

Abdel-Zaher M. Abouzeid (2008) Physical and thermal treatment of phosphate ores — An overview. *International Journal of Mineral Processing*, vol. 85, pp 59–84.

Abriel, W., Reidsdorf, K. and Pannetier, J. (1990) Dehydration reactions of gypsum: a neutron and X-ray study. *Journal of Solid State Chemistry*, vol. **85**, pp 23-30.

Ackers, J.G., De Boer, J.F., De Jong, P. and Wolschrijin, R.A. (1985) Radioactivity and radon exhalation rates of building materials in the Netherlands. *Science of the Total Environment*, vol. **45**, pp 151-156.

Alienov, D.P. *Fertilizer Manual*, Kluwer Academic Publishers, 1998, pp 246-248.

Al-Jundi, J., Al-Ahmad, N., Shehadeh, H., Afaneh, F., Maghrabi, M. and Gerstmann, U. (2008) Investigation on the activity concentrations of U-238, Ra-226, Pb-210 and K-40 in Jordan phosphogypsum and fertilizer. *Radiation Protection Dosimetry*, vol. **131,** no. 4, pp 449-454.

Amrani, A., Zhang, T., Ma, Q., Ellis, G.S. and Tang, Y. (2008) The role of labile sulphur compound in Thermochemical Sulphate Reduction, *Geochimica et Cosmochimica Acta*, pp 2660-2972.

Ball, D. (2001) Theory of Raman Spectroscopy, *Spectroscopy*, vol. 16, no.2, pp. 28-30.

Ball, M.C. and Norwood, L.S. (1969) Studies in the calcium sulphate-water-Part 1. Kinetics of dehydration of calcium sulphate dihydrate. *Journal of Chemical Society*, vol. **A**, pp 1633- 1637.

Ballirano, P. and Melis, E. (2007) Thermal behaviour of anhydrite β-$CaSO_4$ to 1,263K. *Physics and Chemistry of Minerals*, vol. **34**, pp 699-704.

Ballirano, P. and Melis, E. (2009) Thermal behaviour and kinetics of dehydration of gypsum in air from *in situ* real time laboratory parallel-beam X-Ray powder diffraction. *Physics and Chemistry of Minerals*, vol. **36**, pp 391-402.

Ballirano, P., Maras, A., Meloni, S. and Caminiti, R. (2001) The monoclinic *I*2 structure of bassanite, calcium sulphate hemihydrate ($CaSO_4$•$0.5H_2O$). *European Journal of Mineralogy*, vol. **13**, pp 985 - 993.

Bergamin, A., Cavagnero, G., Mana, G. and Zosi, G. (1997) Lattice parameter and thermal expansion of monocrystalline silicon. *Journal of Applied Physics*, vol. **82**, pp 5396-4000.

Bezou, C., Nonat, A., Mutin, J.C., Christensen, A.N., and Lehmann, M.S. (1995) Investigation of the crystal-structure of γ-$CaSO_4$, $CaSO_4$·$0.5H_2O$, and $CaSO_4$·$0.6H_2O$ by powder diffraction methods. *Journal of Solid State Chemistry*, vol.117,pp 165–176.

Brown, M.E. *Introduction to Thermal Analysis: Techniques and Applications*, Chapman and Hill, New York. 1998. pp 7-21

Bushuev, N.N., Maslenikov, B.M. and Borisov, V.M. (1983) Phase transformation in the dehydration of $CaSO_4$•$2H_2O$. *Russian Journal of Inorganic Chemistry*, vol. **28**, pp 1404-1407.

Cammack, KM, Wright, C.L., Austin, P.S., Johnson, P.S., Cockrun, R.R., Kessler, K.L. and Olson, K.C. (2010) Effect of high-sulfur water and clinoptilolite on health and growth performance of steers fed forage-based diets, *Journal of Animal Science*, vol. **88**, pp 1777-1785.

Carbone, M., Ballirano, P. and Caminiti, R. (2008) A kinetic investigation of gypsum dehydration at reduced pressure by energy dispersive X-ray diffraction (EDXRD). *European Journal of Minerals*, vol. **20**, pp 621-627.

Chang, H., Huang, P.J. and Hou, S. (1999) Application of thermo-Raman spectroscopy to study the dehydration of $CaSO_4.2H_2O$ and $CaSO_4.1/2H_2O$. *Materials Chemistry and Physics*, vol. **58**, pp 12-19.

Chio, C.H, Sharma, S.K. and Munenow, D.W. (2004). MicroRaman studies of gypsum in the temperature range between 9 K and 373 K. *American Mineralogy*, vol. **89**, pp 390-395.

Chou, M.I.M., Bruinius, J.A., Li, Y.C., Rostam-Abadi, M., Lytle, J.M. (1995) Manufacture of ammonium sulfate fertilizer from FGD-gypsum. *American Chemical Society Fuel Chemical division*. Chicago. Available online at http://web.anl.gov/PCS/acsfuel/files. Accessed 20 February 2016

Chou, M.I.M., Rosam-Abadi, M. and Lytle, J.M. (1996) Manufacture of ammonium sulfate fertilizer from gypsum-rich by-product of flue gas desulfurisation – A prefeasibility cost estimate. Available online at https://web.anl.gov/PCS/acsfuel/preprint%20archive/Files/41_2_NEW%20ORLEANS_03-96_0579.pdf. Accessed 30 November 2015

Christensen, N., Lehmann, M.S. and Pannetier, J. (2008) Formation and transformation of five different phases in the $CaSO_4$-H_2O system. Crystal structure of the subhydrates β-$CaSO_4$ and soluble anhydrite $CaSO_4$. *Chemistry of Materials*, vol. **20**, pp 2124-2132.

Coles, D.G., Ragaini, R.C. and Ondov, J.M. (1978) Behavior of natural radionuclides in Western Coal-Fired power plants. *Environmental Science and Technology*, vol. **12**, no.4, pp 442-446.

Contract No 96-ET-003, STUK (Finland), Enhanced Radioactivity of Building Material, Radiation Protection 96. 1999.

Curie S (1904) Discovery of Radium. *The Century Magazine*. 461-466.

Curie, M. (1911) Radium and the new concepts in chemistry. Nobel Lecture. www.nobelprize.org/nobelprizez/chemistry/laureates/1911/maire-curie-lecture.html>

Dos Santos, V.A., Pereira, J.A.F.R. and Dantas, C.C. (1997) Kinetics of thermal dehydration of gypsum ore for obtaining beta hemihydrates in a fluidized bed. *Bulletin des Societes Chimiques Belges*, vol. **6**, pp 253-260.

Ellis. G.S., Zhang, T., Ma, Q. and Tang, Y. (2007) Theoretical study on the reactivity of sulfate species with hydrocarbons**.** *Geochimica et Cosmochimica Acta***,** vol. **72**, vol. 18, pp 4565**-**4576.

El-Tahawy, M.S. and Higgy, R.H. (1985) Natural radioactivity in different types of bricks fabricated and used in the Cairo region. *Applied Radioactive Isotopes*, vol. **46**, no. 12, pp 1401-1406.

El-Thaway, M.S. and Higgy, R.H. (1985) Natural radioactivity in different types of bricks fabricated and used in the Cairo region. *Applied Radiation Isotopes,* vol. **46,** no. 12, pp 1401-1406.

Environmental Protection Agency. Radiation Protection: Gamma Rays. Accessed at www.epa.gov/radiation/understand/gamma.html on August 10, 2015.

Genet, M. (1995) The discovery of Uranic Rays: A short step for Henri Becquerel but a giant step for science. *Radiochimica Acta,* vol. **70**, no.70, pp 3-12.

Ghissassi F.E.L., Baan, R., Straif, K., Grosse, Y., Secretan, B., Bouvard, V., Benbrahim-Tallaa, L., Guha, N., Freeman, C., Galichet, L. and Cogliano, V. (2009) A review of human carcinogens—Part D: radiation. *The Lancet Oncology*, vol. **10**, no. 8, pp 751 – 752.

González, D., Miguel, A.M-M. and Garcia, A.B (2003) Graphite materials prepared from anthracite; a structural characterisation. *Energy Fuel*, vol. **17**, pp 1324 -1329.

Gulbrandsen, R.A. (1966) Chemical composition of phosphorites of the phosphoria formation. *Geochimica et Cosmochimica Acta*, vol. **30**, no 8, pp 769-778.

Heizer, W.D. (1997) Intestinal effects of sulphate in drinking water on normal human subjects. *Digestive Diseases and Science*, vol. **42**, no. 5, pp 1055-1061.

Hogarth, D.D. (1988) Chemical composition of fluorapatite and associated minerals from skarn near Gatineau, Quebec. *Mineralogical Magazine*, vol. 52, pp 347–358.

http://beta2.statssa.gov.za/publications/P0318/P03182013

http://en.wikipedia.org/wiki/Standard_enthalpy_change_of_formation

Http://icsd.fiz-karlsruhe.de DemoICSD9160; KETORO

http://icsd.ill.eu/icsd/index.php {Free crystal structure database}

http://www.epa.gov/radiation accessed on 08.08.2015

http://www.nndc.bnl.gov/chart accessed on 15 May 2015

http://www.reade.com/Products/Minerals_and_Ores/calcium_carbonate.html]

http://www.simetric.co.uk/si_materials.htm accessed on 12 Feb 2015

http://www2.lbl.gov/abc/ accessed on 10.03.2014

Hussein, E.M. (1994) Radioactivity of phosphate ore, superphosphate and phosphogypsum in Abu Zaabal phosphate plant, Egypt. *Health Physics*, vol. **48**, pp 87-95.

Ismail, A.F., Yasir, M.S., Majid, A.A., Bahari, I., Yahaya, R. and Rahman, I.A. (2009) Radiological studies of naturally occurring radioactive materials

in some Malaysia's sand used in building construction. *The Malaysian Journal of Analytical Sciences,* vol.**13**, no.1, pp 29-35.

Kato, T., Murakami, K. and Sugawara, K. (2012) Carbon reduction of gypsum produced from flue gas desulphurization. *Chemical Engineering Transactions*, vol. **29**, pp 805-810.

Klinowski, J. "High resolution spectroscopy (Raman)." University of Cambridge 2003.

Lager, G.A., Armbruster, T.H., Protella, F.J., Jorgensen, J.D. and Hinks, D.G. (1984) A crystallographic study of the low temperature dehydration products of gypsum, $CaSO_4.2H_2O$: Hemihydrate $CaSO_4$. $0.5H_2O$, and γ-$CaSO_4$. *American Mineralogist*, vol. **69**, pp 910-918.

Loneragan, G.H., Wagner, J.J., Gould, D.H., Garry, F.B. and Thoren, M.A. (2001) Effect of water sulfate concentration on performance, water intake, and carcass characteristics of feedlot steers. *Journal of Animal Science*, vol. **79**, pp 2941-2948.

Ma, Y.M., Zhou, Q., He, Z., Li, F.F., Yang, K.F., Cui, Q.L. and Zou, G.T. (2007) High-Pressure and High-Temperature study of the phase transition in anhydrite. *Journal of Physics: Condensed Matter*, vol. **19,** no.42, 425221.

Manea, C., Podina, C., Pordea, I., Crutu, G., Ilie, G. and Robu, I. (2010) The radiological risk assessment due to the radioactivity of thermal power station ashes added in building materials. *Revue Roumaine de Chimie*, vol. **55**, no. 1, pp 39-44.

Manea, C., Podina, C., Pordea, I., Crutu, G., Ilie, G. and Robu, I. (2008) The estimation of cements radioactivity obtained by electrofilter ashes addition due to thermal power station based on coal from oltenia coalfired, Romania." *Analele Universitatii din Bucuresti-Chemie*, vol. **1**, pp 45-49.

Mar, S.S. and Okazaki, M. (2012) Investigation of Cd contents in several phosphate rocks use for the production of fertilizers. *Microchemical Journal*, vol. 104, pp 17-21.

McAdie, H.G. (1964) The effect of water vapour upon the dehydration of $CaSO_4.2H_2O$. *Canadian Journal of Chemistry*, vol. **42**, pp 792–801.

Mokaila, G.E. An overview of South Africa's primary industrial mineral imports and exports. Directorate: Mineral Economic. Report R42/2003. 2003.

Molony, B. and Ridge, M.J. (1968) Kinetics of the dehydration of calcium sulphate dihydrate in vacuo. Australian Journal of Chemistry, vol. 21, no.4, pp 1063-1065.

Nakamoto, K. *Infrared and Raman Spectra of Inorganic and Coordination Compounds, 3rd*,1978. (John Wiley-Interscience Publication)

Okada, Y. and Tokumaru, Y. (1984) Precise determination of lattice parameter and thermal expansion coefficient of silicon between 300 and 1500K. *Journal of Applied Physics*, vol. **56**, pp 314- 320.

Pfister, H., Philipp, G. and Pauly, H. (1976) Population dose from natural radionuclides in phosphate fertilizers. *Radiation and Environmental Biophysics*, vol. **13**, pp 247-261.

Popovic D. and Todorovic, D. (2006) Radon indoor concentrations and activity of radionuclides in building materials in Serbia. *Physics, Chemistry and Technology*, vol. **4**, pp 11-20.

Prasad, P., Krishna, C., Prasad, K.S. and Narayan, R.D. (2005) Direct formation of the γ-$CaSO_4$ phase in the dehydration process of gypsum. *In situ* FTIR study. *American Mineralogist*, vol. **90**, pp 672- 678.

Putnis, A., Winkler, B. and Diaz, L.F. (1990) in-situ IR spectroscopy and thermogravimetric study of the dehydration of gypsum. *Journal of Raman Spectroscopy*, vol. **29**, pp 847- 851.

Ratlabala M.E. 2003. An overview of South Africa's mineral based fertilizers. Department of Minerals and Energy. The Republic of South African government.

Ray, W.G., Arbo, J.C. and Gryka, G.E. (1990) Process for recovery of sulphur from a gas stream. US Patent 5057298, PIPco Inc. CT, USA

Sarma, L.P., Prasad, P.S.R. and Ravikumar, N. (1998) Raman spectroscopic study of the phase transition in natural gypsum. *Journal of Raman spectroscopy*, vol. 29, no.9, pp 851-856.

Schofield, P.F., Knight, K.S. and Stretton, I.C. (1996) Thermal expansion of gypsum investigation by neutron powder diffraction. *American Mineralogist*, vol. **81**, pp 847- 951.

Stranden, E. (1976) Some aspects on radioactivity of building materials. *Physica Norvegica*, vol. **8**, pp 167-173.

Stranden, E. (1976) Some aspects on radioactivity of building materials. *Physica Norvegica*, vol. **8**, pp 167-173.

Strydom, C.A., Hudson-Lamb, D.L., Potgieter J.H., Dagg, E. (1995) The thermal dehydration of synthetic gypsum. *Thermochimica Acta*, vol. **269-270**, pp 631- 638.

TECHNICAL UNIVERSITY DRESDEN Institute of Power Engineering Training Reactor. Identification of Unknown Radionuclides (γ - Spectrometry), 2015. Accessed online at: https://tu-dresden.de/die_tu_dresden/fakultaeten/fakultaet_maschinenwesen/iet/wket/akr2/Lehrmaterialien/gaspek_e.pdf on 27 April 2016.

Wagner, J.C. and Van Niekerk, A.M. Quality and treatment of effluents originating from mine and municipality waste sites. *Proceedings of the International Conference on Mining and Industrial waste Management*. Johannesburg.1987. pp 283-286.

Zhang, T., Ellis, G.S., Waters, C.C., Kelemen, S.R., Wang, K. and Tang, Y. (2008) Geochemical signatures of thermochemical sulfate reduction in controlled hydrous pyrolysis experiments. *Organic Geochemistry*, pp 308-328.

Appendix A: Flynn – Wall – Ozawa method: Data for E_a calculation

Conversion	Heating rate (β)				Slope	R^2	Ea (kJ/mol)
	15	20	25	30			
lnβ	2.708050201	2.995732274	3.218875825	3.401197382			
10.0%	2.51268908	2.470905093	2.447381302	2.430310837	-8.325	0.9891	65.800
15.0%	2.467917078	2.418145766	2.393317857	2.380555622	-7.616	0.9673	60.197
20.0%	2.427950567	2.365016673	2.338743627	2.331382743	-6.550	0.9258	51.771
25.0%	1.449128349	1.404967967	1.511395925	1.430574232	1.038	0.0248	-8.208
30.0%	0.934265107	0.9198955	0.914411119	0.906125408	-25.045	0.9840	197.939
35.0%	0.876708486	0.862909558	0.862024378	0.85467894	-31.183	0.9200	246.445
40.0%	0.844601728	0.833277781	0.838166762	0.825832026	-31.498	0.6976	248.934
45.0%	0.821045026	0.81532817	0.819443762	0.804505229	-30.209	0.5672	238.745
50.0%	0.8087932	0.803264467	0.802767944	0.792964816	-41.771	0.8464	330.116
55.0%	0.800717443	0.795431044	0.792374191	0.785558296	-46.227	0.9585	365.336
60.0%	0.794445239	0.789496538	0.785416388	0.779629832	-47.086	0.9786	372.122
65.0%	0.789041788	0.784350636	0.779702777	0.774359411	-47.095	0.9827	372.196
70.0%	0.784092335	0.779356407	0.77468935	0.769295863	-46.747	0.9827	369.444
75.0%	0.779356407	0.774425376	0.769965198	0.764292265	-46.127	0.9812	364.544
80.0%	0.7748154	0.769550429	0.765421326	0.759353335	-45.220	0.9787	357.376
85.0%	0.770249869	0.764543529	0.760560381	0.754193315	-43.752	0.9786	345.775
90.0%	0.765374459	0.759301443	0.7552756	0.748945859	-42.889	0.9824	338.954
95.0%	0.7592265	0.752887323	0.748407762	0.74264411	-42.424	0.9916	335.280

Appendix B: Kissinger – Akahira – Sonuse method: Data for E_a calculation

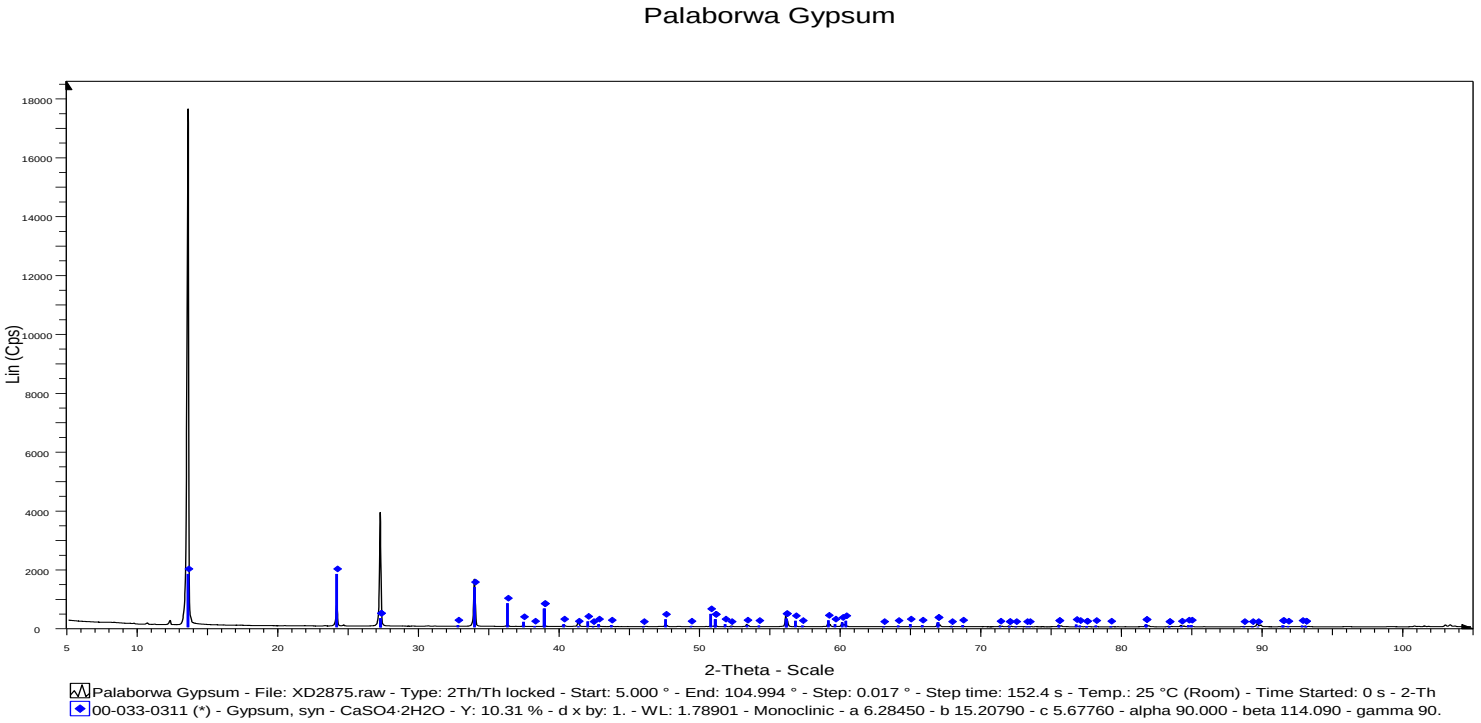
Conversion	Heating rate (β)				Slope	R^2	Y	Ea ($kJ.mol^{-1}$)
	15	20	25	30				
ln (β/T^2)	-9.264	-9.010609249	-8.80659754	-8.638274845				
10.0%	2.51268908	2.470905093	2.447381302	2.430310837	-7.517	0.9868	9.602	62.497
ln (β/T^2)	-9.33336533	-9.09820814	-8.897406986	-8.721390089				
20.0%	2.427950567	2.365016673	2.338743627	2.331382743	-5.7108	0.9202	5.036	47.480
ln (β/T^2)	-11.24345044	-10.98676869	-10.77558475	-10.6114683				
30.0%	0.934265107	0.9198955	0.914411119	0.906125408	-22.873	0.9821	11.849	190.171
ln (β/T^2)	-11.44524054	-11.18455473	-10.94971113	-10.79704095				
40.0%	0.844601728	0.833277781	0.838166762	0.825832026	-29.104	0.6966	14.840	241.968
ln (β/T^2)	-11.5318844	-11.25792083	-11.03601392	-10.87826603				
50.0%	0.8087932	0.803264467	0.802767944	0.792964816	-39.272	0.8499	21.412	326.506
ln (β/T^2)	-11.5676828	-11.29249794	-11.07971727	-10.91218527				
60.0%	0.794445239	0.789496538	0.785416388	0.779629832	-44.544	0.9810	24.618	370.343
ln (β/T^2)	-11.59391734	-11.31835192	-11.10722107	-10.93887247				
70.0%	0.784092335	0.779356407	0.77468935	0.769295863	-44.172	0.9852	23.938	367.245
ln (β/T^2)	-11.6177213	-11.34367587	-11.13129242	-10.96488934				
80.0%	0.7748154	0.769550429	0.765421326	0.759353335	-42.612	0.9810	22.469	354.280
ln (β/T^2)	-11.64224051	-11.37049113	-11.15797986	-10.99249034				
90.0%	0.765374459	0.759301443	0.7552756	0.748945859	-40.248	0.9840	20.451	334.617
ln (β/T^2)	-11.65837061	-11.38745768	-11.17624936	-11.00938986				
95.0%	0.7592265	0.752887323	0.748407762	0.74264411	-39.7608	0.9928	19.878	330.572

Appendix C: High temperature X-Ray diffractometer set-up

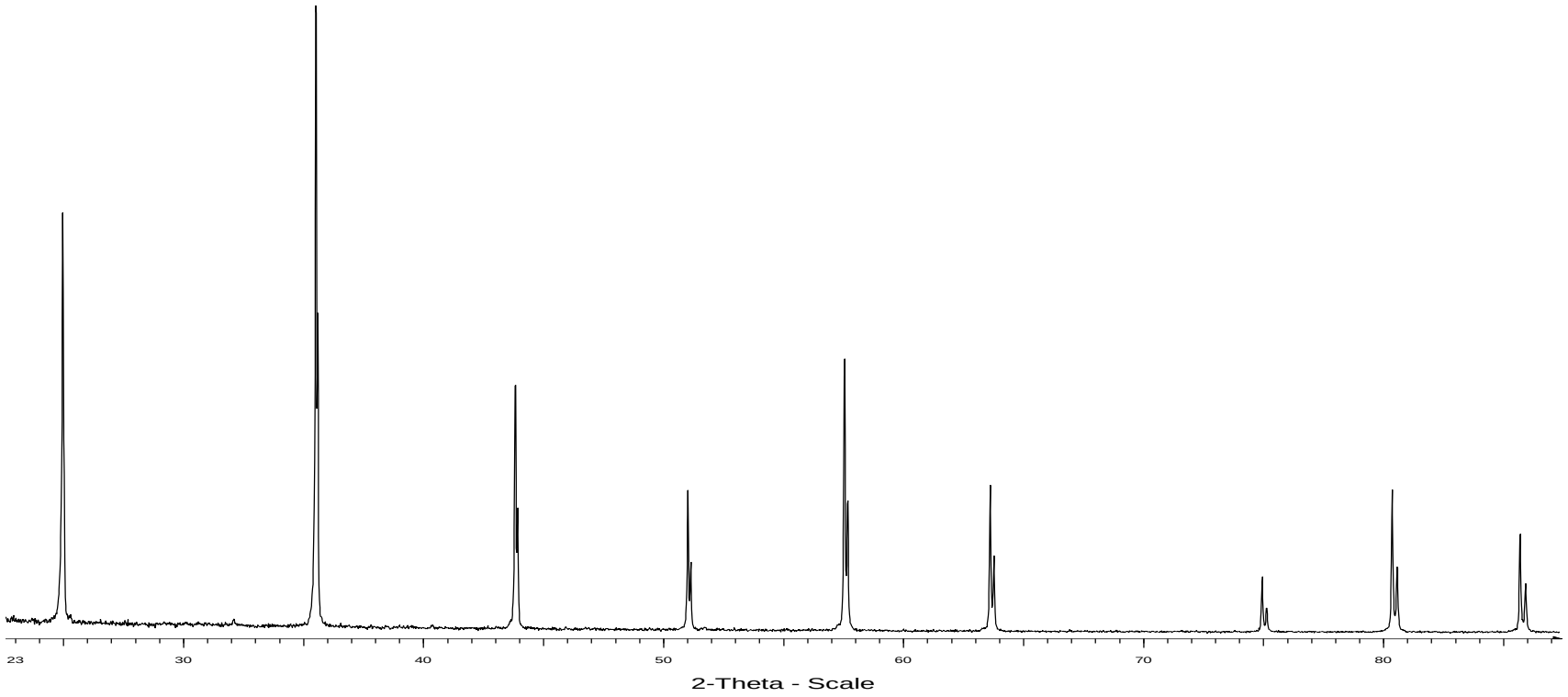
Measurement Date / Time	1/13/2013 6:36:05 PM
Raw Data Origin	XRD measurement (*.XRDML)
Scan Axis	Gonio
Start Position [°2Th.]	5.0064
End Position [°2Th.]	89.9894
Step Size [°2Th.]	0.0170
Scan Step Time [s]	14.6050
Scan Type	Continuous
PSD Mode	Scanning
PSD Length [°2Th.]	2.12
Offset [°2Th.]	0.0000

Divergence Slit Type	Automatic
Irradiated Length [mm]	5.00
Specimen Length [mm]	10.00
Measurement Temperature [°C]	25.00
Anode Material	Co
K-Alpha1 [Å]	1.78901
K-Alpha2 [Å]	1.79290
K-Beta [Å]	1.62083
K-A2 / K-A1 Ratio	0.50000
Generator Settings	50 mA, 35 kV
Goniometer Radius [mm]	240.00
Dist. Focus-Diverg. Slit [mm]	100.00

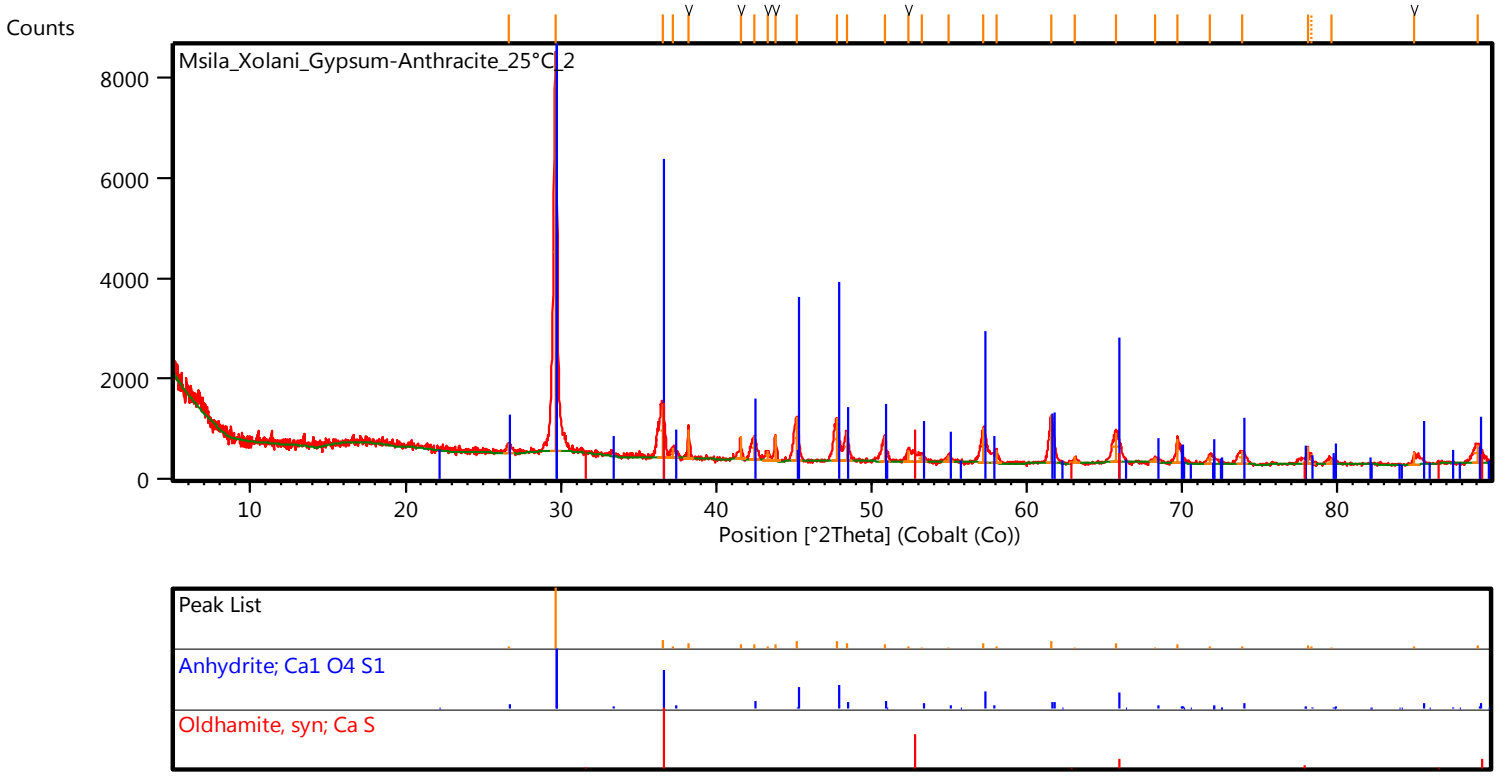
Appendix D: Diffractogram of the Phalaborwa phosphogypsum



Appendix E: Diffractogram of the LAB_6 standard used for peak position verification of the X-Ray diffractometer



Appendix F: Diffractogram of phosphogypsum and graphite reaction mixture at temperature 25-1080 ºC under continuous nitrogen flow.



Appendix G: Gamma-ray spectrum of the grab sample from the pile

